The Biophysics of Vertebrate Hearing: A Single-Molecule Approach

The Biophysics of Vertebrate Hearing: A Single-Molecule Approach

A dissertation presented

by

Mounir Ahmad Koussa

to

The Division of Medical Sciences

in partial fulfilment of the requirements

for the degree of

Doctor of Philosophy

In the subject of

Neurobiology

Harvard University

Cambridge, Massachusetts

April 2015

Dissertation Advisors:
Dr. David P. Corey and Wesley P. Wong Mounir Ahmad Koussa

The Biophysics of Vertebrate Hearing: A Single-Molecule Approach

Inner-ear mechanotransduction relies on tip links, fine protein filaments made of cadherin-23 and protocadherin-15 that convey tension to mechanosensitive channels at the tips of hair-cell stereocilia. The tip-link cadherins are thought to form a heterotetrameric complex, with two cadherin-23 molecules forming the upper part of the filament and two protocadherin-15 molecules forming the lower end. The interaction between cadherin-23 and protocadherin-15 is mediated by their N-terminal tips. Missense mutations that modify the interaction interface impair binding and lead to deafness. We have developed molecular tools to perform single-molecule force spectroscopy on the tip-link bond. Self-assembling DNA nanoswitches are functionalized with the interacting tips of cadherin-23 and protocadherin-15 using the enzyme sortase under conditions that preserve protein function. These tip-link-functionalized nanoswitches are designed to provide a signature force-extension profile, which allows us to identify single-molecule rupture events that result from applying force. Using this system, we have been able to measure the cadherin-23-protocadherin-15 single-molecule force-dependent off rate, as well as the concentration-dependent on rate for a single pair of these proteins. The rates suggest that a single bond is inadequate to withstand physiological forces for physiological times, but we construct a new model for tip-link dynamics which greatly alters our understanding of tip-link function and explains the necessity for a two-filament tip link.

Table of contents

Acknowledgements

I, first and foremost, want to thank my advisors Drs. David P. Corey and Wesley P. Wong. They have both worked very hard to ensure that my doctoral training has been challenging, fun, stimulating, and exciting.

I have an immense amount of respect for David as both a scientist, and an extremely principled human being. His motivations as a scientist are pure in nature, he has a keen ability to seek out biological questions which are inherently interesting, and his clarity of thought is unparalleled. David does all of this while being a phenomenal mentor who gives his trainees the perfect balance of freedom and guidance.

Wesley has provided an extremely fun environment for technology development. He is a master problem solver and an extremely creative thinker. Additionally, Wesley is extremely fair, caring, and kind; all of which make him a phenomenal mentor.

I am extremely grateful for having had the opportunity to work with both David and Wesley. Their combined mentorships was crucial in my ability to develop the technologies necessary to answer the fundamental questions addressed in this thesis. I would like to thank all of the members of the Corey and Wong labs who have been extremely helpful during my time here. I would especially like to thank Drs. Marcos Sotomayor, Ken Halvorsen, and Andrew Ward for all of their help, training, and feedback, without which my thesis work would not have been possible.

I would also like to thank the many other faculty here at Harvard who have made my experience here extremely enjoyable. I would especially like to thank Dr. Rachel Wilson who has provided me with sage advice when I needed it most, and for serving on my Dissertation Advisory Committee (DAC). I would like to thank Dr. Richard Born for shaping a lot of the culture in the program, and for teaching me "Panicking is NEVER a good thing. Remain calm and you'll be more likely to think of the best course of action, no matter how dire the circumstances." I would also like to thank Drs. Bruce Bean and Gary Yellen for an amazing set of lectures on neurophysiology. Bruce was also extremely generous in allowing me to rotate in his lab to learn how to do electrophysiology on acutely isolated mouse neurons. I would like to thank Gary Yellen for serving on my DAC and for providing very insightful and critical feedback on my work over the last four years. I wish to acknowledge Jeffrey Holt for serving on my DAC, for inviting me to assist in the composition of a review on the TMC-family of proteins, and for having me as a teaching fellow for two years in the Neurology 200 course.

I would also like to thank Drs. Hidde Plough, Jonathan Cohen, Joshua Kaplan, Gary Yellen, and Michael Do for their feedback, and their willingness to serve on my examination committee.

In addition to my scientific development, there have been many people here at Harvard who have helped make my time at Harvard truly fulfilling. I would like to thank Karen Harmin for being a phenomenal program administrator, therapist, and friend. I wish to thank Carla Fujimoto for being extremely supportive in all my efforts, and for always being able to put a smile on my face. I wish to thank Drs. Joseph B. Martin and Sheila Nutt for many wonderful

conversations, and for their efforts in the Health Professions Recruitment and Exposure Program (HPREP).

Working on the leadership team of HPREP has brought me in touch with some of the kindest, most purely motivated people I have ever met. I would like to thank all of the high school students who have come through HPREP during my tenure at Harvard; you have all had a part in changing my world view, and bettering me as a person. I would like to thank all of my fellow "HPREP Enthusiasts" for teaching me so much about the world and its complexities. I would especially like to thank Jason Yamada-Hanff for the hours and hours of fun lesson planning and organizational revamping. I would like to thank Anna Chambers for constantly pushing me to be a better person, and her patience with me as I tried to do so. I would also like to thank Zhi-Yang Tsun for being my best friend, confidant, cooking partner, toughest critic, and biggest cheerleader; I cannot imagine my time here without him, nor do I have any desire to.

Before coming to Harvard, I had a lot of help and support from wonderful caring people in Arizona. I would like to thank Steve Laturco for believing in me, and sparking my curiosity, science and the world in the second grade. I would like to thank Christina Rossetti and Joanne Steele for fueling the fire through middle school with their engaging lectures, and for introducing me to the world of neuroscience. In high school I was very fortunate to have Dr. Fernier and Dr. Margaret Wilch as teachers. Dr. Fernier got me hooked on physics, and Dr. Wilch greatly altered my life trajectory by introducing me to the world academic research.

I would like to thank Dr. John Pollard for showing me the wonders of chemistry; Drs. Andrei Sanov and Oliver Monti for making accessible to me the worlds of thermodynamics and quantum mechanics respectively; Drs. Milsom and Jackson for providing me with a solid foundation in thinking like a physicist; Dr. Anne Padias for the opportunity to teach organic chemistry labs; and Dr. Hazzard for an amazing set of technical skills and life lessons.

I was very fortunate to work in the lab of Drs. Pélagie Beeson and Steven Rapcsak as a senior in high school. As I transitioned into my undergraduate career I had the immense pleasure of spending four years working in the lab of Drs. Lynne Oland and Leslie Tolbert. I cannot express how pivotal this experience was for me. I am thankful for my interactions with everyone in that lab, but I owe my most sincere gratitude to Lynne Oland. She taught me how to be a scientist, how to think, how to write, and how to make the most of what one has lying around the lab to solve problems.

The wonderful opportunities and ubiquitous nature of undergraduate research at the University of Arizona would not be possible without the tireless efforts of Carol Bender who has built a community of undergraduates, teaching us leadership and collaboration.

Throughout the years I could not have made it without the people in this world who keep me sane. I wish to thank Colin Shepard for starting me on a path to personal growth; Sasha Rayshubskiy and Masha Lezhen-Rayshubskiy for continually challenging me and supporting me through my struggles both scientific in nature and otherwise; Ahmed Badran for being like a brother, and my molecular biology guru; Pallav Kosuri for your joy, enthusiasm,

and criticism; and Rodrigo Lopez for always knowing how to call my bluff and make me face the truth.

Last, but certainly not least, I wish to thank my family for their amazing support. I want to thank my father Ahmad Koussa for his unwavering support of my curiosities, for being an amazing role model, and for being the best friend-of-a-lifetime anyone could ask for! I would like to thank my mother Rima Koussa for her unconditional love; for inspiring my love for educational reform; and for teaching me how to be in touch with my emotions, and how to truly love. I would like to thank my sister Reina Koussa for being the bestest little sister in the whole world! Additionally, I wish to thank my cousins Jalal Adada and Drs. Wassim and Ahmad Shatila for support and discussions. I want to thank my uncles Mohammad AbdulSater, Abu Omar, and Mehdi for being truly inspirational to me throughout my development. Finally I wish to thank my grandmother Fariha, and my aunts Halima Koussa and Maha Adada for their full support and encouragement.

Dedication

I dedicate this thesis to my sister Reina Koussa. She is my inspiration, my muse, and my biggest supporter. I cannot think of anyone in this world whose accomplishments I am more proud of, or whose genuine and candid nature I more wish to emulate. She is the light of my life, the fuel for my fire, and the wind beneath my wings.

Quotes:

The following quotes have greatly influenced my passion for science:

> The scientist does not study nature because it is useful to do so. He studies it because he takes pleasure in it, and he takes pleasure in it because it is beautiful. If nature were not beautiful it would not be worth knowing, and life would not be worth living.
>
> - Jules Henri Poincaré

> **Senator Pastore:** Is there anything connected in the hopes of this accelerator that in any way involves the security of the country?
>
> **Dr. Robert R. Wilson:** No, sir; I do not believe so.
>
> Senator Pastore. Nothing at all?
>
> **Dr. Wilson:** Nothing at all.
>
> **Senator Pastore:** It has no value in that respect?
>
> **Dr. Wilson:** It only has to do with the respect with which we regard one another, the dignity of men, our love of culture. It has to do with those things. It has nothing to do with the military. I am sorry.
>
> **Senator Pastore:** Don't be sorry for it.
>
> **Dr. Wilson:** I am not, but I cannot in honesty say it has any such application.
>
> **Senator Pastore:** Is there anything here that projects us in a position of being competitive with the Russians, with regard to this race?
>
> **Dr. Wilson:** Only from a long-range point of view, of a developing technology. Otherwise, it has to do with: Are we good painters, good sculptors, great poets? I mean all the things that we really venerate and honor in our country and are patriotic about. In that sense, this new knowledge has all to do with honor and country but it has nothing to do directly with defending our country except to help make it worth defending.

Chapter One: General Introduction

Mechanotransduction allows us to sense our world both directly through somatosensation, and at a distance through hearing. Hearing in humans is unique among the senses in that it allows simultaneous detection of stimuli from any direction. The auditory system is also central to our means of communicating with one another. The cochlea in the inner ear affords us the ability to listen to and appreciate music and the ability to detect threats from visually occluded regions of our environment. Our hearing works over a large dynamic range. This results in the ability to hear the sound of a pin drop in a quiet room, while also allowing us to hold and maintain a conversation with an individual in a noisy environment. Although much of this ability comes from higher order rejection of sound, the sensory epithelium of the cochlea is sensitive to motions of atomic dimensions and has built-in mechanisms for adapting to constant stimuli. The inner ear, specifically the saccule, utricle and semicircular canals, provides us with our sense of balance, which includes the senses of linear acceleration, head rotation, and of up and down.

Mechanotransduction also complements our other senses. We are primarily visual creatures but our vision is limited to having high acuity only at the fovea. This is not very noticeable in daily life as a result of compensatory mechanisms, some of which rely on mechanotransduction in the inner ear. For instance, the vestibular-ocular reflex (VOR) allows one to remain foveated on a target while the head moves. In order to do this, the semi-circular canals in the inner ear sense angular velocity of the head and converts it to electrical signals. In the brainstem these signals are integrated and relayed to the ocular muscles to counter roll the eyes, resulting in the eye remaining still while the head rotates. Similarly, although we usually

use vision to track a target, it is often an auditory signal which first alerts us to the presence of something that requires our visual attention.

In order to accomplish these feats, the ear must convert mechanical motions—from sound waves, movements of the head, or movements induced by gravity—into electrical signals. This sensory information is transmitted to the brainstem and ultimately to the cortex, the cerebellum, or the ocular muscles. Although the means by which these sensory stimuli are relayed to their sensory epithelium differ, the mechanism of transduction is highly conserved both across these sensory modalities and across different mechanosensitive organs in different species. This mechanotransduction is carried out by hair cells.

Hair cells in the inner ear convert mechanical stimuli in the vestibular and auditory systems into electrical signals which can be processed by the brain. Hair cells are highly polarized cells with a unique elaboration of modified microvilli at their apical surface known as stereocilia. These stereocilia are organized in a staircase formation and their bases are tapered, allowing them to pivot about their insertion into the cuticular plate at the apical surface of the hair cell (**Figure 1.1a**).

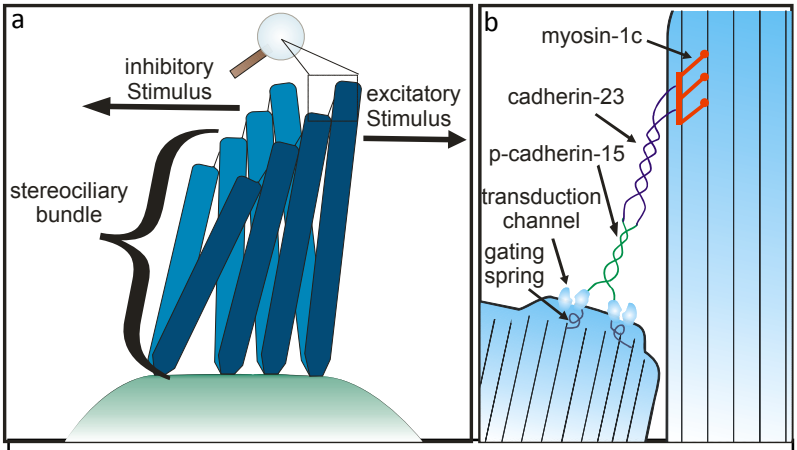

Figure 1.1| a) Schematic of the apical surface of a hair cell showing the staircase arrangement of stereocilia at rest (light blue) and experiencing an excitatory stimulus (dark blue). b) Magnification of the region indicated in a. Highlighting the putative organization of components of the mechanotransduction apparatus.

Sensory stimuli such as sound waves of a particular frequency result in oscillations of the stereociliary bundle at a location in the cochlea corresponding that frequency. Movements of the bundle result in changes in the open probability of ion channels at the tips of the stereocilia. This transduction is achieved by a complicated transduction apparatus which affords the system both high sensitivity, and the ability to adapt to maintained stimuli **(Figure 1.1b**).

Bundle motions thus produce an oscillating current across the membrane, which in turn produces an oscillating receptor potential at frequencies below ~4 kHz. Hearing extends up to ~20 kHz in humans. At these higher frequencies however the receptor potential is filtered by the cell capacitance, and the asymmetry of the positive and negative phases of the current produces a depolarization with a progressively smaller oscillatory component.

The remarkable sensitivity of the ear has intrigued scientists for centuries. As early as 1877 Lord Rayleigh set out to determine the sensitivity of the ear. He wrote

> The source of sound in my experiment was a whistle, mounted on a Wolf's bottle, in connexion with which was a siphon manometer for the purpose of measuring the pressure of wind. This apparatus was inflated from the lungs through an india-rubber tube, and with a little practice there was no difficulty in maintaining a sufficiently constant blast of the requisite duration…. The first point to be determined was the distance from the source to which the sound remained clearly audible. The experiment was tried in the middle of a fine still winter's day, and it was ascertained that the whistle was heard without effort at a distance of 820 metres.

Lord Rayleigh then calculated the vibration of air particles 820 m away from the source, arriving at the conclusion that the ear can detect motions as small as 10 nm, and stating that he was "inclined to think that on a still night a sound of this pitch, whose amplitude is only a hundred-millionth of a centimetre [0.1 nm], would still be audible." This estimate is remarkably close to the threshold of hearing measured with modern instruments.

In 1928 Georg von Békésy showed that, in response to sound stimuli, the basilar membrane carries a traveling wave. Békésy was able to see this traveling wave by monitoring cochleas under a microscope with stroboscopic illumination. At high frequencies Békésy observed that the base of the basilar membrane was more active than at the apex. This was the first evidence to support the notion that the basilar membrane acted as a mechanical filter stimulating different portions of sensory epithelia as a function of frequency. Soon thereafter, people began combining the Békésy's findings with Corti's anatomical description of the cochlea to develop theories of auditory transduction.

Huggins and Licklider postulated in 1951 that deformations of the bundles atop hair cells may underlie transduction of the mechanical motions from the traveling wave to the electrical signals measured as the cochlear microphonic. Békésy noticed in 1952 that the electrical energy

of the mammalian microphonic potential, an extracellular signal produces by sound, was greater than the sound energy required to produce this potential. He thus inferred that there must be some "pool (source) of electrical energy." To investigate this further Békésy recorded the potential difference between different regions within the cochlea with respect to an indifferent electrode in the vestibular canal (ground). Upon entering the endolymphatic space, Békésy was confronted with a potential ~100mV above ground. Today we refer to this as the endolymphatic potential, and know it to be crucial to the sensitivity of the mammalian cochlea.

Békésy was eventually awarded the Nobel prize in 1962 but his ideas were not immediately accepted. Many were skeptical of his work on the traveling wave as it was performed on "dead" cochleas. Others criticized the fact that the mechanical tuning of the basilar membrane was too broad to explain the sharp tuning curves measured from VIIIth nerve fibers. Eventually *in vivo* experiments were performed, measuring the traveling wave and mechanical tuning via the Mössbauer effect, capacitive vibration sensors, and laser Doppler-shift velocimetry (Rhode, 1984). They revealed that the mechanical tuning in live cochleas was far sharper and did match the tuning curves, showing that the tuning was fundamentally biomechanical in origin.

Békésy's skeptics even included himself. Békésy had proposed that transduction is a function of the amplitude of movement of the basilar membrane. Ernest Wever and Merle Lawrence were suggesting that it was membrane velocity—not displacement—which determined the amplitude of the cochlear microphonic. Békésy eventually agreed with Wever and Lawrence. It was not until Békésy performed a series of experiments measuring the response of the cochlear microphonic to a trapezoidal stimulus that it was decided that Békésy's

original conclusion was in fact correct (Huggins & Licklider, 1951; Wever, Lawrence & Békésy 1954; Békésy, 1962).

The next goal was to understand the function of the cells responsible for mechanotransduction. Engström et al. (1962) showed via light-, phase-contrast-, and electron-microscopy imaging studies, that the stereocilia of hair bundles are rigid and move like levers as the bundle is deflected. Engström et al. proposed that the levering action might relay the motion to the cuticular plate where transduction would be conducted by the basal body. In 1977 David Corey and Jim Hudspeth showed definitively that hair cells have a sound-activated conductance that produces a robust receptor potential. In 1979 Hudspeth and Jacobs showed that mechanotransduction was carried out by stereocilia and did not require the kinocilium, and in 1982 Hudspeth showed that the transduction occurs at the tips of stereocilia and not at the cuticular plate.

After confirmation that hair cells were the mechanotransducers of the inner ear and characterization of their sensitivity, polarity, and conductance changes in response to mechanical stimuli (Hudspeth & Corey 1977), the search for the "mechanical transformer of molecular dimensions" began. Two years later the response latency of frog saccular hair cells was measured to be ~13μs at 37^{o} C (Corey & Hudspeth, 1979). The response latency and its temperature dependence (Q_{10} = 2.5) suggested that the mechanotransduction resulted from a direct mechanical gating of an ion channel. After putting forth the notion of a mechanosensitive channel David Corey and Jim Hudspeth presented the notion of some elastic element whose stretch conveys tension to these mechanotransduction channels (Corey & Hudspeth, 1983; Hudspeth, 1983). It was not until 1984, however, that Pickles et al., using electron microscopy,

discovered both tip links and horizontal top connectors. The horizontal crosslinks are thought to allow the bundle to move coherently during stimulation, resulting in shearing rather than splaying of the bundle. This shearing motion causes the stereocilia to slide along one another, thus tensing the tip link and applying force to the mechanotransduction channels.

In 1975 Sand, and later in 1979 Corey and Hudspeth noted that hair cell mechano-transduction required Ca^{2+}. Sand suggested that the transduction channel was Ca^{2+} selective, but Corey and Hudspeth showed that Ca^{2+} was only a necessary cofactor. It was later shown, however, that calcium plays a role in maintaining tip-link stability (Assad et al., 1991). Assad showed, using scanning and transmission electron microscopy, that addition of a calcium chelator resulted in a loss of tip links. It was not until 2007 that the proteins that make up the tip links were identified as protocadherin-15 (PCDH15) and cadherin-23 (CDH23) (Kazmierczak et al., 2007). Five years later crystallography and molecular dynamics simulations have revealed mechanisms by which calcium stabilizes the interaction of PCDH15 and CDH23 (Sotomayor et al., 2012). Sotomayor et al. found that these atypical cadherins interact by forming an anti-parallel dimer (**Figure 1.2a and c**). Ca^{2+} was shown to stabilize the regions between EC domains of each protein thus making the protein more rigid and indirectly stabilizing the interaction between the two proteins, providing new mechanistic insights into the role of Ca^{2+} in tip link stability.

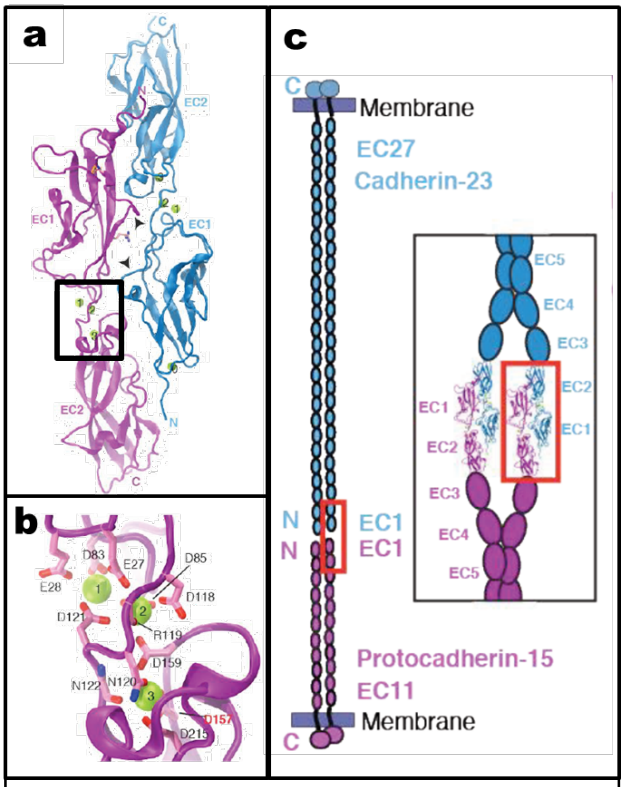

Figure 1.2| Crystal structure of PCDH15 and CDH23 interaction. a) Ribbon diagram based on crystal structure of the last two extracellular domains (EC 1 and 2) of PCDH15 and CDH23 interacting . b) Magnified view of boxed region in a green spheres represent Ca^{2+} ions. c) Schematic of postulated arrangement of tip-link proteins. (inset shows ribbon structure from a). (Adapted from Sotomayor et al. 2012)

Hair cells have developed an amazingly elegant system for adapting to maintained stimuli. On the upper end of the tip link a motor controls the resting tension on the tip link, positioning the cell in its maximally sensitive range and allowing it to adapt to maintained stimuli. Myosin-1c motors are thought to regulate adaptation (Eatock et al., 1987; Howard & Hudspeth, 1987; Holt et al., 2002; Staufer et al., 2002; Gillespie and Cyr, 2004). (**Figure 1.1b**). The thought is that the myosin-1c motor is constantly trying to climb up the actin core of the stereocilia. This results in a constant resting tension on the tip links which yields a resting

channel open probability of ~20%. In response to a maintained stimulus, however, the motor can slip causing the tip link to slacken, thus reducing the channel's open probability. At the termination of a stimulus that produced adaptation, the motor will climb until the resting tension is restored.

The adaptation motor complex has been studied extensively and several models have been designed to explain its effects on bundle compliance and mechanotransduction (Howard & Hudspeth, 1987; Assad & Corey, 1992). Ca^{2+} has been shown to interact with myosin-1c through calmodulin to regulate adaptation (Cyr et al., 2002). It is thought that Ca^{2+}, entering through transduction channels, would interact with myosin-1c and reduce its climbing. This allows the resting tension to be modulated by the open probability of the channel in addition to the stall tension of the myosins. This is more robust as it corrects for any deviation in mechanical coupling between the motor, tip link, and channel.

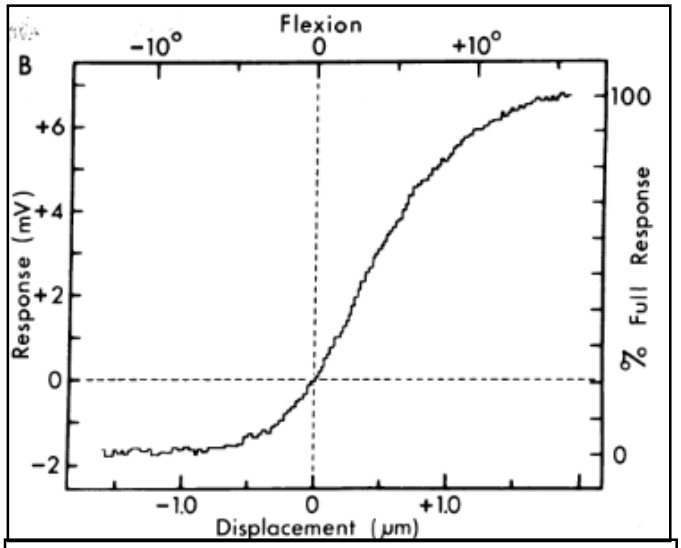

Figure 1.3| Reproduced from Hudspeth and Corey 1977. Shows receptor potential of bullfrog sacculus hair cells in response to displacements of the stimulus probe.

Perhaps the most well studied aspect of mechanotransduction, however, is the electrical response to mechanical stimuli (Hudspeth & Corey, 1977; Hudspeth & Jacobs, 1979; Corey & Hudspeth, 1979a,b;1980; 1983a,b; Hudspeth, 1982;1983; Shotwell et al., 1982; Crawford et al., 1991; Cheung & Corey, 2003; Beurg, 2006). These studies have demonstrated that mechanotransduction occurs only along the axis of mirror symmetry (deflections towards the tallest stereocilium), and that the hair cells have a non-linear current-displacement curve (**Figure 1.3**). The curve's midpoint is set to make excitatory responses more prominent than inhibitory responses. The plateauing at either extreme is a result of the channels being either all closed or all open.

Arguably the most crucial part of the transduction apparatus is the mechanotransduction channel itself. Although the identity of the channel is not definitively known, a very strong candidate has recently emerged (Kawashima et al. 2011). Even without knowing the molecular identity of the channel much work has centered around characterizing it (Corey & Hudspeth, 1979a & b; Hudspeth, 1983; Holton & Hudspeth, 1986; Hudspeth & Holton, 1986; Crawford et al., 1991; Lumpkin et al., 1997). These studies indicate that the pore appears to be rather similar to acetylcholine receptor channels. They are nonselective cation channels with a reversal potential around 0 mV. They are nearly equally permeable to Li^+, Na^+, K^+, Rb^+, and Cs^+. The pore is also permeable to some charged molecules such as tetra-methyl ammonium and is in fact roughly 30% more permeable to NH_4^+ than to K^+. The first successful attempt to record from a single transduction channel was done by Crawford et al. in 1991 where they titrated BAPTA to sever tip links until only one remained. They thus measured the single-channel conductance to be ~100 pS in turtle hair cells.

The ultimate goal in understanding the mechanosensitivity of this channel is to determine the effect of force on the gating of the channel. As probing the channel directly has not been possible, the approach thus far has been to understand the geometry, motion, and dynamics of the bundle to infer the forces experienced by the channel as a result of bundle movements (Hudspeth, 1983; Crawford and Fettiplace, 1985; Howard and Hudspeth 1987; 1988; Hacohen et al., 1989; Denk et al., 1989; Benser et al., 1993; Jarmillo and Hudspeth, 1993). Many of these studies were performed using flexible fibers to allow measurements of forces produced by the bundle. Although these measurements do not directly probe forces experienced by the channel, much has been inferred about the channel's properties from bundle mechanics. For example the gate swing, or conformational change of the channel upon transitioning from the closed to open state, has been estimated to be ~4 nm (Howard & Hudspeth, 1988).

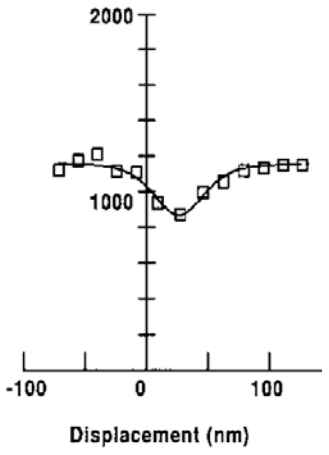

Figure 1.4. Bundle stiffness as a function of displacement. (Howard and Hudspeth 1988)

One of the most interesting features of hair bundle mechanics is the compliance of the transduction apparatus. The biophysical properties of components of the transduction apparatus have been studied by stimulating the bundle and monitoring both electrical activity of the cell and movements of the bundle. Although these experiments have yielded much information about the system (Hudspeth, 1983; Sukharev & Corey 2004), much has to be inferred due to the indirect means of stimulation. For instance, hair bundles have a stiffness of about 1 mN/m, measured at the tip (**Figure 1.4**), which is thought to represent the parallel stiffnesses of the stereocilia pivoting and the hypothetical elastic element (the gating spring) that stretches when tip-link tension is increased. Over the 100-nm range of displacements that open mechanotransduction channels, hair bundles display a decreased stiffness (Howard & Hudspeth 1988) (**Figure 1.4**). This compliance is thought to reflect the release of tension when channels open. With certain assumptions, the stiffness of pivots and gating springs can be separated, but the measurements still reflect the average behavior of a hundred or more channels; good numbers have yet to be successfully attributed to a specific component of the transduction apparatus.

More recently a novel approach was used to probe the bundle. Instead of a flexible glass probe, a glass bead held in an optical trap was used to deflect bullfrog saccular hair bundles, and to monitor the forces produced by the bundle (Cheung & Corey, 2006). The optical trap both produced and measured small and fast bundle motions. Although these studies eliminate the issues associated with measuring many channels at once, much information is lost about the forces experienced by, and gating kinetics of the channel itself. As Jim Hudspeth pointed out in 1984:

> …if the stimulating spring has a vanishingly small stiffness, the transduction element is subjected to a pure force. Even if a hair bundle is stimulated via a very flexible fiber, however, viscosity and steric constraints within the bundle may prevent all the transduction elements from experiencing pure forces. Because the fluid surrounding the hair bundle provides a viscous damping of about 200 nN·s /m, bundle motion is damped with a time constant of about 200 μs.

Scientists have been fascinated by the sensitivity of the ear to microscopic movements since at least the mid 1800's (Rayleigh 1877). Throughout the years, many have studied mechanisms of hearing in many forms, including the mechanics of the middle ear, movements of the basilar membrane, and mechanotransduction by hair cells. Georg von Békésy brilliantly devised experiments to measure the motion of the basilar membrane, but was frustrated by the technology of his time in going beyond that to a molecular description:

> We now return to the problem of the high sensitivity of the ear. From a purely physical point of view, it is startling that a displacement whose magnitude is the diameter of an atom can produce enough voltage to trigger a nerve ending. I have no solution for this problem. But since we have seen how, step by step, the anatomical structures in the ear localize the vibration forces in smaller and smaller compartments, it does not seem impossible that the final mechanical transformer is of molecular dimensions. (von Békésy 1962)

Attempts to identify molecular elements of the transduction apparatus have included biochemical assays which have identified the adaptation motor as myosin-1c (Eatock et al. 1987, Holt et al. 2002, Staufer et al. 2002, Gillespie and Cyr 2004), and imaging studies which have successfully broadened our understanding of the development and regeneration of tip links (Kazmierczak et al. 2007, Lelli et al. 2010). Most recently crystallography and molecular dynamics studies have bettered our understanding of the structure of tip links (Sotomayor et al. 2012). Still lacking, however, are the identity of the mechanotransduction channel, the elastic elements that mechanically gate the channel, and molecular mechanics experiments on the

compliance and rupture force of tip links at a physiologically relevant range of solution and mechanical conditions. A greater understanding of these properties will shape the way we understand mechanotransduction in the ear and elsewhere. These experiments may also lead to the discovery of therapeutics for patients with deafness mutations.

Here, we have focused especially on the tip links of the transduction apparatus, which convey tension to the mechanotransduction channel. Tip links, however, present an interesting developmental challenge. As there are no vesicles in stereocilia, all membrane proteins must be synthesized in the cell body. Thus if the tip link were a single protein, two myosin motors would have to work in synchrony in two stereocilia to move the tip link up the stereocilia while the tip link spanned the extracellular space between them. The space, up to a micrometer in some hair cells, is longer than most extracellular proteins. To solve this problem, tip links are made up of two proteins. Each half can be trafficked up the stereocilia separately and subsequently assembled. This lack of a covalent linkage, however, means that there is a potential for the tip links to break. Exposure to loud sounds can rupture tip links resulting in a temporary threshold shift lasting many hours while tip links recover (Husbands et al., 1999). It has also been shown that tip-link integrity is highly dependent on Ca^{2+} (Assad et al., 1991). Rupture of tip links by calcium chelation has been used as a model of noise-induced tip link damage. More recently, the regeneration of tip links after damage has been studied (Lelli et al., 2010), and Sotomayor et al. (2012) elucidated the interaction interface between PCDH15 and CDH23 and the role of Ca^{2+} in bond stability. Specifically, simulations carried out without Ca^{2+} predict that Ca^{2+} does not affect the interface but rather reduces flexure of the proteins (Sotomayor et al., 2012). The disruption of the interaction interface by either of two deafness

mutations explained how these mutations could result in deafness. Crystallography and molecular dynamics simulation have provided a very good understanding of the tip link structure. However, an understanding of how real PCDH15 and CDH23 fragments interact in physiologically relevant ionic and mechanical conditions is lacking.

In this thesis I discuss the development of novel tools for single-molecule-biophysics techniques, and their use to measure the rupture force of a tip link under various conditions. This single molecule approach is the only way to directly probe the rupture force and its dependence on solution conditions and mechanical stresses. This set of experiments has reshaped our understanding of the molecular mechanism of hair-cell mechanotransduction.

References

1. Ahmed, Z.; Goodyear, R.; Riazuddin, S.; Lagziel, A.; Legan, P.; Behra, M.; Burgess, S.; Lilley, K.; Wilcox, E.; Riazuddin, S.; Griffith, A.; Frolenkov, G.; Belyantseva, I.; Richardson, G. & Friedman, T. (2006), 'The tip-link antigen, a protein associated with the transduction complex of sensory hair cells, is protocadherin-15.', The Journal of neuroscience : the official journal of the Society for Neuroscience 26(26), 7022--7034.

2. Assad, J. & Corey, D. (1992), 'An active motor model for adaptation by vertebrate hair cells.', *The Journal of neuroscience : the official journal of the Society for Neuroscience* **12**(9), 3291--3309.

3. Assad, J.; Shepherd, G. & Corey, D. (1991), 'Tip-link integrity and mechanical transduction in vertebrate hair cells.', *Neuron* **7**(6), 985--994.

4. Benser, M.; Issa, N. & Hudspeth, A. (1993), 'Hair-bundle stiffness dominates the elastic reactance to otolithic-membrane shear.', *Hearing research* **68**(2), 243--252.

5. Beurg, M.; Evans, M.; Hackney, C. & Fettiplace, R. (2006), 'A large-conductance calcium-selective mechanotransducer channel in mammalian cochlear hair cells.', *The Journal of neuroscience : the official journal of the Society for Neuroscience* **26**(43), 10992--11000.

6. Cheung, E. & Corey, D. (2006), 'Ca2+ changes the force sensitivity of the hair-cell transduction channel.', *Biophysical journal* **90**(1), 124--139.

7. Cheung, E. & Corey, D. (2003), 'A gradient of single-channel conductance in the cochlea:

tuning the cochlea's strings?', *Neuron* **40**(5), 875--876.

8. Corey, D. & Hudspeth, A. (1983), 'Kinetics of the receptor current in bullfrog saccular hair cells.', *The Journal of neuroscience : the official journal of the Society for Neuroscience* **3**(5), 962--976.

9. Corey, D. & Hudspeth, A. (1983), 'Analysis of the microphonic potential of the bullfrog's sacculus.', *The Journal of neuroscience : the official journal of the Society for Neuroscience* **3**(5), 942--961.

10. Corey, D. & Hudspeth, A. (1980), 'Mechanical stimulation and micromanipulation with piezoelectric bimorph elements.', *Journal of neuroscience methods* **3**(2), 183--202.

11. Corey, D. & Hudspeth, A. (1979), 'Ionic basis of the receptor potential in a vertebrate hair cell.', *Nature* **281**(5733), 675--677.

12. Corey, D. & Hudspeth, A. (1979), 'Response latency of vertebrate hair cells.', *Biophysical journal* **26**(3), 499--506.

13. Crawford, A.; Evans, M. & Fettiplace, R. (1991), 'The actions of calcium on the mechano-electrical transducer current of turtle hair cells.', *The Journal of physiology* **434**, 369--398.

14. Crawford, A. & Fettiplace, R. (1985), 'The mechanical properties of ciliary bundles of turtle cochlear hair cells.', *The Journal of physiology* **364**, 359--379.

15. Cyr, J.; Dumont, R. & Gillespie, P. (2002), 'Myosin-1c interacts with hair-cell receptors through its calmodulin-binding IQ domains.', *The Journal of neuroscience : the official journal of the Society for Neuroscience* **22**(7), 2487--2495.

16. Denk, W.; Webb, W. & Hudspeth, A. (1989), 'Mechanical properties of sensory hair bundles are reflected in their Brownian motion measured with a laser differential interferometer.', *Proceedings of the National Academy of Sciences of the United States of America* **86**(14), 5371--5375.

17. Eatock, R.; Corey, D. & Hudspeth, A. (1987), 'Adaptation of mechanoelectrical transduction in hair cells of the bullfrog's sacculus.', *The Journal of neuroscience : the official journal of the Society for Neuroscience* **7**(9), 2821--2836.

18. EngstrÃ¶m, H.; Ades, H. & Hawkins, J. (1962), 'Structure and functions of the sensory hairs of the inner ear', *The Journal of the Acoustical Society of America* **34**(9B), 1356--1363.

19. Gillespie, P. & Cyr, J. (2004), 'Myosin-1c, the hair cell's adaptation motor.', *Annual review of physiology* **66**, 521--545.

20. Grati, M. & Kachar, B. (2011), 'Myosin VIIa and sans localization at stereocilia upper tip-link density implicates these Usher syndrome proteins in mechanotransduction.', *Proceedings of the National Academy of Sciences of the United States of America* **108**(28), 11476--11481.

21. Hacohen, N.; Assad, J.; Smith, W. & Corey, D. (1989), 'Regulation of tension on hair-cell transduction channels: displacement and calcium dependence.', *The Journal of neuroscience : the official journal of the Society for Neuroscience* **9**(11), 3988--3997.

22. Halvorsen, K.; Schaak, D. & Wong, W. (2011), 'Nanoengineering a single-molecule mechanical switch using DNA self-assembly.', *Nanotechnology* **22**(49), 494005--.

23. Halvorsen, K. & Wong, W. (2010), 'Massively parallel single-molecule manipulation using centrifugal force.', *Biophysical journal* **98**(11), --5.

24. Holt, J.; Gillespie, S.; Provance, D.; Shah, K.; Shokat, K.; Corey, D.; Mercer, J. & Gillespie, P. (2002), 'A chemical-genetic strategy implicates myosin-1c in adaptation by hair cells.', *Cell* **108**(3), 371--381.

25. Holton, T. & Hudspeth, A. (1986), 'The transduction channel of hair cells from the bull-frog characterized by noise analysis.', *The Journal of physiology* **375**, 195--227.

26. Howard, J. & Hudspeth, A. (1988), 'Compliance of the hair bundle associated with gating of mechanoelectrical transduction channels in the bullfrog's saccular hair cell.', *Neuron* **1**(3), 189--199.

27. Howard, J. & Hudspeth, A. (1987), 'Mechanical relaxation of the hair bundle mediates adaptation in mechanoelectrical transduction by the bullfrog's saccular hair cell.', *Proceedings of the National Academy of Sciences of the United States of America* **84**(9), 3064--3068.

28. Hudspeth, A. (1983), 'Mechanoelectrical transduction by hair cells in the acousticolateralis sensory system.', *Annual review of neuroscience* **6**, 187--215.

29. Hudspeth, A. (1982), 'Extracellular current flow and the site of transduction by vertebrate hair cells.', *The Journal of neuroscience : the official journal of the Society for Neuroscience* **2**(1), 1--10.

30. Hudspeth, A. & Corey, D. (1977), 'Sensitivity, polarity, and conductance change in the response of vertebrate hair cells to controlled mechanical stimuli.', *Proceedings of the National Academy of Sciences of the United States of America* **74**(6), 2407--2411.

31. Hudspeth, A. & Holton, T. (1986), 'Ensemble-variance analysis of transduction in saccular hair cells', *Hearing Research* **22**(1-3), 30--30.

32. Hudspeth, A. & Jacobs, R. (1979), 'Stereocilia mediate transduction in vertebrate hair cells (auditory system/cilium/vestibular system).', *Proceedings of the National Academy of Sciences of the United States of America* **76**(3), 1506--1509.

33. Huggins, W. & Licklider, J. (1951), 'Place mechanisms of auditory frequency analysis', *The Journal of the Acoustical Society of America* **23**(3), 290--299.

34. Husbands, J.; Steinberg, S.; Kurian, R. & Saunders, J. (1999), 'Tip-link integrity on chick tall hair cell stereocilia following intense sound exposure.', *Hearing research* **135**(1-2), 135--145.

35. Indzhykulian, A.A. et al. Poster, Midwinter Meeting of the Association for Research in Otolaryngology. (2011)

36. Jaramillo, F. & Hudspeth, A. (1993), 'Displacement-clamp measurement of the forces exerted by gating springs in the hair bundle.', *Proceedings of the National Academy of Sciences of the United States of America* **90**(4), 1330--1334.

37. Kawashima, Y.; GÃ©lÃ©oc, G.; Kurima, K.; Labay, V.; Lelli, A.; Asai, Y.; Makishima, T.; Wu, D.; Della Santina, C.; Holt, J. & Griffith, A. (2011), 'Mechanotransduction in mouse inner ear hair cells requires transmembrane channel-like genes.', *The Journal of clinical investigation* **121**(12), 4796--4809.

38. Kazmierczak, P.; Sakaguchi, H.; Tokita, J.; Wilson-Kubalek, E.; Milligan, R.; MÃ¼ller, U. & Kachar, B. (2007), 'Cadherin 23 and protocadherin 15 interact to form tip-link filaments in sensory hair cells.', *Nature* **449**(7158), 87--91.

39. Kuo, S. (2001), 'Using optics to measure biological forces and mechanics.', *Traffic (Copenhagen, Denmark)* **2**(11), 757--763.

40. Lelli, A.; Kazmierczak, P.; Kawashima, Y.; MÃ¼ller, U. & Holt, J. (2010), 'Development and regeneration of sensory transduction in auditory hair cells requires functional interaction between cadherin-23 and protocadherin-15.', *The Journal of neuroscience : the official journal of the Society for Neuroscience* **30**(34), 11259--11269.

41. Lumpkin, E.; Marquis, R. & Hudspeth, A. (1997), 'The selectivity of the hair cell's mechanoelectrical-transduction channel promotes Ca2+ flux at low Ca2+ concentrations.', *Proceedings of the National Academy of Sciences of the United States of America* **94**(20), 10997--11002.

42. Pickles, J.; Comis, S. & Osborne, M. (1984), 'Cross-links between stereocilia in the guinea pig organ of Corti, and their possible relation to sensory transduction.', *Hearing research* **15**(2), 103--112.

43. Powers, R.; Roy, S.; Atilgan, E.; Brownell, W.; Sun, S.; Gillespie, P. & Spector, A. (2012), 'Stereocilia membrane deformation: implications for the gating spring and mechanotransduction channel.', *Biophysical journal* **102**(2), 201--210.

44. Rayleigh, L. (1877), 'On the Amplitude of Sound-Waves', *Proceedings of the Royal Society of London* **26**, --.

45. Rhode, W. (1984), 'Cochlear mechanics.', *Annual review of physiology* **46**, 231--246.

46. Rhode, W. & Geisler, C. (1967), 'Model of the displacement between opposing points on the tectorial membrane and reticular lamina.', *The Journal of the Acoustical Society of America* **42**(1), 185--190.

47. Sotomayor, M.; Corey, D. & Schulten, K. (2005), 'In search of the hair-cell gating spring elastic properties of ankyrin and cadherin repeats.', *Structure (London, England : 1993)* **13**(4), 669--682.

48. Sotomayor, M.; Weihofen, W.; Gaudet, R. & Corey, D. (2010), 'Structural determinants of cadherin-23 function in hearing and deafness.', *Neuron* **66**(1), 85--100.

49. Sotomayor, M.; Weihofen, W.; Gaudet, R. & Corey, D. (2012) Structure of a force-conveying cadherin bond essential for inner-ear mechanotransduction.' Nature

50. Stauffer, E.; Scarborough, J.; Hirono, M.; Miller, E.; Shah, K.; Mercer, J.; Holt, J. & Gillespie, P. (2005), 'Fast adaptation in vestibular hair cells requires myosin-1c activity.', *Neuron* **47**(4), 541--553.

51. Sukharev, S. & Corey, D. (2004), 'Mechanosensitive channels: multiplicity of families and gating paradigms.', *Science's STKE : signal transduction knowledge environment* **2004**(219), --.

52. VON BEKESY, G. (1952), 'Resting potentials inside the cochlear partition of the guinea pig.', *Nature* **169**(4293), 241--242.

53. Wever, E.; Lawrence, M. & Von Békéy, G. (1954), 'A NOTE ON RECENT DEVELOPMENTS IN AUDITORY THEORY.', *Proceedings of the National Academy of Sciences of the United States of America* **40**(6), 508--512.

54. Wong, Wesley P. Exploring Single-molecule Interactions through 3D Optical Trapping

and Tracking: From Thermal Noise to Protein Refolding. Thesis. Harvard University, 2006. Print

Chapter Two

DNA Nanoswitches: A quantitative platform for gel-based biomolecular interaction analysis

Mounir A Koussa[1,6], Ken Halvorsen[2,3,6], Andrew Ward[3], Wesley P Wong[3,4,5]

[1]Program in Neuroscience, Department of Neurobiology, Harvard Medical School, Boston, MA, United States. [2] The RNA Institute, University at Albany, Albany, NY, United States [3]Program in Cellular and Molecular Medicine, Boston Children's Hospital, Boston, MA, United States. [4]Department of Biological Chemistry and Molecular Pharmacology, Harvard Medical School, Boston, MA, United States. [5]Wyss Institute for Biologically Inspired Engineering, Harvard University, Boston, MA, United States. [6]These authors contributed equally to this work.

Correspondence should be addressed to K.H. (khalvorsen@albany.edu) and W.P.W (Wesley.wong@childrens.harvard.edu).

Nature Methods. 2015 Feb; 12(2):123-6

Contributions: KH and MAK worked closely on the development of the assay, and the majority of the Biotin-Streptavidin on-rate and off-rate experiments. MAK developed the majority of the non Biotin-Streptavidin Experiments, and MAK and AW worked very closely on the development of the multistate assay. MAK performed the majority of the control experiments to validate the results. All authors contributed to data analysis.

Abstract:

We introduce a nanoscale experimental platform that enables kinetic and equilibrium measurements of a wide range of molecular interactions using a gel electrophoresis readout. Programmable, self-assembled DNA nanoswitches serve both as templates for positioning molecules, and as sensitive, quantitative reporters of molecular association and dissociation. We demonstrate this low cost, versatile, "lab-on-a-molecule" system by characterizing 10 different interactions, including a complex 4-body interaction with 5 discernable states.

Gel electrophoresis has been a workhorse of biological research for over 50 years, providing a simple way to determine size, topology, and quantity of DNA, RNA, and protein[1,2,3]. However, quantitative kinetic and thermodynamic characterization of molecular interactions on gels remains a challenge. For example, electrophoretic mobility shift assays (EMSA) are primarily used for qualitative analysis of protein-nucleic acid interactions[4]. Quantitative biomolecular interaction analysis typically requires specialized techniques such as Surface Plasmon Resonance (SPR) (e.g. Biacore), radiolabeling, or Isothermal Titration Calorimetry (ITC), with cost, required technical expertise, and material requirements sometimes posing barriers to their use (**Table 2.1**). Furthermore, quantitative analysis of long-lived interactions, small molecule interactions, and multi-component complexes are difficult, even with these advanced approaches.

Technique	Equipment Cost[a]	Sample Cost[b]	Protein Usage[c]	Surface Free[c]
DNA Nanoswitches	**low**	**low**	**< 1ng**	**yes**
Surface Plasmon Resonance (SPR)	medium/high	medium	<10 µg	no
Nuclear Magnetic Resonance (NMR)	high	low	15-5000 µg	yes
Scintillation Proximity Assay (SPA)	medium	high	0.1-10 µg	yes
Fluorescence	medium/high	low/medium	1 µg	yes
Bio-Layer Interferometry (BLI)	medium	medium	< 1ng	no
Quartz crystal microbalance (QCM)	medium	low	< 1ng	no
Isothermal calorimetry (ITC)	high	low	0.1-0.4 mg	yes

[a] low: <$5k, medium: $5-$50k, high: >$50k
[b] low: <$0.1, medium: $0.1-$1, high: >$1
[c] Most values taken from Table 1.1 in A. Dejaegere, et. al.

Table 2.1| Comparison of biomolecular interaction analysis techniques

We introduce an instrument-free platform, based on DNA self-assembly[5,6,7], that meets these challenges by enabling quantitative analysis of molecular interactions using standard gel electrophoresis, for pennies per sample (**Table 2.1**). DNA oligonucleotides (60 nt) are functionalized with interacting molecules, and hybridized to specific locations on a single-stranded DNA scaffold (M13mp18, 7,249 nt) to form DNA nanoswitches. These nanoswitches report molecular associations and dissociations through induced topological changes. By exploiting the ability to separate DNA based on topology[8], the different interaction states can be easily resolved as distinct bands on a gel (**Figure 2.1a**).

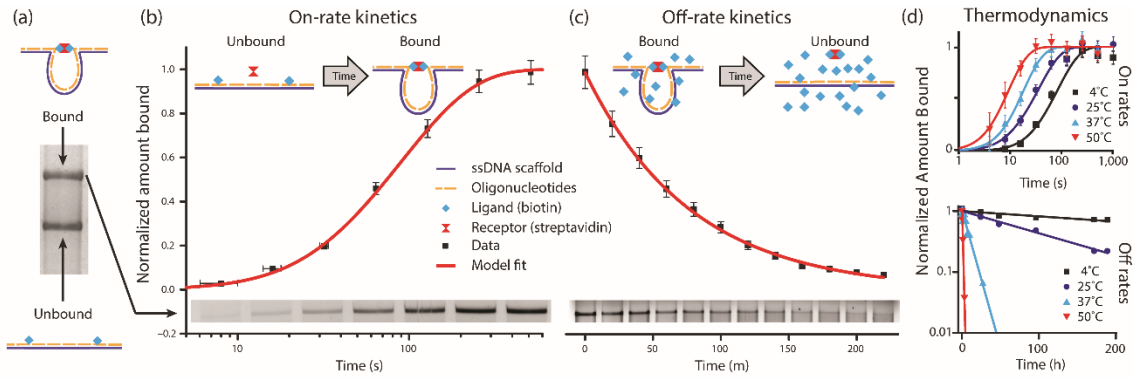

Figure 2.1| Kinetic measurements using DNA nanoswitches. a) The two (bound and unbound) states of the DNA nanoswitches can be distinguished by gel electrophoresis. b) With two biotins integrated into the nanoswitch, loop formation begins when unlabeled streptavidin is introduced, and progresses over time as evidenced by increasing intensity in the bound (looped) band across different lanes of a gel (bottom). The growth curve is fit with a kinetic model to determine the on rate. c) Addition of excess biotin blocks loop formation, making bond rupture irreversible, which leads to the exponential decay of nanoswitches from the bound state into the unbound state, as shown by the decreasing contrast in the unbound band across different lanes of a gel (bottom). d) Temperature dependence of on rates and off rates for the biotin-streptavidin interaction at 150mM NaCl. Horizontal error bars represent uncertainty in mixing time ($\pm$ 2 seconds), and vertical error bars indicate $\pm$ 7% uncertainty in the intensity (this is the one-sigma confidence interval determined from 48 repeated measurements of the same construct–see Data Analysis section of methods for more detail).

These nanoswitches have several useful features. Their programmable nature enables precise control over relative concentrations and stoichiometries on a per molecule basis. The large DNA construct causes interaction-triggered topological changes to yield distinct and

repeatable gel shifts, even with the integration of large proteins[5]. Additionally, the large size of the DNA allows for the incorporation of thousands of dye molecules, dramatically amplifying the signal per interaction, and making readout of the nanoswitches orders of magnitude more sensitive than most other techniques (**Table 2.1**). Together, these features make DNA nanoswitches a versatile, accessible, and inexpensive tool for studying multimolecular interactions.

By monitoring changes in the nanoswitch states over time, we can determine equilibrium and kinetic rate-constants for a variety of molecular systems using standard gel electrophoresis. Loop closure over time is used to determine association rate-constants, while loop opening over time, in the presence of a competitor, is used to determine the dissociation rate-constant (**Figure 2.1b, 2.1c, and Figure 2.2**). These kinetic processes take place in solution and are "quenched" to halt kinetics at various time points, with the gel acting as a post-experiment readout, enabling experimental conditions that are independent of gel running conditions. Ease of readout and other nanoswitch characteristics can be optimized by tuning key design parameters, including oligonucleotide length, ligand positioning, reaction concentrations, and temperatures (methods).

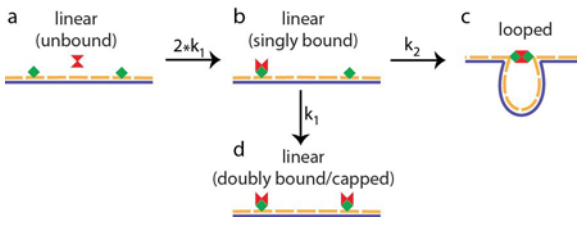

Figure 2.2 (Continued)| Graphical representations of kinetic model. The linear unbound construct (a) has two free ligands (green). The two free ligands result in the receptor (red) binding with twice its solution on-rate ($2*k_1$) to form the singly bound state (b). This now singly bound construct can either form a loop (c) by the same receptor binding to the second ligand at some loop closure rate (k_2), or a second receptor can bind to the scaffold at the receptor solution-on-rate (k_1) resulting an a doubly bound, or capped state (d).

We first assessed the nanoswitch platform using the ubiquitous biotin-streptavidin system. At physiological salt conditions and 25˚C, we measured a dissociation time of 9.7 ± 0.4 days (all values are reported as the error-weighted fit parameter ± its one-sigma confidence interval), closely matching previously reported values[9]. To demonstrate parallel exploration of a broad range of experimental conditions, we measured off-rates at 16 different conditions, by measuring the fraction dissociated at 6 time points per condition, and running all 96 samples on a single gel (**Figure 2.3**). Each condition showed exponential decay over time, yielding 16 uniquely determined off-rates ranging from 0.8 hours to 3 months with an uncertainty typically less than 10% (**Figure 2.3**). Dissociation kinetics varied nearly 1,000 fold over our temperature range (4-50 ˚C) but only about 2 fold over our salt range (25-500 mM) (**Figure 2.1d and Figure 2.4**). Based on these results, we present a semi-empirical model for dissociation kinetics between streptavidin and biotin-labeled oligonucleotides from 25 ˚C to 50 ˚C and 25 mM to 500 mM NaCl:

$$k_{\text{off}} \approx T e^{\left(42.4 - \frac{18300}{T} - 0.033\sqrt{I}\right)}$$

Where k_{off} is the value of the off-rate in s^{-1}, T is the value of the absolute temperature in K, and I is the value of the ionic strength of the solution in mM (**methods and Figure 2.4d**). This model does not describe the behavior at 4 ˚C, presumably due to temperature dependent changes in heat capacity[10].

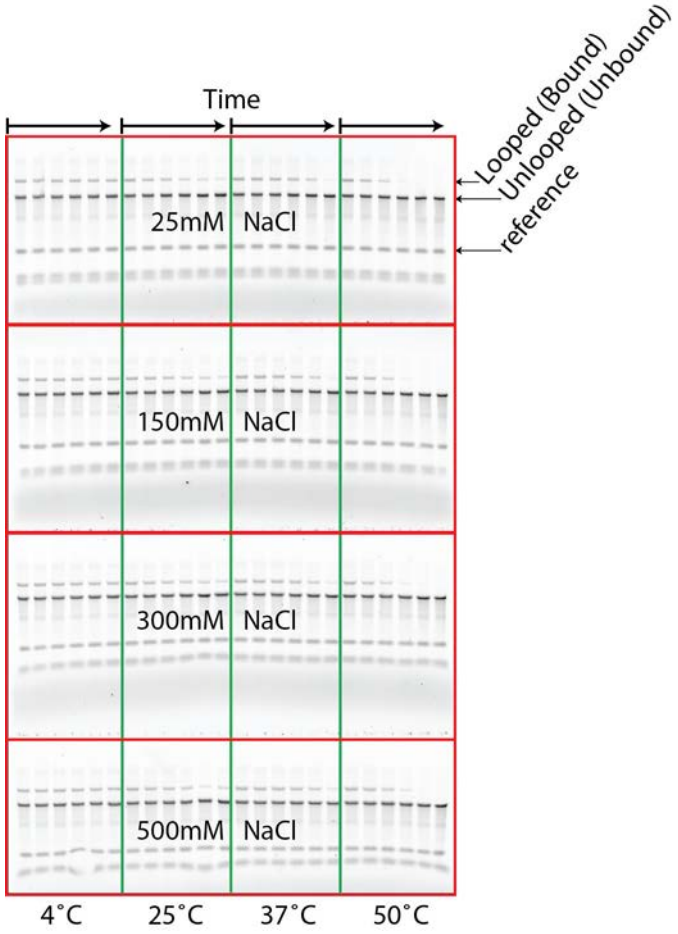

Figure 2.3| Parallel measurements: biotin-streptavidin exploring a broad range of experimental conditions. A highly parallel biotin-streptavidin off-rate measurement where an array of 16 different experimental conditions with 6 time points each were tested on a single 96-

lane gel. Each of the 4 combs corresponds to a different salt condition, and within each comb experiments were conducted at 4 different temperatures. The band below the linear band is thought to be the result of enzyme promiscuity during the linearization process, and all lower bands result from the addition of a ladder used as a reference band to help alleviate the effects of pipetting error.

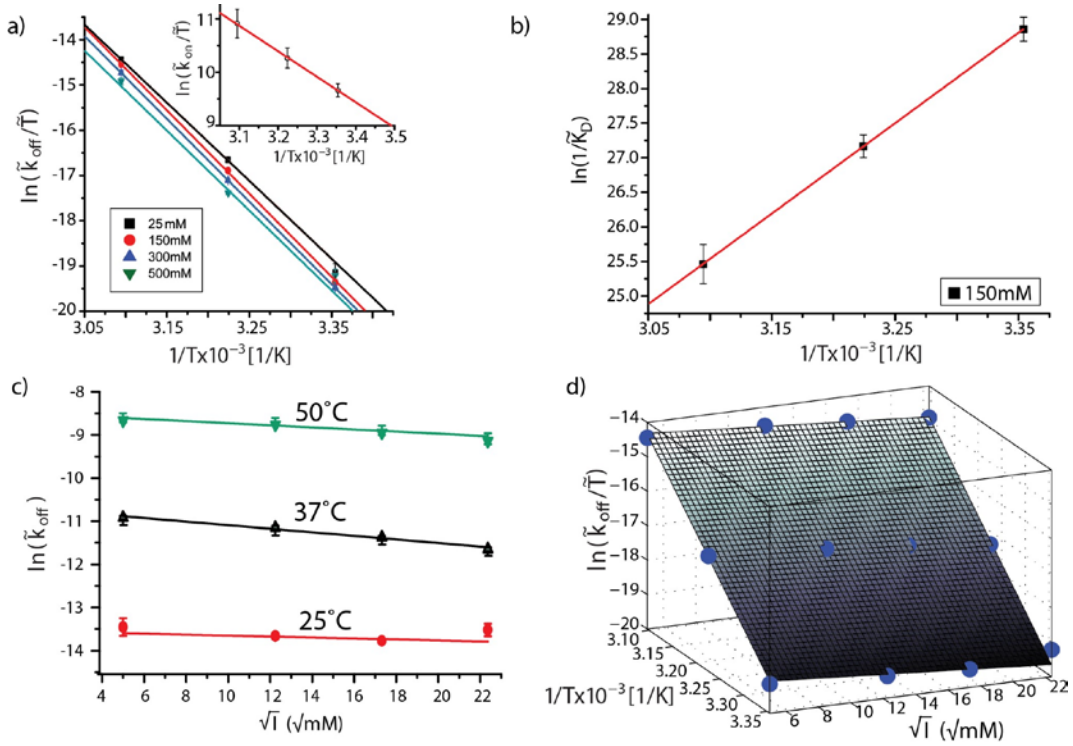

Figure 2.4|Temperature and salt dependence of biotin-streptavidin interaction kinetics. a) Eyring̃ plot of the temperature dependence of the off-rate shows similar slopes for each salt condition but varying offsets. The off-rate and temperature were made dimensionless by scaling them by our reference units, i.e $k_{!""} = \frac{k}{!\ s^{-1}!""}$ and $T = \frac{T}{1K}$. Fits were performed for data in the temperature range 25˚C to 50˚C Inset shows the temperature dependence of the on-rates. Inset

shows Eyring analysis of on rates over the same temperature range of 25˚C to 50˚C. From linear fits to these data we obtain a transition-state enthalpies of $\Delta H\ddagger_{on}$ = 9.48 ± 0.18 kcal/mol, and $\Delta H\ddagger_{off}$ = 36.64 ± 0.50 kcal/mol b) Van't Hoff plot from 25˚C to 50˚C. The dissociation constant was made dimensionless by scaling it by our reference units, i.e $\widetilde{K_D} = K_D/(1M^{-1})$. The red curve indicates a linear fit to the data. The fit was of the form $\ln\left(\frac{1}{\widetilde{K_D}}\right) = \frac{\Delta S}{R} - \frac{\Delta H}{R} \cdot \frac{1}{T}$, where R is 1.99 x 10-3 kcal K-1 mol-1, and T is the absolute temperature in K. This fit yielded the following values: ΔH = -26.01 ± 0.05 kcal mol-1, and ΔS = -0.0298 ± 0.0002 kcal K-1 mol-1. c) Plot showing salt dependence, again with similar slopes across all temperature conditions but with varying offsets. d) a 3D plot of the data fit with a least squares surface. All error bars represent the propagated error in the values taken from **Table 2.2**.

We measured on-rate kinetics for the biotin-streptavidin interaction, at a variety of temperatures, by monitoring loop formation over time. Loop closure occurs through two separate binding events, the binding of a molecule from solution to the nanoswitch, and then the closing of the loop. Thus, we fit loop closure data to a two-step kinetic model to extract these rates (**Figure 2.1b, 2.1d, methods, Table 2.3, Figure 2.2**). At 150 mM salt we measured a room-temperature on-rate of 4.0 ± 0.7 x 10^6 $M^{-1}s^{-1}$. Combining our on-rate and off-rate measurements, we calculated a dissociation constant of 2.94 ± 0.51 x 10^{-13} M, an equilibrium free energy change, ΔG^0, of -17.1 ± 0.1 kcal/mol, and an equilibrium enthalpy change, ΔH, of 26.01 ± 0.05 kcal/mol (**Table 2.3**). In general, our measurements are consistent with values reported in the literature (**Table 2.2**). Specifically, we are within 15% of the reported off-rate of a biotin-labelled oligonucleotide[9], within 30% of on-rate measurements from SPR[11], and within 5% of both

equilibrium ΔH measurements by ITC[12] and equilibrium ΔG measurements made by monitoring kinetics of radiolabeled biotin[13].

	k_{off} (10^{-7} s^{-1})			
Sample (Salt conc.)	**4°C**	**25°C**	**37°C**	**50°C**
Streptavidin (25mM)	2.02±0.22	14.38±2.92	181.8±7.6	1725±67
Streptavidin (150mM)	2.77±0.68	11.66±0.70	143.8±5.8	1565±25
Streptavidin (300mM)	2.84±0.60	10.39±0.51	115.1±3.6	1299±68
Streptavidin (500mM)	0.64±0.37	13.45±1.99	87.5±3.8	1073±81
Avidin (150mM)	--	2.25±0.32	45.6±10.3	--
Neutravidin (150mM)	--	1.84±0.83	91±23	--

	k_{on}/molecule[b] (10^6 M^{-1} s^{-1})			
Sample (Salt conc.)	**4°C**	**25°C**	**37°C**	**50°C**
Streptavidin (150mM)	1.7±0.4	4.0±0.7	9.0±1.4	17.9±5.1
Avidin (150mM)	--	6.21±0.24[a]	18.86±2.0[a]	--
Neutravidin (150mM)	--	0.37±0.27	1.47±0.42	--

	Equilibrium properties (150mM NaCl) Per Molecule			
Measurement	**4°C**	**25°C**	**37°C**	**50°C**
Streptavidin K_D (10^{-14} M)	16.1±5.6	29.4±5.1	159.5±26	870±248
Streptavidin ΔG^0 (kcal/mol)	-16.2±.2	-17.1±0.1	-16.7±0.1	-16.4±0.2
Avidin K_D (10^{-14} M)	--	3.6±0.5[a]	24.2±6.0[a]	--
Avidin ΔG^0 (kcal/mol)	--	-18.3±0.1[a]	-17.9±0.2[a]	--
Neutravidin K_D (10^{-14} M)	--	49±42	617±236	--
Neutravidin ΔG^0 (kcal/mol)	--	-16.8±0.5	-15.9±.2	--

[a]Non-specific avidin interactions may result in additional uncertainty in k_{on}

[b]Divide these k_{on} measurments by 4 to get the k_{on} per binding site

Table 2.3: Kinetic and thermodynamic values obtained from studying the interactions of biotin with Streptavidin, Avidin, and Neutravidin. Errors indicate the 67% confidence interval on the fit parameters (a 3 parameter model fit to 6 data points for each condition).

Without modifying the DNA construct, we were also able to measure kinetic and equilibrium properties for avidin and Neutravidin (**Table 2.3**). Although Neutravidin's affinity for biotin is 20 times weaker than avidin's, they surprisingly have similar off-rates,

underscoring the limitation of relying solely on affinity measurements to characterize an interaction.

	Units	Condition	Our values	Literature Range	References
off-rate	1/s	25˚C	**(1.2 ± 0.1) x 10^{-6}**	1.4 x 10^{-6} to 5.4 x 10^{-6}	Green, 1990; Piran, 1990; Chilkoti, 1995; Klumb, 1998; Hyre, 2006; Levy, 2008; Deng, 2012
		37˚C	**(1.4 ± 0.1) x 10^{-5}**	2.9 x 10^{-5} to 6.8 x 10^{-5}	Hyre, 2000; Howarth, 2006; Chivers, 2010; Magalhaes, 2011
on-rate*	1/(M*s)	25˚C	**(4.0 ± 0.7) x 10^{6}**	1.4 x 10^{6} to 8.5 x 10^{7}	Burunda, 1999; Qureshi, 2001; Hyre, 2006; Srisa-Art, 2008; Takakura, 2009; Magalhaes, 2011
		37˚C	**(9.0 ± 1.4) x 10^{6}**	5.5 x 10^{7} to 6.7 x 10^{7}	Chivers, 2010; Magalhaes, 2011
ΔH	kcal/mol	25˚C	**-26 ± 0.1**	-24.5 to -29.4	Chilkoti, 1995; Klumb, 1998; Hyre, 2000; Magalhaes, 2011
ΔG	kcal/mol	25˚C	**-17.1 ± 0.1**	-16.7 to -18.9	Green 1990; Chilkoti, 1995; Qureshi, 2001; Hyre, 2006; Magalhaes, 2011
		37˚C	**-16.7 ± 0.1**	-16.3 to -16.8	Chivers, 2010; Magalhaes, 2011
K_d	1/M	25˚C	**(2.9 ± 0.5) x 10^{-13}**	1.4 x 10^{-14} to 5.5 x 10^{-13}	Green, 1990; Chilkoti, 1995; Qureshi, 2001; Hyre, 2006; Magalhaes, 2011
		37˚C	**(1.6 ± 0.3) x 10^{-12}**	6.0 x 10^{-13} to 1.0 x 10^{-12}	Chivers, 2010; Magalhaes, 2011

*Our on-rates are reported per molecule of streptavidin. Literature range may contain a mixture of both per molecule and per binding site on rates as it is rarely specified.

Notes: 1) References that quoted either K_d or ΔG were included in both parameters using the relationship $\Delta G = RT*\ln(K_d)$

2) References that measured the on and off rates were included in both K_d (k_{off}/k_{on}) and ΔG

Table 2.2: Comparison of our kinetic and thermodynamic values for the biotin-streptavidin interaction to those in previously-published works.

To demonstrate the ability to measure weaker interactions, we incorporated desthiobiotin, a biosynthetic precursor to biotin that binds streptavidin with far lower affinity, into our nanoswitch[14]. By optimizing gel running conditions, we resolved the looped and unlooped constructs in as little as 6 minutes, measuring the off-rate of streptavidin-desthiobiotin as 35.3 ± 7.5 minutes at 4 ˚C and 8.6 ± 1.2 minutes at room temperature (**Figure 2.5**). We note that while the system is ideal for quantification of long lived interactions, even those out of the range of surface plasmon resonance, the time required to resolve the bands in a gel currently sets the lower limit of detectable dissociation life-times to minutes.

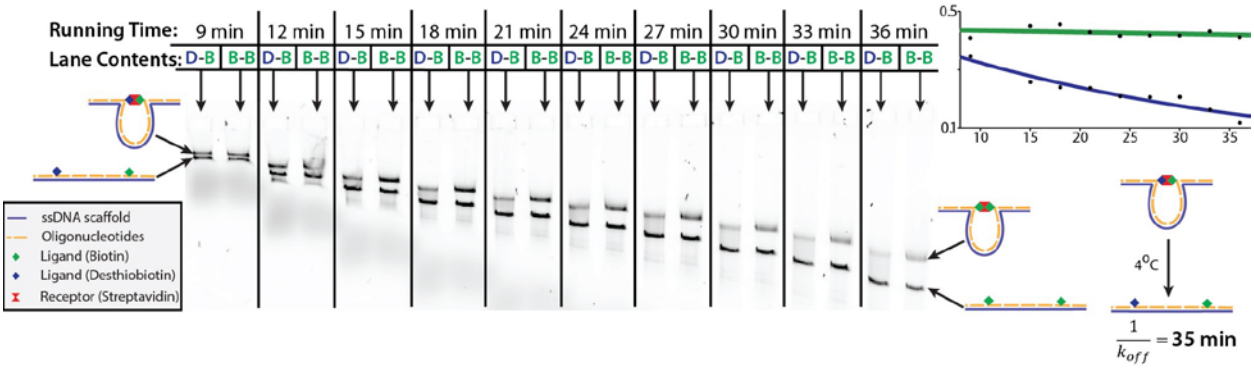

Figure 2.5| Measurement of weak interactions.The nanoswitches have proven very useful for the study of strong interactions. To extend the range of interactions which could be studied we modified the gel running procedure (see methods). Noting that reptation of the DNA through the gel matrix acts as a quencher by preventing open loops from closing we are able to monitor the ratio of looped to unlooped as a function of time run in a gel. To indicate the location of the looped band a nanoswitch with a negligible off rate was run alongside each time point. A desthiobiotinstreptavidin-biotin (D-B) bridge was used for the weak interaction, and a biotin-streptavidin-biotin (B-B) bridge was used as the strong interaction. The B-B nanoswitches

stayed relatively unchanged as a function of running time. The D-B constructs however show significant decay which was fit with a single exponential yielding a time constant of 35.3 ± 7.5 minutes.

The modularity of the DNA nanoswitch facilitates the easy incorporation of different types of molecules. We exploited this feature to measure several biologically relevant interactions including a covalent bond taking weeks to dissociate (**Figure 2.6a**), a protein-small-molecule interaction dissociating over days **(Figure 2.6b**), an antibody-antigen interaction taking hours to dissociate at room temperature (**Figure 2.6c**), and a 20bp DNA oligonucleotide dissociating over hours at 50˚C (**Figure 2.6d**). Additionally we were able to study peptide ligation kinetics with a time constant of minutes (**Figure 2.6e**), and restriction enzyme cleavage over seconds (**Fig 2.6f**). As with many techniques including SPR, assay preparation requires the derivatization of at least one molecule of interest. Here, we attach our molecules of interest to a DNA oligonucleotide, which can be accomplished using a variety of techniques. In addition to Sulfosuccinimidyl-4-(N-maleimidomethyl)cyclohexane-1-carboxylate-crosslinking[5], we previously described the use of click-chemistry to attach peptides to oligonucleotides, and the use of the enzyme sortase[15] to rapidly and efficiently attach proteins to our nanoswitches while preserving protein function[16].

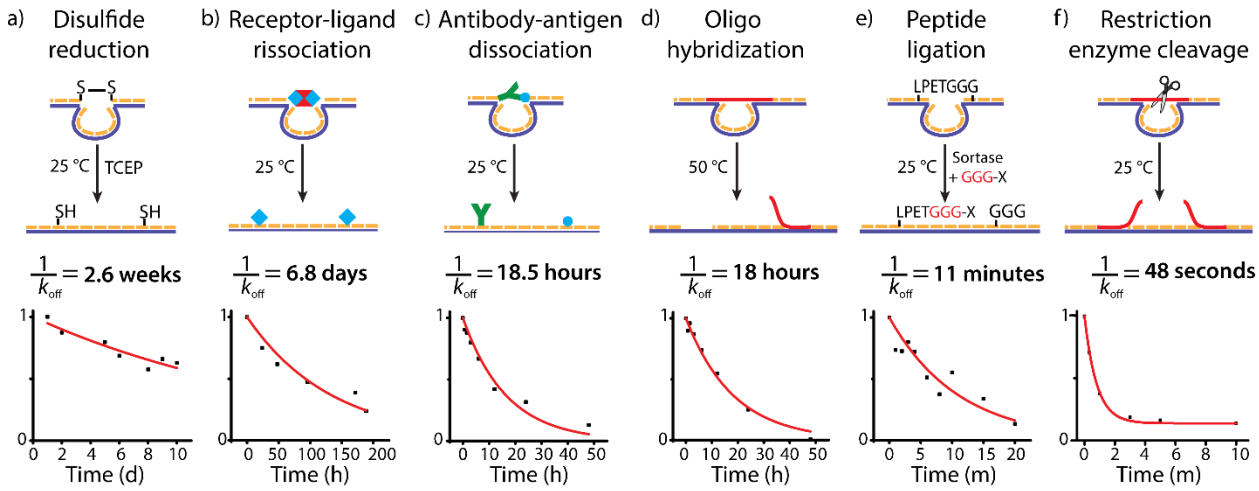

Figure 2.6| **Various biological measurements using the nanoswitch platform.** Schematic representation of each measurement, with data and model fit shown beneath. a) Disulfide bond reduction in 10μM TCEP at room temperature (k_{off} = 2.6 ± 0.4 weeks). b) Biotin-streptavidin dissociation in 300mM NaCl at room temperature (k_{off} = 6.8 ± 0.8 days). c) Dissociation kinetics of digoxigenin and its antibody at room temperature (k_{off} = 18.5 ± 2.0 hours). d) Melting kinetics of a 20nt oligonucleotide at 50˚C (k_{off} = 18 ± 1.6 hours). e) Sortase-catalyzed transpeptidation at room temperature ($k_{ligation}$ = 11 ± 1.3min). f) XhoI restriction-enzyme kinetics at room temperature (k_{cut} = 48 ± 2 sec). Each value is reported as an error-weighted fit parameter ± its one-sigma confidence interval).

The platform's versatility is facilitated by its universal gel readout. An extreme example of this is our characterization of the reduction of a disulfide bond at 25˚C in 10μM TCEP yielding a time constant of 2.6 ± 0.4 weeks (**Figure 2.6a**). Since the signal per molecule is only dependent on the nanoswitch size, this two-atom system yields the same level of signal per interaction as a 150kDa antibody binding to its antigen (**Figure 2.6c**).

Additionally, the programmability of these nanoswitches enables multiple topological states to be individually distinguished on a gel, facilitating the analysis of complex multicomponent interactions (**Figure 2.7**). We engineered nanoswitches with three integrated ligands, placed strategically to form two asymmetric loops when simultaneously bound by a bi-specific receptor. The resulting nanoswitch adopts 5 resolvable states that can be identified with control experiments (**Figure 2.7a and 2.8**). We measured bi-directional transitions for all 5 states, thus determining all rate constants (**Figure 2.7, 2.9, and 2.10, and Table 2.4**). This ability to monitor the fraction of molecules populating each state over time would be difficult or impossible to achieve with most other measurement techniques.

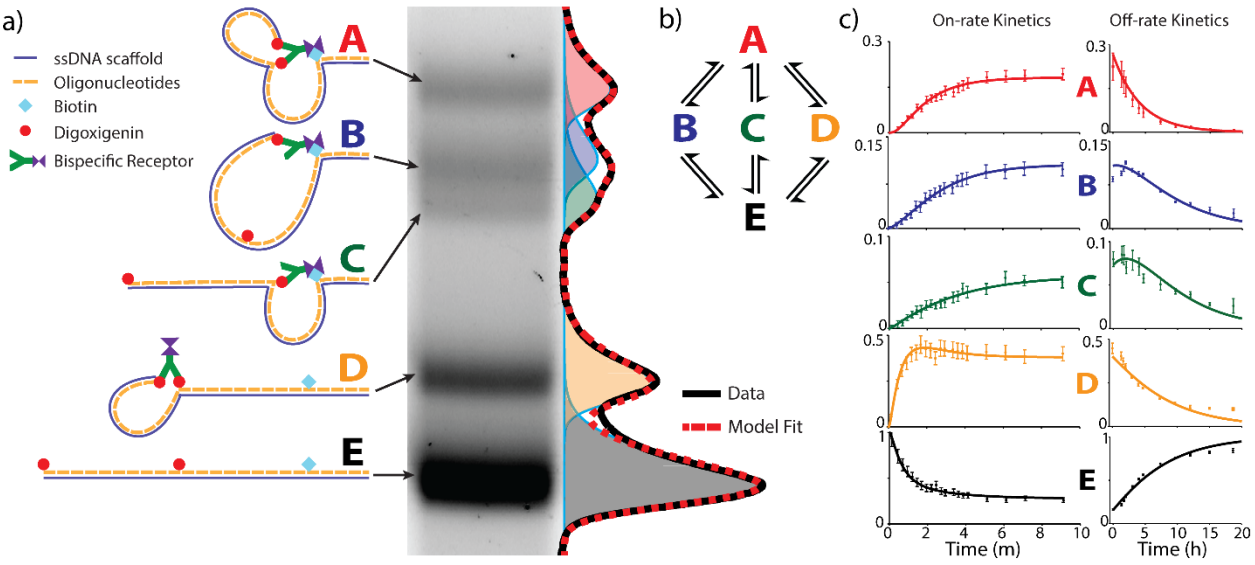

Figure 2.7| **Multistate kinetic analysis.** a) A nanoswitch functionalized with two digoxigenin molecules and one biotin molecule can adopt 5 discernable states upon addition of a bispecific receptor. All 5 topological states, **A**-**E** (**Figure 2.9**), can be resolved within a single lane of an agarose gel. These bands can be fit globally with a single fit of a sum of skewed Gaussian

curves. The black curve represents the median pixel intensity, the dashed red curve represents the fit which is the sum of 5 skewed Gaussians, and the individual skewed Gaussians are shaded by state. b) A reaction diagram illustrating the possible transitions between each of the 5 states. c) (left) on-rate measurements indicating the value of each state at 20 different time points. Solid curves indicate the result of a global fit of all states to the kinetic model illustrated in c. (right) off-rate measurements indicating the value of each state at 12 different time points. Solid curves indicate the result of a global fit of all states to the kinetic model illustrated in b. These fits taken together allowed for the determination of all rate constants from 32 lanes which can be run on a single gel (**Figure 2.10 and Table 2.4**). Error bars are based on one-sigma confidence-intervals of the least squares fit to each band (see Gel Image Analysis in Methods for details). The on-rate model was fit using 100 measurements while the off-rate model was fit using 60 measurements.

Our approach enables low-cost, accessible, and parallel multicomponent biomolecular interaction analysis using a basic laboratory technique, gel electrophoresis. We have demonstrated our platform's ability to characterize interactions with time constants ranging from seconds to months (~6 orders of magnitude), for a wide variety of molecular interactions, temperatures and buffer conditions. The signals are robust and highly amplified, giving detection limits in the range of attomoles and allowing quantitative kinetic- and thermodynamic-analysis of proteins as shown here with femtomoles of material (~1ng for a 50kDa protein). In contrast to other techniques that provide one signal to analyze (e.g. SPR, radiolabeling, and ITC), our technique has the ability to perform independent measurement of 5 signals simultaneously, allowing complete characterization of a complex 5-state system. The

modularity and programmability of the nanoswitches affords control over the relative concentrations and stoichiometries of interacting components, independent of the nanoswitch concentration. This feature suggests that in addition to monitoring reactions, nanoswitches could be used as a template-directed synthesis technique to control complex reactions. Overall, this unique lab-on-a-molecule platform promises to be a powerful research tool, accessible to anyone able to perform gel electrophoresis.

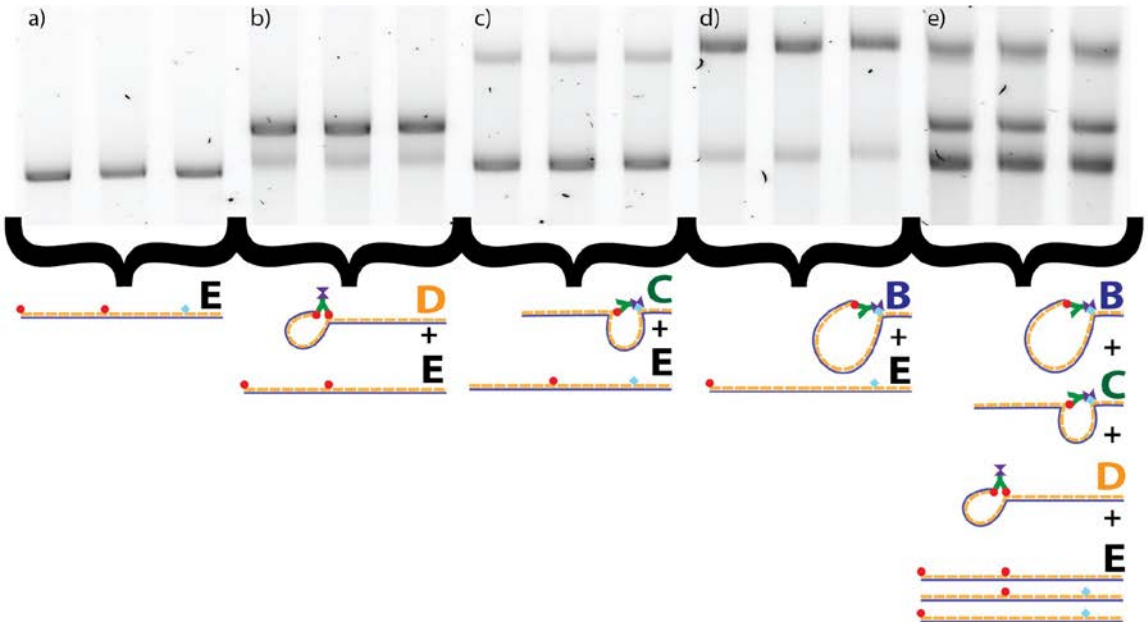

Figure 2.8| Multistate band verification. To determine the location of the bands which represent the different states of the bispecific receptor binding to the trifunctionalized nanoswitch, we made nanoswitches capable of forming one or a subset of states (each set was run in triplicate). a) trifunctionalized nanoswitches without the bispecific receptor result in only a linear band (E). b) Nanoswitches with both digoxigenin functionalizations but lacking the biotin can form the E and D states. c) Nanoswitches lacking the terminal digoxigenin can form the E and C states. d) Nanoswitches lacking the central digoxigenin can form the E and B states. e) In this lane the samples from the lanes in b, c, and d were mixed in a 1:1:1 volumetric ratio before running on the gel to simulate the conditions seen in the multistate experiments. Note that it was not possible to make a construct which could exclusively form state A in Figure 2.7 but this state is attributed to the only remaining band, and selective quenching experiments (data not shown) indicate that this construct contains both digoxigenin and biotin dependent interactions which collapse into the appropriate states upon quenching exclusively with digoxigenin or biotin.

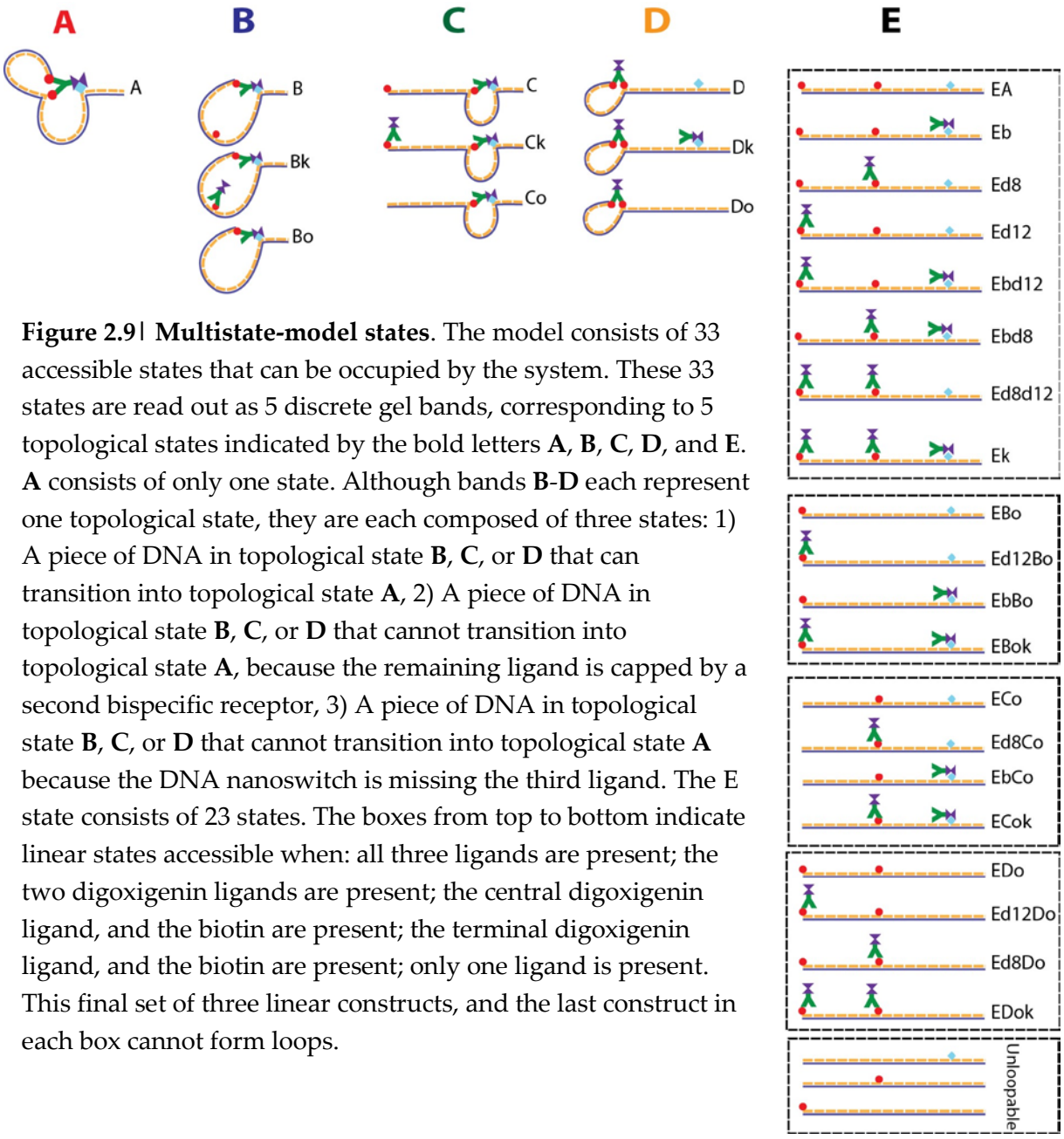

Figure 2.9| Multistate-model states. The model consists of 33 accessible states that can be occupied by the system. These 33 states are read out as 5 discrete gel bands, corresponding to 5 topological states indicated by the bold letters **A**, **B**, **C**, **D**, and **E**. **A** consists of only one state. Although bands **B**-**D** each represent one topological state, they are each composed of three states: 1) A piece of DNA in topological state **B**, **C**, or **D** that can transition into topological state **A**, 2) A piece of DNA in topological state **B**, **C**, or **D** that cannot transition into topological state **A**, because the remaining ligand is capped by a second bispecific receptor, 3) A piece of DNA in topological state **B**, **C**, or **D** that cannot transition into topological state **A** because the DNA nanoswitch is missing the third ligand. The E state consists of 23 states. The boxes from top to bottom indicate linear states accessible when: all three ligands are present; the two digoxigenin ligands are present; the central digoxigenin ligand, and the biotin are present; the terminal digoxigenin ligand, and the biotin are present; only one ligand is present. This final set of three linear constructs, and the last construct in each box cannot form loops.

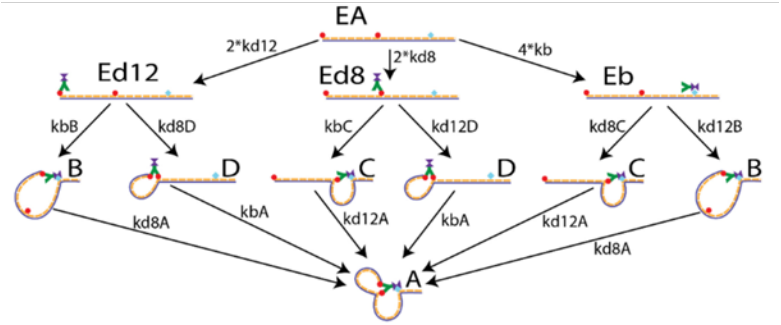

Rate Constant	Description	
kb	Per-site solution on rate for biotin	
kd8	Per-site solution on rate for the dig on var 8	
kd12	Per-site solution on rate for the dig on var 12	
Rate Constant	**Description**	**Definition**
kbC	Rate of biotin binding to form state C	$kbC = 4*kb*L_C$
kbB	Rate of biotin binding to form state B	$kbB = 4*kb*L_B$
kd8C	Rate of dig on var 8 binding to form state C	$kd8C = 2*kd8*L_C$
kd8D	Rate of dig on var 8 binding to form state D	$kd8D = kd8*L_D$
kd12B	Rate of dig on var 12 binding to form state B	$kd12B = 2*kd12*L_B$
kd12D	Rate of dig on var 12 binding to form state D	$kd12D = kd12*L_D$
kbA	Rate of biotin binding to form state A	$kbA = 4*kb*L_{DA}$
kd8A	Rate of dig on var 8 binding to form state A	$kd8A = kd8*L_{BA}$
kd12A	Rate of dig on var 12 binding to form state A	$kd12A = kd12*L_{CA}$

Figure 2.10| Multistate on-rate kinetic model schematic. The kinetic on-rate model consists of 3 solutions on rates and 6 effective loop concentrations resulting in effective on loop rate constants referred to as kbB, kbC, kd8C, kd8D, kd12B, kd12D, kbA, kd8A, and kd12A. The figure illustrates the kinetic model, excluding the capping phenomenon for clarity, and the table indicates the physical meaning and mathematical definition of each rate constant in the figure. The effective loop concentrations are as follows: L_B is the effective concentration between the biotin on var 4 and the dig on var 12, L_C is the effective concentration between the biotin on var 4 and the dig on var 8, L_D is the effective concentration between the dig on var 8 and the dig on var 12, L_{BA} is the effective concentration of the dig on var 8 relative to the var 4-var 12 complex, L_{CA} is the effective concentration of the dig on var 12 relative to the var 4-var 8 complex, L_{DA} is the effective concentration of the biotin on var 4 relative to the var 8-var 12 complex.

Parameter	kb on	kb off	kd on	kdoff	kd8 on	kd12 on	kd8 off	kd12 off	L_B	L_C	L_D	L_{BA}	L_{CA}	L_{DA}
Units	10^6 /$M^{-1}s^{-1}$	$days^{-1}$	10^6 /$M^{-1}s^{-1}$	$days^{-1}$	10^6 /$M^{-1}s^{-1}$	10^6 /$M^{-1}s^{-1}$	$days^{-1}$	$days^{-1}$	10^{-9} M	10^{-9} M	10^{-9} M	10^{-9} M	10^{-9} M	10^{-9} M
Upper Bound	0.12	2.08	5.24	1.85	2.69	5.24	1.82	1.85	27.45	11.33	245.31	19.51	30.76	35.98
Average	**0.10**	**2.05**	**2.65**	**1.81**	1.62	2.24	1.80	1.82	15.51	10.85	112.32	15.28	7.84	31.02
Lower Bound	0.09	2.01	1.15	1.77	1.15	1.54	1.77	1.80	11.14	10.39	90.12	11.45	4.30	28.26

Table 2.4| Results from multistate on-rate and off-rate fits, where LB is the effective concentration between the biotin on var 4 and the dig on var 12, LC is the effective concentration between the biotin on var 4 and the dig on var 8, LD is the effective concentration between the dig on var 8 and the dig on var 12, LBA is the effective concentration of the dig on var 8 relative to the var 4-var 12 complex, LCA is the effective concentration of the dig on var 12 relative to the var 4-var 8 complex, LDA is the effective concentration of the biotin on var 4 relative to the var 8-var 12 complex. Additionally, to verify that the solution on-rate measurements are independent of how we scaffold the ligands, we redid the measurements using a construct containing two biotin molecules and a single digoxigenin molecule, and found that these solution on-rates were in close agreement with our prior measurements (data not shown).

Acknowledgments:

The authors gratefully acknowledge D. Corey, G. Yellen, R. Wilson, J. Holt, H. Ploegh, G. Wong, A. Badran, Z. Tsun, A. Golden, and members of the Wong and Corey Labs for critical discussions, and T. Kao for her early work on the project. Funding for this project was provided by NIH R01 DC02281 to D.P.C, M.K. was supported by National Science Foundation USA GRFP 2012147612; W.P.W. was supported by BCH startup funds and Takeda New Frontier Science.

Author contributions:

The initial idea was conceived by K.H. and W.P.W. Experiments were designed by all authors. Method was expanded by M.A.K. and A.W., and experiments were carried out by K.H. M.A.K. and A.W. All authors participated in data analysis, critical discussion, and writing of the manuscript.

References

1. Thorne, H. V. *Virology.* **29**, 234-239 (1966).

2. Bishop, D. H. L., Claybrook J. R. & Spiegelman S. *J. Mol. Bio.* **26**, 373-387 (1967).

3. Smithies, O. *Biochem J.* **61**, 629-641 (1955).

4. Hellman, L. M. & Fried, M. G. *Nat. Prot.* **2**, 8 (2007).

5. Halvorsen K., Schaak D. & Wong W.P. *Nanotechnology.* **22**, pp. 1-8 (2011).

6. Saccà, B. & Niemeyer, C. M. *Angew. Chem. Int. Ed.* **51**, 58–66 (2012).

7. Seeman, N.C. *Annual Reviews Biochemistry.* **79**, 65-87 (2010).

8. Aaij, C. & Borst P. *BIOCHIMICA ET BIOPHYSICA ACTA.* **269**, 192-200 (1972).

9. Levy, M. & Ellington, A.D. *Chemistry & Biology.* **15**, 979–989 (2008).

10. Prabhu, N.V. & Sharp, K.A. *Annual Reviews Physical Chemistry.* **56**, 521-48 (2005).

11. Qureshi, M. H., Yeung, J. C., Wu, S. C. & Wong, S. L. *J Biol Chem.* **276**, 46422–46428 (2001).

12. Klumb, L.A., Chu, V. & Stayton P.S. *Biochemistry.* **21**, 7657-63 (1998).

13. Chivers, C. E. et al. *Nature Methods.* **7**, 391–393 (2010).

14. Florin, E. L., Moy V.T., and Gaub H.E. *Science.* **264**, 415-417 (1994).

15. Chen I., Dorr, B. M., and Liu D. R. Proc. Natl. Acad. Sci. USA **108**, 11399-11404 (2011).

16. Koussa M.A., Sotomayor M., Wong W.P. *Methods.* **67** 134-141 (2014).

Methods:

Note that we provide a **Detailed Protocol** that includes lists of reagents needed and detailed step by step instructions for performing on-rate and off-rate experiments.

General nanoswitch formation:

The nanoswitches were constructed as previously described in detail[5]. Circular-single-stranded DNA from the 7249 nt bacteriophage M13 (New England Biolabs) was linearized by enzymatic cleavage of a single site using BtscI (New England Biolabs) and a site specific oligonucleotide. Oligonucleotides (from Bioneer or Integrated DNA Technologies (IDT)) were designed to complement the linearized M13 DNA along the backbone, resulting in 120 60-nt oligonucleotides and a single 49 nt oligonucleotide. The first and last oligonucleotide along with 10 evenly distributed oligonucleotides are intended to be interchangeable and will be referred to as variable oligonucleotides (var 1-12, with var 1 representing the first oligonucleotide and var 12 representing the last oligonucleotide—see **Detailed Protocol**). These variable oligonucleotides were stored separately from the remaining 109, referred to as backbone (bb) oligonucleotides, which were mixed in equimolar concentration in a single tube. Mixing a molar excess of the oligonucleotides (10:1 unless otherwise noted) with the ssDNA scaffold and subjecting the mixture to a temperature ramp (90 ˚C to 20 ˚C at 1 ˚C/minute unless otherwise noted) produced double stranded DNA. Final constructs were spiked with a low concentration of DNA ladder (BstNI Digest of pBR322 DNA, New England Biolabs) to aid in quantification. For many experiments the constructs were PEG precipitated after annealing to remove excess

oligonucleotides. The PEG precipitation was performed as described in section 3.3 of the **Detailed Protocol** and as previously described in[16].

Key Design Considerations:

The nanoswitches were designed with several key design considerations to ensure that they function properly and robustly over a wide range of conditions. The oligonucleotide length was selected to be 60 nt to ensure both site specificity, and to ensure that the oligonucleotides would not spontaneously fall off even at temperatures as high as 50 ˚C. At 50 ˚C even a 20-mer oligonucleotide has a long lifetime of ~18 hours (**Figure 2.6d**), and the lifetime of a 60-mer oligonucleotide is predicted to be orders of magnitude longer than the 20-mer oligonucleotide[17].

The ligands were positioned at locations that allow for easy resolution of the looped and unlooped bands. Placement of the oligonucleotides on variable regions 4 and 5 yields two bands that are quite close to one another under our standard gel running conditions. The further apart the ligands are, the more easily resolvable the two bands become. The spacing of ligands on the DNA scaffold also controls their effective concentration, with the effective concentration of one ligand to the other generally decreasing as they are spaced further apart (though if the ligands are brought within one persistence length of the polymer, the effective concentration may decrease dramatically). We have found that the use of variable regions 4 and 8 provides a nice middle ground (**Table 2.6**).

Streptavidin concentration (nM)	Solution on-rate (10^6 M^{-1} s^{-1}) (per binding site)
1	1.15 ± 0.18
3	1.00 ± 0.09
10	0.88 ± 0.10
Mean	1.01 ± 0.08

Table 2.6| Solution on-rate is independent of receptor concentration. Solution on-rate values reported are the solution on-rate fit parameter from an error weighted fit of 10 data points with a 3 parameter model. The errors for measurements are the one-sigma confidence intervals of the fit parameter. The mean value is the mean of the solution on-rates from the three different concentrations with the error given by the standard error of the mean. All values are reported as a per-binding site onrate. To get the per-molecule on-rate, one would need to divide these values by one molecule per four binding sites (i.e. multiply by 4).

There are three concentrations that can be independently tuned in an on-rate experiment. There is the concentration of the scaffold, the concentration of the receptor, and the effective concentration between the two ligands on the polymer. If these concentrations are adjusted carefully, many problems can be avoided. For example, if the effective concentration between the two tethered ligands is significantly higher than the concentration of the receptor, then one can minimize capping (the binding of two receptors to a single scaffold resulting in an unloopable construct). We note, however, that since our model accounts for capping, the values obtained outside this optimal regime will still be correct, the looped-band intensities will simply be weaker, resulting in a lower signal-to-noise. Although not usually a problem, one can avoid

higher order aggregation by ensuring that the scaffold concentration is significantly lower than the effective concentration between the two ligands on the scaffold. One can also simplify the analysis by selecting a receptor concentration that is significantly higher than the scaffold concentration so that the receptor concentration stays effectively constant over the course of the experiment. Following these experimental design principles, in our experiments using variable oligonucleotides 4 and 8, the effective concentration between the two ligands on the loop is ~30 nM, the scaffolds are used at a concentration of 80 pM, and the receptor is used at a nominal concentration of 3 nM.

In addition to the ratio of concentrations there are some important lower and upper limits of concentration to keep in mind. We have found that working with protein concentrations below 1 nM can be unreliable due to losses of protein to the walls of the tubes. We have performed on-rate experiments with streptavidin concentrations as low as 0.3 nM but losses of protein can be as high as 80% even in protein LoBind tubes (Eppendorf technical data sheet). Unless a means of eliminating protein loss to tubes and pipette tips is implemented, we do not recommend working below 1 nM. The upper limit is not a hard limit. We have found that the on-rate for streptavidin is very fast at 30 nM, making it difficult to pipette fast enough to take multiple time points before the plateau. If one has a means of more rapidly mixing solutions (i.e. microfluidics), or a protein with a slower on rate, higher protein concentrations can be used. We have found that 3 nM provides a nice middle ground, though one may wish to optimize the

protein concentration used based on the speed of mixing, and the solution on-rate of the protein being studied.

Following these design principles and those laid out in[5], is key to the successful use of this platform. The **Detailed Protocol** provides information on reagents needed, and detailed step-by-step instructions on how to succesfully perform on-rate and off-rate experiments.

Electrophoretic conditions

All looped constructs were run in 0.7% agarose gels, cast from LE agarose (Seakem) or Ultrapure Agarose (Life Technologies) dissolved in 0.5x Tris-borate EDTA (TBE) (Biorad). Before loading, samples were mixed with a Ficoll-based loading solution (Promega), which we found to give sharper bands than glycerol-based loading dyes, simplifying quantification. Gels were run for 90-100 minutes at 4 V/cm, unless otherwise noted, and subsequently stained in 1x SYBRGold stain (Invitrogen) for a minimum of 30 minutes before being imaged with a gel imager (Biorad) or laser gel-scanner (GE Typhoon). It is important to note that the standard output file of this imager is often set to a .gel file which has a non-linear intensity scaling. .gel images can be linearized using the imageJ Linearize gel Data plugin (http://rsb.info.nih.gov/ij/plugins/linearize-gel-data.html). Alternatively the gel image can be saved as a linear .tiff file off of the imager. We would like to point out that these expensive imagers are not required for quantification, and we obtained similar results using a blue transilluminator (Invitrogen) and a point and shoot camera (Canon S95).

Biotin-streptavidin nanoswitch experiments

This construct used biotinylated versions of two oligonucleotides (var 4 and var 8), which were used in 4x molar excess to the scaffold, while all other oligonucleotides were used in a 10x molar excess. The reason for this lesser amount is twofold: 1) to be less wasteful of the more expensive functionalized oligonucleotides, and 2) because excess biotin oligonucleotide in solution could interfere with our measurements. The final DNA construct was then diluted 100x from its original concentration of ~16 nM (to 160 pM), and mixed in equal volumes with streptavidin (Rockland) at 6 nM nominal concentration to form the loops, yielding final nominal concentrations of ~80 pM and 3nM, respectively.

On-rate experiments were performed by mixing equal volumes of 160 pM DNA construct with a nominal 6 nM streptavidin concentration, followed by taking 10 μL aliquots of the mixture at various times and mixing them with 1μL of a saturated biotin solution to quench the formation of loops. The 25 ˚C experiment was performed at room temperature, the 4 ˚C experiment was performed in a cold room, and the 37 ˚C and 50 ˚C experiments were performed using a thermal cycler. For on-rate experiments, using low binding tubes (Eppendorf LoBind) was important for getting repeatable results due to significant streptavidin adsorption to the tubes when incubated at 6 nM. Actual concentrations used to determine the on-rates were measured using spectrophotometry and a HABA assay to determine streptavidin activity. We found that the

actual streptavidin concentration was within 10% of the nominal concentration, and over 85% of the protein was active based on the HABA assay.

Off-rate measurements were performed by forming looped construct as described above, and letting the solution sit for at least 24 hours to allow the system to reach equilibrium. Aliquots of the looped construct were mixed at various times with a quenching solution consisting of biotin and sodium chloride to achieve the proper experimental salt concentrations, and immediately put at the experimental temperature. The 4 ˚C condition was done in a refrigerator, the 25 ˚C sample was done in a water bath, and the 37 ˚C and 50 ˚C temperatures were done in a thermal cycler. To run all the samples on a single gel, the quenching times were determined relative to the predetermined gel running time.

Preparations with avidin and neutravidin were prepared in the same way, but protein concentrations were sometimes altered to enable on-rate measurements over a similar time scale as the streptavidin experiments.

Desthiobiotin-Streptavidin

Desthiobiotin experiments were conducted in a similar manner as the biotin experiments with slight modifications. The var 4 oligonucleotide was changed to a desthiobiotin-functionalized oligonucleotide while the var 8 oligonucleotide remained biotin functionalized. The off-rate of the desthiobiotin interaction is much faster than the typical 100 minute gel run time. Noting that once a loop opens in the gel, the reptation of the DNA prevents the loop from closing again, we ran samples for different amounts of time in the gel at 15 V/cm and 4 ˚C, and quantified the fraction looped as a function of running time (**Figure 2.5**). In addition to allowing the

determination of the desthiobiotin-streptavidin off rate, this gel also allowed us to determine the minimum amount of time required to achieve separation of the looped and unlooped bands in the gel. This enabled the use of the standard quenching technique for measuring desthiobiotin off-rates as described in the previous section; these gels were run at 15 V/cm for 10 minutes in pre-chilled electrophoresis buffer.

DNA hybridization experiments

This construct used a 50 nt "bridge" oligonucleotide to span the last 30 nt of the var 4 region and the first 20 nt of the var 8 region. Thus, the normal var 4 and var 8 oligonucleotides were omitted from the mixture and replaced with 3 oligonucleotides: the aforementioned "bridge" oligonucleotide and two small "filler" oligonucleotides to fill the remaining bases so that the M13 scaffold would be fully hybridized. In this case, the bridge oligonucleotide was added in equimolar concentration with the scaffold strand, while the other oligonucleotides remained at 10x molar excess. Off-rate measurements were quenched with 500 nM 20 nt oligonucleotide corresponding to the loop closure site. Kinetics were accelerated by performing the measurement at 50 °C.

Enzyme cleavage experiments

These constructs were made as described above, but with a bridge oligonucleotide containing an inserted sequence recognized by the XhoI enzyme (New England Biolabs). The compliment to this restriction sequence was also added to ensure that this region was double stranded. Cleavage measurements were performed by adding enzyme to the loops (with final

concentrations of 2.2 nM and 1,000 units/mL for the loops and enzyme, respectively) in the recommended buffer (New England Biolabs) and quenching the enzyme activity with 75 mM EDTA at various times at room temperature.

Antibody-antigen experiments

This construct used a 3′ digoxigenin labeled version of the var 8 oligonucleotide (Integrated DNA Technologies) and a 5′ anti-dig labeled version of the var 4 oligonucleotide. The antibody labeled oligonucleotide was made by chemically crosslinking a free amine on the antibody (Polyclonal Sheep Antibody from Roche) to a thiol labeled oligonucleotide, and purified by electroelution as described previously[5]. The construct was made with two annealing steps. First, all the oligonucleotides with the exception of the antibody-labeled oligonucleotide were mixed with the scaffold strand and annealed following our standard protocol described above (except a 1:1, rather than 10:1, molar ratio was used for the digoxigenin oligonucleotide). Second, the purified antibody oligonucleotide was added in a 1:1 molar ratio and annealed from 37 °C to 4 °C at 0.5 °C/minute to facilitate annealing of the antibody-modified var 4 oligonucleotide. Off-rate measurements were performed by quenching with 335nM of antibody at various times at room temperature.

Sortase Catalyzed Peptide Ligation experiments

This construct was created in 3 steps. 1) Var 4 and var 5 oligonucleotides with a 3′ and a 5′azide respectively, were functionalized with sortase compatible peptides. 2) These two oligonucleotides were linked together with sortase. 3) The peptide-bridged oligonucleotides

were hybridized onto the DNA nanoswitch. All custom peptides were purchased from NeobioLab.

1) To create the sortase-compatible oligonucleotides, sortase-compatible peptides were covalently attached using click chemistry as previously[16]. Pra-LPETGHHHHHH, where Pra is a Propargyl glycine which adds an alkyne functionality, was coupled to var 4-azide using copper-catalyzed click chemistry. Azide-var 5 was then functionalized with a Flag-TEV-GGG-Pra peptide, where Flag denotes a Flag-tag and TEV denotes a cleavage site for the Tobaco etch virus protease. After the click chemistry the oligonucleotides were processed with a qiagen nucleotide removal kit and run on a polyacrylamide gel. The bands corresponding to the peptide-oligonucleotide chimeras were cut out and the products were extracted via electroelution as previously described.
2) Once purified the Flag-TEV-GGG-var 5 was treated with TEV (Sigma) and the two oligonucleotides were concentrated as previously[16]. These oligonucleotides were then at a concentration of ~10uM as judged by running on a precast 4-20% gradient polyacrylamide TBE gel (BioRad). Equal volumes (10μL each) of the sortase-compatible oligonucleotides were mixed with 5 μL of 14.1mg/ml sortase (Chen et al., 2011), and 25 μL of 2x Sortase Reaction buffer (600 mM Tris HCl pH 7.5, 300 mM NaCl, 10 mM $MgCl_2$, and 10 mM $CaCl_2$). This was allowed to sit for 3 hours at room temperature before running on a polyacrylamide gel and purifying the dimer band via electroelution. Yielding var 4-LPETGGG-var 5 (Note that the GGG indicates the amino acid string Gly-Gly-Gly.

3) The var 4-LPETGGG-var 5 was used instead of the normal var 4 and var 5. This was annealed onto the linear M13 backbone at a 1:1 ratio and was added along with the other oligonucleotides at the beginning of the annealing, as peptide denaturation was not a concern. This yielded loops with the peptide LPETGGG bridging variable regions 4 and 5.

With these loops in hand we could observe loop opening as a result of sortase ligating free GGG-X peptide. To accomplish this a mixture was made with the following concentrations. 2 nM DNA nanoswitches, 10 μM sortase, 40 μM GGG-S-S-CH_3, 300 mM Tris HCl pH 7.5, 150 mM NaCl, 5 mM $CaCl_2$, and 5 mM $MgCl_2$. Catalysis by sortase is highly calcium dependent thus the transpeptidation could be quenched at different times by adding an equal volume of 100mM EDTA in water. 10 time points were collected over 20 minutes at room temperature.

Disulfide Reduction:

This construct was created in 3 steps. 1) Var 4 and a truncated version of var 8 with a 3′ and a 5′ thiol respectively, were reduced in 50 mM TCEP (BondBreaker Thermo Scientific). 2) These two oligonucleotides were linked by a disulfide. 3) The disulfide-bridged oligonucleotides were hybridized onto the DNA nanoswitch.

1) To reduce the thiols on the oligonucleotides they were incubated in 50 mM TCEP for 1 hour at RT.
2) Equal volumes of the two oligonucleotide-TCEP mixtures were then combined. The TCEP was removed using a QIAGEN nucleotide-removal kit. The oligonucleotides were

then allowed to form disulfides in the absence of reducing agent in PBS for 1 hour before running the products on a precast 4-20% gradient polyacrylamide TBE gel. As the oligonucleotides were different sizes (60 and 30nt) the appropriate heterodimer could be easily identified and purified using electroelution as previously described[5].

3) The var 4-S-S-var 8 was used instead of the normal var 4 and var 8. This was annealed onto the linear M13 backbone at a 1:1 ratio and was added along with the other oligonucleotides at the beginning of the annealing. This yielded loops with a disulfide bridging variable regions 4 and 8.

With these loops in hand we could observe loop opening as a result of TCEP reduction of the disulfide bond. To accomplish this equal volumes of 20 μM TCEP and 160 nM loops, both of which were diluted in NEB buffer 2, were mixed at different time points before running the gel. 7 time points were collected over 10 days at room temperature before running the gel.

MultiState Loops

The bispecific receptor was formed by using a lightning link kit (Innova Biosciences) to attach streptavidin to sheep polyclonal antidig (Roche 11333089001). The antidig, suspended in PBS, was added in a 1:1 ratio to the streptavidin, and the kit protocol was followed exactly. This was then diluted 1:1250 into NEB Buffer 2 with added 150mM NaCl before use in forming multistate loops. The multistate loop was formed by using var 4 with a 3′ biotin, var 8 with a 5′ digoxigenin, and var 12 with 3′ digoxigenin in place of the normal var 4, 8, and 12 oligonucleotides. On-rate and off-rate measurements were performed using the same procedure

used for the biotin-streptavidin experiments with slight modifications. Rather than adding streptavidin, the diluted bispecific receptor was added, samples were quenched with 2 μL of 5 μM digoxigenin-functionalized oligonucleotide (an oligonucleotide was used as digoxigenin is not water soluble) suspended in a saturated biotin solution. Gels were run 6.25 V/cm for 125 minutes with buffer chilled to 4 ˚C before running

Gel Image Analysis

We analyzed gel images in one of two ways:

1) All non-multistate (only two bands) gels were analyzed in the following way:

The amount of material in each gel band was quantified by analyzing the scanned gel images with the gel analysis tool in the freely available ImageJ software package. Using rectangular regions of interest that just capture the width of the gel bands, this toolbox produces intensity profiles whose area can be measured to quantify the total brightness in each band. We applied the same rectangular window size to each lane within a single gel. In many gels the highest molecular weight band of the added ladder was used as a normalizing reference lane. This relaxed the constraints of pipetting perfectly across all lanes.

2) All multistate (with 5 bands) gels were analyzed as follows

A custom MATLAB interface, available upon request, was developed for fitting the intensity profiles of the imaged gel bands. The software interface was modeled after the ImageJ interface. Rectangular boxes are drawn around each lane to define a region of interest. Median filtering is a common technique used to remove speckle noise in images. Rather than filtering the entire image, each individual lane was median filtered by row to remove speckle noise without

sacrificing resolution in the direction of band migration. After plotting the median-intensity profile the background was subtracted using a 4-6 point piece-wise linear function to outline the background. The background was found to be very similar across lanes and often the same background profile could be subtracted from the majority of the lanes. Once the profiles were extracted, least-squares fitting of each profile to the model was performed in MATLAB. Individual bands run on their own show a skewed Gaussian profile, also known as a skew normal distribution, with a skew parameter of ~-2.5 (Figure 2.8). Thus, the entire multistate median-intensity profile (from just above the highest band to just below lowest) was fit using a sum of 5 skewed Gaussians. A common skew parameter was used for all 5 bands, and a common initial guess of band width was used with a fitting range of ±10 pixels. These input parameters allowed for converging fits across all lanes, and resulted in fits that closely matched the observed intensity profiles (**Figure 2.7b**). The areas of the individual bands were calculated by integrating the individual skewed Gaussians. Error in the fitted areas was estimated by calculating the areas within the one-sigma confidence interval of the fit parameters. These areas were all normalized by the total area (the sum of all of the skewed Gaussian areas). The identities of the bands were validated by analyzing gels in which individual loop sizes were formed (**Figure 2.8**). Accuracy of band quantification was confirmed by mixing these individual loops in known ratios—the measured values of the individual bands were found to be within 10% of their true values.

Equation for a skew normal/skewed Gaussian distribution:

$$A \cdot \mathrm{e}^{-\left(\frac{x-b}{c}\right)^2} \cdot (1 + \mathrm{erf}(a\frac{x-b}{c})$$

Data Analysis

Based on a gel we ran to establish repeatability of pipetting and imaging, we conservatively estimate the error per lane at ± 5% plus the detection limit (which will vary by imager). For lanes that used a reference band to normalize brightness, the 5% error per band was propagated to yield roughly 7% error per measurement. Error bars were produced based on this analysis, and all fitting procedures used an error weighted least squares fit. Timed pipetting for on-rate experiments was conservatively assumed to have an error of 2 seconds, which was propagated to overall y-error by multiplying by the derivative of a preliminary fit.

Model

The time evolution of DNA nanoswitch states are modeled using multistep reaction kinetics. On rates are modeled as a two-step process:

$$Unbound\ Linear\ \rightarrow Singly\ Bound\ Linear\ \rightarrow Looped$$

Step 1 represents the binding of a free receptor in solution to a ligand on the scaffold (yielding the solution on-rate), Step 2 represents the subsequent binding of this receptor to another ligand on the same scaffold to form a loop (yielding the loop-closure rate). On-rate and off-rate models for both the two-state and five-state systems are detailed in **Note** 2.

Thermodynamic Analysis

The dissociation constant K_D was determined by the ratio of the off- and on-rates, and the equilibrium free energy ΔG^0 was determined by:

$$\Delta G^0 = -RT\ln(\widetilde{K}_{\mathrm{D}})$$

Where R is the gas constant, T is the absolute temperature, and the dissociation constant, which is determined by dividing the off rate by the on rate, and is made dimensionless by dividing it by a reference concentration, i.e. $\widetilde{K}_{\mathrm{D}} = K_{\mathrm{D}}/(1M)$. We additionally used Eyring analysis to fit the temperature dependence of the kinetic rates:

$$\ln\left(\frac{k}{T}\right) = \frac{-\Delta H}{R}\left(\frac{1}{T}\right) + \ln\left(\frac{k_B}{h}\right) + \frac{\Delta S}{R}$$

Where k is the kinetic rate constant, k_B is the Boltzman constant, h is Plank's constant, and ΔH and ΔS are the enthalpy and entropy of activation, respectively.

For the salt dependence, we used the kinetic salt relationship:

$$\log(k) = \log(k_0) + 2A \cdot Z_{\mathrm{A}} \cdot Z_{\mathrm{B}}\sqrt{I}$$

Where k is the kinetic rate constant, k_0 is the rate constant without the salt, A is the Debye-Hückel constant, Z_A and Z_B are the charges on the two interacting species, and I is the ionic strength of the solution.

References:

17. Strunz T, Oroszlan K, Schäfer R, & Güntherodt HJ. *Proc. Natl. Acad. Sci. USA* **96** 11277-11282 (1999).

Competing financial interests: Patent applications have been filed for various aspects of this work by KH, MAK and WPW

Note 1: Kinetic Models

Two-state kinetic model

For off-rate measurements of two-band systems, the data was fit to a single exponential decaying to zero. In the case of biotin-streptavidin measurements, the time constants were multiplied by two since each streptavidin has two pathways to cause the loop to dissociate. For on-rate measurements of two-band systems, we used a kinetic model consisting of 4 states and two kinetic rate constants. Reverse rates were not considered to play a role since they were many orders of magnitude slower. This model results in a nonlinear system of differential equations that can be solved numerically (using NDsolve in Mathematica, for example). In our case, however, we were able to reduce these to a linear system of differential equations by using the assumption that the concentration of streptavidin is constant, which is a good approximation for our experimental conditions since the streptavidin was at a much higher concentration than the biotin-looped construct (3nM vs. 80pM). Furthermore, we validated this approximation by comparing our results with the full numerical solution, and saw no discernable differences. Thus, the effective system of differential equations for the on-rate measurement s is:

$$
\begin{aligned}
a'(t) &= -S \cdot k_1 \cdot 2a(t) \\
b'(t) &= S \cdot k_1 \cdot \big(2a(t) - b(t)\big) - k_2 \cdot b(t) \\
c'(t) &= k_2 \cdot b(t) \\
d'(t) &= S \cdot k_1 \cdot b(t)
\end{aligned}
$$

Where a(t) is the concentration of unlooped construct with no ligands bound, b(t) is the concentration of unlooped construct with only one ligand bound to one receptor, c(t) is the

concentration of looped construct with two ligands bound to a single common receptor molecule, d(t) is concentration of unlooped construct with both ligands bound to different receptor molecules, S is the concentration of streptavidin, and k1 and k2 are the per-site kinetic rates for streptavidin binding from solution and loop closure, respectively (accounting for the fact that in solution streptavidin has 4 binding sites, and after binding there are only 3 avaliable binding sites for loop closure). Note that k2 does not depend on the concentration of strepavidin in solution, since the loop closure rate is governed by an effective local concentration within the nanoswitch that is set by the loop length. This system of equations results in an analytical expression:

$$c(t) = \frac{A_o[3k_2 - 3k_2e^{-8k_1St} - 4k_1S - 4k_1Se^{-8k_1St} + 8k_1Se^{(-3k_2-4k_1S)t}]}{(3k_2 - 4k_1S)}$$

$$A_o = \lim_{t\to\infty} c(t)$$

C(t) was fit to the data with three free parameters, *k1*, *k2*, and Ao. In the regime of concentrations that we used (local biotin > free streptavidin > nanoswitches), the on-rate fi ing was less sensitive to *k2* than *k1*, and constraining *k2*/*k1* for the fits resulted in solution on-rates that overlapped within error with fits using *k1* and *k2* as free parameters.

This model allows for the determination of both the solution on-rate, which is independent of the polymer looping kinetics, and the loop closure rate as illustrated in **Figure 2.5**.

Additionally, to examine the effect of ligand placement on the determination of the solution on rate, we conducted biotin-streptavidin on-rate experiments with a variety of ligand positions at room temperature. The results, shown in **Table 2.5**, indicate that the solution on-rate

measurements are in reasonable agreement, exhibiting a relative standard error of the mean (1.29×10^6 M^{-1} s^{-1}) of 13%.

Ligand Positions	Solution on-rate (10^6 M^{-1} s^{-1}) (per binding site)
4-8	1.03 ± 0.15
8-12	1.34 ± 0.28
4-12	1.06 ± 0.29
1-12	1.75 ± 0.21
Mean	1.29 ± 0.17

Table 2.5| Solution on-rate is independent of loop size. Solution on-rate values reported are the weighted means of 3 experiments with the errors being the weighted standard deviation. The mean value is the mean of the solution on-rates from the four different ligand positions with the error given by the standard error of the mean. All values are reported as a per-binding site on-rate. To get the per-molecule on-rate, one would need to divide these values by one molecule per four binding sites (i.e. multiply by 4).

To further test the robust nature of the system we analyzed the effect of keeping the ligand positions constant while altering the concentration of the receptor (**Table 2.6**). We found that the measured solution on-rates are in reasonable agreement even when varying the receptor concentrations by an order of magnitude, yielding a relative standard deviation of 13%. Note that working outside this range may be difficult as protein concentrations become unreliable below 1 nM, and the rate of loop formation becomes very fast above 10 nM (see methods for details).

Multistate off-rate model

For off-rate measurements of multistate (5 band) systems we used a model consisting of 5 topological states and 3 rate constants. Reverse rates were not considered to play a role as the presence of excess quencher prevents the closure of loops. This model results in a linear system of differential equations.

$$\mathbf{A}'(t) = -(kb + kd8 + kd12) * \mathbf{A}(t)$$

$$\mathbf{B}'(t) = kd8 * A(t) - (kb + kd12) * \mathbf{B}(t)$$

$$\mathbf{C}'(t) = kd12 * A(t) - (kb + kd8) * \mathbf{C}(t)$$

$$\mathbf{D}'(t) = kb * A(t) - (kd8 + kd12) * \mathbf{D}(t)$$

$$\mathbf{E}'(t) = (kb + kd12) * \mathbf{B}(t) + (kb + kd8) * \mathbf{C}(t) + (kd8 + kd12) * \mathbf{D}(t)$$

Where kb is the biotin off rate, kd8 is the off rate of the digoxigenin on var 8, kd12 is the off rate of the digoxigenin on var 12, $\mathbf{A}(0)$-$\mathbf{E}(0)$ are the starting fractions of construct in each state A-E illustrated in Figure 2.7. These differential equations can be easily solved analytically (for example, using Dsolve in Mathematica), resulting in the following set of equations:

$$\mathbf{A}(t) = \mathbf{A}(0)e^{(-kb - kd12 - kd8)t}$$

$$\mathbf{B}(t) = \mathrm{e}^{(-\mathrm{kb}-\mathrm{kd12}-\mathrm{kd8})\mathrm{t}}\left(-\mathbf{A}(0)\left(\mathrm{e}^{(kd8)t}-1\right)+\mathbf{B}(0)\mathrm{e}^{(kd8)t}\right)$$

$$\mathbf{C}(t) = \mathrm{e}^{(-\mathrm{kb}-\mathrm{kd12}-\mathrm{kd8})\mathrm{t}}\left(-\mathbf{A}(0)\left(\mathrm{e}^{(kd12)t}-1\right)+\mathbf{C}(0)\mathrm{e}^{(kd12)t}\right)$$

$$\mathbf{D}(t) = \mathrm{e}^{(-\mathrm{kb}-\mathrm{kd12}-\mathrm{kd8})\mathrm{t}}\left(-\mathbf{A}(0)\left(\mathrm{e}^{(kb)t}-1\right)+\mathbf{D}(0)\mathrm{e}^{(kb)t}\right)$$

$$\begin{aligned}\mathbf{E}(t) = \mathrm{e}^{(-\mathrm{kb}-\mathrm{kd12}-\mathrm{kd8})\mathrm{t}}&\left(\mathbf{A}(0)\left(2-\mathrm{e}^{(kb)t}-\mathrm{e}^{(kd12)t}-\mathrm{e}^{(kd8)t}+\mathrm{e}^{(\mathrm{kb}+\mathrm{kd12}+\mathrm{kd8})\mathrm{t}}\right)\right.\\&+\mathbf{B}(0)\left(\mathrm{e}^{(\mathrm{kb}+\mathrm{kd12}+\mathrm{kd8})\mathrm{t}}-\mathrm{e}^{(kd8)t}\right)+\mathbf{C}(0)\left(\mathrm{e}^{(\mathrm{kb}+\mathrm{kd12}+\mathrm{kd8})\mathrm{t}}-\mathrm{e}^{(kd12)t}\right)\\&+\mathbf{D}(0)\left(\mathrm{e}^{(\mathrm{kb}+\mathrm{kd12}+\mathrm{kd8})\mathrm{t}}-\mathrm{e}^{(kb)t}\right)+\mathbf{E}(0)\mathrm{e}^{(\mathrm{kb}+\mathrm{kd12}+\mathrm{kd8})\mathrm{t}}\end{aligned}$$

These equations were then fit to the data using fminsearch to minimize the chi-squared in MATLAB with kb, kd8, kd12, **A**(0), **B**(0), **C**(0), **D**(0), and **E**(0) as free parameters.

Multistate on-rate model

For the on-rate measurements of multistate (5 band) systems we used the model described below. This model results in a system of differential equations that can be solved numerically (using ODE15s in matlab, for example) with the following assumptions: The reverse rates were not considered to play a role since they were many orders of magnitude slower, and the concentration of the bispecific receptor is considered to be constant, which is a good approximation for our experimental conditions since the bispecific receptor was at a much higher concentration than the nanoswitches (3nM vs. 80pM).

The on rate model is schematized generally in the figures s5 and s6, followed by the differential equations that comprise the model.

Models were fit to experimental data using fminsearch in matlab to find the minimum of the χ^2:

$$\chi^2 = \sum_{i=1}^{N} \frac{\left(y_i^{exp} - y_i^{model}\right)^2}{\sigma_i^2}$$

y_i^{exp} is the ith experimental data point. y_i^{model} is the theoretical prediction given by the model of the ith data point, and σ_i^2 is the variance in the ith experimental data point.

To estimate errors on the fit parameters obtained using fminsearch, we calculated the local curvature of the χ^2as a function of each fit parameter. The variance of the fit parameter is estimated by $\left(\sigma_{x_i}\right)^2 = 2\left(\frac{\partial^2 \chi 2}{\partial x_i^2}\right)^{-1}$ where x_i is the ith fit parameter.

Multistate on-rate model details

In addition to loop formation our model accounts for the presence of scaffolds that lack one or more ligand, and for the phenomenon of capping, in which two or more receptor molecules bind to a single scaffold. The model assumes that the concentration of the bispecific receptor molecule, S, is constant, as it is in great excess compared to the scaffold. Additionally, as the time scales for the on rate are much smaller than those for the off rate, the model assumes no unbinding events occur during loop formation.

Bold letters **A**, **B**, **C**, **D**, and **E** represent topological states composed of the individual states, illustrated in figure s5, as follows:

$$\mathbf{A}(t) = A(t)$$

$$\mathbf{B}(t) = B(t) + Bk(t) + Bo(t)$$

$$\mathbf{C}(t) = C(t) + Ck(t) + Co(t)$$

$$\mathbf{D}(t) = B(t) + Dk(t) + Do(t)$$

$$\mathbf{E}(t) = EA(t) + Eb(t) + Ed8(t) + Ed12(t) + Ebd8(t) + Ebd12(t) + Ed8d12(t) + Ek(t) + EBo(t) + Ed12Bo(t) + EbBo(t) + EBok(t) + ECo(t) + Ed8Co(t) + EbCo(t) + ECok(t) + EDo(t) + Ed12Do(t) + Ed8Do(t) + EDok$$

A linear piece of DNA that has all three ligands, and therefore has the ability to enter state A, is referred to as being in state EA.

Molecules can transition from state EA into either state Eb, Ed8, or Ed12 indicating a linear strand of DNA with a receptor bound to the biotin, var 8-dig, or var 12-dig respectively. Additionally molecules can transition out of these states either by binding a second receptor, or by forming a loop as indicated by the following equations:

$$Eb'(t) = 4\ kb\ \ S\ \ EA(t) - (\ kd12B + kd8C\ )\ \ Eb(t) - 2\ \ kd8\ \ S\ \ Eb(t) - 2\ \ kd12\ \ S\ \ Eb(t)$$

$$Ed8'(t) = 2 * kd8 * S * EA(t) - (\ kbC + kd12D\ ) * Ed8(t) - 4 * kb * S * Ed8(t) - 2 * kd12 * S * Ed8(t);$$

$$Ed12)'(t) = 2 * kd12 * S * EA(t) - (\ kbB + kd8D\ ) * Ed12(t) - 4 * kb * S * Ed12(t) - kd8 * 2 * S * Ed12(t);$$

Where kb, kd8, and kd12 are the per-site solution on rates for biotin, the dig on var 8, and the dig on var 12 respectively, and S is the concentration of the bi-specific receptor, assumed to be constant in time.

The formation of linear constructs with two receptor molecules bound can be modeled with the following equations:

Ebd8′(t) = 2 * kd8 * S * Eb(t) + 4 * kb * S * Ed8(t) – (kd12D + kd12B + 2 * kd12 * S) * Ebd8(t);

Ebd12′(t) = 2 * kd12 * S * Eb(t) + 4 * kb * S * Ed12(t) – (kd8C + kd8D + 2 * kd8 * S) * Ebd12(t);

Ed8d12′(t) = 2 * kd12 * S * Ed8(t) + kd8 * 2 * S * Ed12(t) – (kbC + kbB + 4 * kb * S) * Ed8d12(t);

Where Ebd8 indicates a linear scaffold with a receptor molecule bound to the biotin and a receptor molecule bound to the dig on var 8, Ebd12 indicates a linear scaffold with a receptor molecule bound to the biotin and a receptor molecule bound to the dig on var 12, Ed8d12 indicates a linear scaffold with a receptor molecule bound to the dig on var 8, and a receptor molecule bound to the dig on var 12

The linear EA state can also be capped by 3 separate receptor molecules.

Ek′(t) = 2 * kd12 * S * Ebd8(t) + 2 * kd8 * S * Ebd12(t) + 4 * kb * S * Ed8d12(t);

A linear piece of DNA that is missing one ligand cannot form state A. These linear pieces of DNA are referred to by the highest order loop they can form. Thus, a scaffold that only has a biotin on var 4 and a dig on var 12, and can therefore only form loop B, is referred to as EBo; a scaffold that only has a biotin on var 4 and a dig on var 8, and therefore can only form loop C, is

referred to as ECo; a scaffold that only has a dig on var 8 and a dig on var 12, and can therefore only form loop D, is referred to as EDo.

Molecules can transition from state EBo into either state EbBo, or Ed12Bo indicating a linear molecule with a receptor bound to the biotin, or var 12-dig respectively. Additionally molecules can transition out of these states either by binding a second receptor, or by forming a loop as indicated by the following equations:

EbBo'(t) = 4 * kb * S * EBo(t) – kd12B * EbBo(t) – 2 * kd12 * S * EbBo(t);

Ed12Bo'(t) = 2 * kd12 * S * EBo(t) – kbB * Ed12Bo(t) – 4 * kb * S * Ed12Bo(t);

Molecules can transition from state ECo into either state EbCo, or Ed8Co indicating a linear molecule with a receptor bound to the biotin, or var 8-dig respectively. Additionally molecules can transition out of these states either by binding a second receptor, or by forming a loop as indicated by the following equation:

EbCo'(t) = 4 * kb * S * ECo(t) – kd8C * EbCo(t) – 2 * kd8 * S * EbCo(t);

Ed8Co'(t) = 2 * kd8 * S * ECo(t) – kbC * Ed8Co(t) – 4 * kb * S * Ed8Co(t);

Molecules can transition from state EDo into either state Ed8Do, or Ed12Do indicating a linear molecule with a receptor bound to the var 8-dig, or var 12-dig respectively. Additionally molecules can transition out of these states either by binding a second receptor, or by forming a loop as indicated by the following equation:

Ed12Do′(t) = 2 * kd12 * S * EDo(t) – kd8D * Ed12Do(t) – 2 * kd8 * S * Ed12Do(t);

Ed8Do′(t) = 2 * kd8 * S * EDo(t) – kd12D * Ed8Do(t) – 2 * kd12 * S * Ed8Do(t);

The following three equations represent scaffolds which have only two ligands, and become capped by the binding of two separate receptors.

EBok′(t) = 2 * kd12 * S * EbBo(t) + 4 * kb * S * Ed12Bo(t);

ECok′(t) = 2 * kd8 * S * EbCo(t) + 4 * kb * S * Ed8Co(t);

EDok′(t) = 2 * kd8 * S * Ed12Do(t) + 2 * kd12 * S * Ed8Do(t);

The rate of loop closure is described by the following equations.

A′(t) = kd8A * B(t) + kd12A * C(t) + kbA * D(t);

B′(t) = kd12B * Eb(t) + kbB * Ed12(t) – kd8A * B(t) – 2 * kd8 * S * B(t);

C′(t) = Eb(t) * kd8C + Ed8(t) * kbC – kd12A * C(t) – 2 * kd12 * S * C(t);

D′(t) = Ed8(t) * kd12D + Ed12(t) * kd8D – kbA * D(t) – 4 * kb * S * D(t);

Where kbB is the rate of biotin binding to form state B, kbC is the rate of biotin binding to form state C, kd8C is the rate of dig binding to var-8 form state C, kd8D is the rate of dig binding to var-8 form state D, kd12B is the rate of dig binding on var-12 to form state B, kd12D is the rate of dig binding on var-12 to form state D.

Loops which could transition into state A but are capped by having a second receptor molecule bind to the remaining ligand can be described as follows:

$$Bk'(t) = 2 * kd8 * S * B(t) + kd12B * Ebd8(t) + kbB * Ed8d12(t);$$

$$Ck'(t) = 2 * kd12 * S * C(t) + kd8C * Ebd12(t) + kbC * Ed8d12(t);$$

$$Dk'(t) = 4 * kb * S * D(t) + kd12D * Ebd8(t) + kd8D * Ebd12(t);$$

Where Bk, Ck, and Dk are the capped versions of Loops B, C, and D respectively.

A linear piece of DNA that is missing one ligand cannot form state A. These linear pieces of DNA are referred to by the highest order loop they can form. Such that a scaffold that only has a biotin on var-4 and a dig on var-12, and can therefore only form loop B, is referred to as EBo; a scaffold that only has a biotin on var-4 and a dig on var-8, and therefore can only form loop C, is referred to as EBo; a scaffold that only has a dig on var-8 and a dig on var-12, and can therefore only form loop D, is referred to as Edo.

$$Bo'(t) = kd12B * EbBo(t) + kbB * Ed12Bo(t);$$

$$Co'(t) = kd8C * EbCo(t) + kbC * Ed8Co(t);$$

$$Do'(t) = kd12D * Ed8Do(t) + kd8D * Ed12Do(t);$$

Given these equations the amount of EA, EBo, ECo, and EDo can be described as follows:

EA(t) = EA_Start – Eb(t) – Ed8(t) – Ed12(t) – A(t) – B(t) – C(t) – D(t) – Ebd8(t) – Ebd12(t) – Ed8d12(t) – Ek(t) – Bk(t) – Ck(t) – Dk(t);

EBo(t) = EB_Start – EbBo(t) – Ed12Bo(t) – Bo(t) – EBok(t);

ECo(t) = EC_Start – EbCo(t) – Ed8Co(t) – Co(t) – ECok(t);

EDo(t) = ED_Start – Ed12Do(t) – Ed8Do(t) – Do(t) – EDok(t);

Multistate Kinetics Results:

Fi ing the data with these on-rate and off-rate models, and using fminsearch to reduce the chi squared yielded the values reported in **Table 2.4** for the fit parameters.

Note 2: Semiempirical formula for temperature and salt dependence

The temperature and salt dependence were analyzed using Eyring analysis and kinetic salt effect theory, respectively[9] (Figure 2.2). Empirically, we found that these dependencies were separable over our measurement range, giving the following expression for the off -rate of DNA-linked biotin from streptavidin as a function of salt (25mM-500mM) and temperature (25°C-50°C):

$$\ln\left(\frac{k_{off}}{T}\right) \approx A + \frac{B}{T} + C\sqrt{I}$$

where koff is the value of the off-rate in s^{-1}, T is the value of the absolute temperature in K, and I is the value of the ionic strength of the solution in mM. From a 2D least squares fit of our data,

we found an offset A of 42.41 ± 1.7, an enthalpic prefactor B of -1.83 ± 0.06 x 10^4, and a salt dependence C of -0.033 ± 0.01. We note that the off rates used in developing this formula match off rates measured using a radiolabeled biotin-functionalized oligo under similar conditions, and are slower than the off rates measured using a free biotin.

Detailed Protocol

Preface:

This document serves as a detailed protocol to provide you with all the information needed to implement the nanoswitch platform in your lab. The protocol will walk you through all the steps required to form nanoswitches, and use them to make on-rate and off-rate measurements. The protocol goes through the specific steps required to make measurements on the ubiquitous biotin-streptavidin system, with notes about where changes can be made to adapt the platform to your system of interest. While supplies last, we are happy to provide a starter kit, which contains all of the oligonucleotides needed to perform these measurements, to any interested labs. The detailed contents of the kit are described in section 2 of this protocol. Anyone interested in obtaining a starter-kit for their lab should visit http://wonglab.tch.harvard.edu/nanoswitch/ .

Protocol:

1. Linearizing the M13 Scaffold

To begin one must first prepare the linear single-stranded M13 scaffold. We do this by using a synthetic oligonucleotide complementary to the site where we want to cut that creates a double stranded region allowing the restriction enzyme BtsCI to cleave the M13 scaffold. The following will walk you through the procedure needed to make the linear scaffold.

Note: We recommend using Eppendorf LoBind tubes and Corning DeckWorks Lowbind Tips (Corning Product #s: 4121 and 4147) for all liquid handling.

1.1 Reagents needed:

1.1.1 250µg/ml (~100nM) Circular single-stranded M13 DNA (New England Biolabs Catalog#: N4040S)

1.1.2 100µM Synthetic oligonucleotide complementary to the BtsCI restriction site (sequence 5′->3′: CTACTAATAGTAGTAGCATTAACATCCAATAAATCATACA).

1.1.3 BtsCI (20,000 units/ml) Restriction Enzyme (New England Biolabs Catalog#: R0647S or R0647L)

1.1.4 10x NEBuffer 2 (New England Biolabs Catolog #: B7002S)

1.1.5 Nuclease Free Water (Invitrogen Ultrapure Distilled Water DNAse and RNAse free Catalog # 10977-015)

1.2 Mix the following in a PCR tube (Axygen PCR-02D-C)

1.2.1 ____ 5µl of 100nM circular single-stranded M13 DNA

1.2.2 ____ 2.5µl of 10x NEBuffer 2

1.2.3 ____ 0.5µl of 100µM BtsCI restriction-site complimentary-oligonucleotide

1.2.4 ____ 16µl of Nuclease Free Water

1.2.5 ____ Pipette to mix thoroughly being sure to avoid air bubbles

1.3 ____ Place the tube in a thermocycler and subject to the following linearization protocol:1

1.3.1 ____ Bring to 95° C and hold for 30 seconds

1.3.2 ____ Cool to 50° C

1.3.3 ____ Add 1µl of the BtsCI enzyme

- Mix thoroughly with a pipette to ensure enzyme is well mixed. The enzyme is in glycerol and will sink to the bottom if not mixed well. It is best to use a pipette set to ~10µl to do this as the 1µl pipette may not provide adequate mixing. Failure to do this may greatly lower linearization efficiency.

1.3.4 ____ Allow the mixture to sit at 50° C for 1 hour

1.3.5 ____ Bring the mixture up to 95° C for 1 minute to heat deactivate the enzyme

- For convenience you may want to set the thermocycler to hold at 4°C after completion

1.3.6 This will result in 25µl of ~20nM linearized circular M13 in NEBuffer 2

- We have scaled this up as much as 4 times resulting in 100µl of final product with no obvious reduction in linearization efficiency
- Additionally we have found the linearization to be equally efficient in NEBuffers 2, 2.1,4, and cutsmart

- To aid in quantification the linearized DNA can be spiked with 1 µl BstNI Digest of pBR322 DNA (New England Biolabs). This provides low molecular weight bands which can be used as intensity references to combat errors in pipetting at later stages

Now that linear single-stranded scaffold is made you will need the set of oligonucleotides that are complementary to the scaffold. We have chosen to use 60 nt oligonucleotides. This yields 120 60 nt oligonucleotides and one 49 nt oligonucleotide. We have divided these oligonucleotides into two groups to avoid having to mix 121 oligonucleotides for each construct. A mixture of 12 oligonucleotides evenly spaced along the backbone are each stored in their own tubes and referred to as variable regions or Vars. The remaining 109 oligonucleotides are all pre mixed together and we refer to these as backbone oligonucleotides. We have created a SnapGene DNA file which has these regions highlighted and labeled (in the SnapGene file, the bottom strand is the M13 sequence while the top strand represents the oligonucleotide sequences). SnapGene Viewer is freely available software that can be downloaded at: http://www.snapgene.com/products/snapgene_viewer/ . Images exported from SnapGene can be found below. The SnapGene file can be found at: https://drive.google.com/file/d/0B_SawyS5qEUaldiUFlGbHkwczQ/view?usp=sharing , an excel file with the 109 backbone oligonucleotides can be found at: https://drive.google.com/file/d/0B_SawyS5qEUcEF3OF9ZQkRTeWM/view?usp=sharing , and an excel file with the 12 variable oligonucleotides can be found at: https://drive.google.com/file/d/0B_SawyS5qEUbTVHdUp6V0NUUjQ/view?usp=sharing.c

Additionally, these files are available in the online supplementary materials on nature method's website (http://www.nature.com/nmeth/journal/v12/n2/full/nmeth.3209.html).

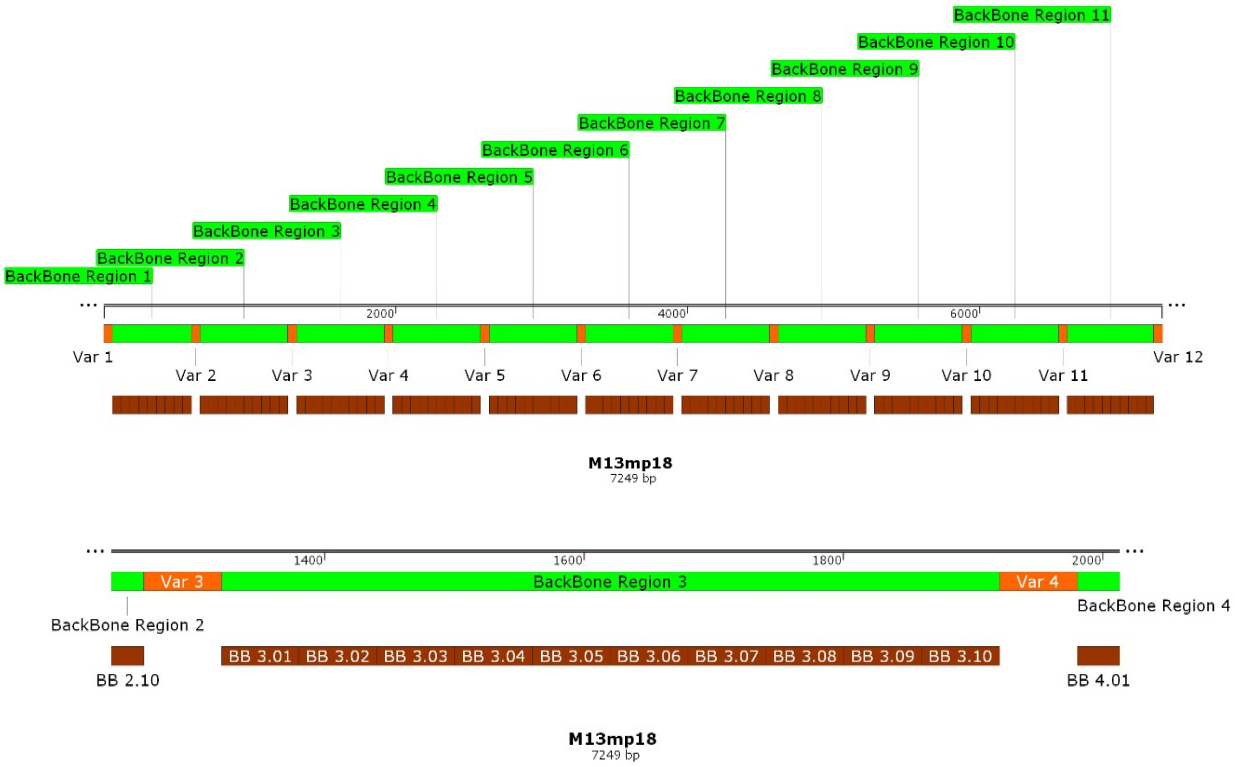

Figure 2.11| (Top) Linearized M13 showing the 12 evenly spaced Var 1-Var 12(orange) oligonucleotides interrupted by 11 back bone regions (green), each of which is filled with 10 backbone oligonucleotides (maroon) (with the exception of backbone region 1 which only has 9 backbone oligonucleotides). (**Bottom)** we have zoomed in on the region between Var 3 and Var 4.

2. Materials available upon request:

To facilitate trying the nanoswitch platform in your lab, we have ordered some materials for starter kits that we will provide while supplies last. We will provide a mixture of the 109 backbones, a mixture of the 10 Vars (Vars 1, 2, 3, 5, 6, 7, 9, 10, 11, and 12), and a mixture of Var 4-3'biotin and 5'biotin-Var 8. The 109 mix can be used in conjunction with the provided Var oligos to create scaffolds capable of forming loops between Vars 4 and 8 upon the addition of streptavidin. Additionally, one could use the 109 mix in conjunction with 12 separately purchased Var oligonucleotides (or the 10 var mix and separately purchased Var 4 and Var 8 oligonucleotides) which can be functionalized to your specific needs. Protocols for functionalizing oligonucleotides for incorporation into this scaffold can be found in Halvorsen et al. 2011 and Koussa et al. 2014.

Below we provide a protocol for using the included 109 mix, the 10 Var Mix, and the mix of the two biotinylated oligonucleotides, to make biotin-SA on-rate and off-rate measurements.

3. Building the construct:

3.1 Hybridize the 121 oligonucleotides to the scaffold

3.1.1 ____ Hydrate provided oligonucleotides

3.1.2 ____ Hydrate the 109 backbone oligonucleotide mixture with nuclease free water to achieve a total oligonucleotide concentration of 100μM (10μl per nanomole).

3.1.3 ____ Hydrate the 10 var mixture with nuclease free water to achieve a total oligo concentration of 100μM (10μl per nanomoles).

3.1.4 ____ Hydrate the mixture of the two biotinylated vars with nuclease free water to achieve a total oligonucleotide concentration of 100μM (10μl per nanomoles)

3.1.5 ____ Create a mixture of 119 unfunctionalized oligonucleotides

- To help ensure that each scaffold has all of its oligonucleotides hybridized we recommend putting the oligonucleotides in at a 10 fold excess to the scaffold. As having many excess biotinylated oligonucleotides would be costly and problematic for on-rate experiments, the biotinylated oligonucleotides will only be put in at a 4x excess to the scaffold. As all of the oligonucleotides are mixed in an equimolar fashion, adding 1.09 μl of the 109 mixture is simply like adding 0.01 μl of each of the 109 oligonucleotides at 100μM.

3.1.6 ____ Mix the following in an Eppendorf DNA LoBind tube (0030 108.035)

a. ____ 10.9µl of the 100µM 109 backbone mix

b. ____ 1.0 µl of the 10 Var mixture

3.2 Mix the single stranded scaffold, unfunctionalized oligonucleotides, and functionalized oligonucleotides

3.2.1 Mix the following in an Axygen PCR tube

a. ____ 5µl of 20nM linear single-stranded M13 DNA (see Section 1)

b. ____ 1.19µl the mixture of 119 unfunctionalized oligonucleotides

- This is essentially like adding 0.01 µl of each oligonucleotide at 100µM which gives a 10 fold excess to the 5µl of 20nM scaffold

c. ____ 0.8 µl of 100x dilute biotinylated Var mixture (1µl of the mixture of functionalized Var 4 and Var 8 + 99µl of nuclease free water)

- This is essentially like adding 0.004 µl of each of the biotinylated Vars at 100µM thus giving a 4 fold excess compared to the scaffold

d. ____ 0.22 µl of 10x NEBuffer 2

e. ____ Pipette to mix thoroughly

3.2.2 Place the mixture in a thermocycler and subject it to the following protocol

a. ____ Heat the sample to 90° C

b. ____ Cool the sample 1°C per minute until it reaches 20°

- Note: if non-thermostable custom functionalized-oligonucleotides are used these oligonucleotides should not be added in until after the mixture has reached a temperature compatible with the functionalized oligonucleotide
- For convenience you may want to set the thermocycler to hold at 4°C after completion

3.3 Optional PEG precipitation step to remove excess oligonucleotides.

Large pieces of DNA such as the scaffold will precipitate out, while smaller pieces of DNA such as the oligonucleotides will remain in the supernatant. (This is not necessary for the biotinstreptavidin experiments but may be useful for custom applications).

Note: that the precipitation efficiency is very sensitive to the concentration of the PEG so it helps to make a large stock of PEG that you can calibrate so that you do not have to calibrate your

concentration every time you make a new PEG stock

3.3.1 Make a 30% (by weight) stock of 8k PEG (Polyethylene Glycol 8000 Amresco 0159-500G)

a. ____ Add 15g of 8k PEG to a 50 ml falcon tube

b. ____ Bring this up to 50 ml with nuclease free water

3.3.2 Make 2 dilutions of your PEG stocks in protein LoBind tubes as follows (As mentioned above, the efficiency is very sensitive to PEG concentration thus the following percentages may not work for you and you may have to tweak the percentages for your 30% stock

a. 4.75% PEG in 30mM MgCl2 (This is higher so that when mixed with the 40µl of

DNA the final PEG concentration will be ~3.5%)

i. ____ 38 µl of 30% PEG stock

ii. ____ 24 µl of 300mM MgCl2

iii. ____ 178 µl of nuclease-free water

b. 3.5% PEG in 30mM MgCl2

i. ____ 28 µl of 30% PEG stock

ii. ____ 24 µl of 300mM MgCl2

iii. ____ 188 µl of nuclease-free water

3.3.3 Dilute your hybridized construct to 40 µl in 30mM MgCl2 in a DNA LoBind tube □

For example, if you have 8 µl of the hybridized DNA/oligonucleotide mix then to this mix you should add 4 µl of 300mM MgCl2 and 28 µl of nuclease-free water

3.3.4 Perform the PEG precipitation

a. ____ Add 115 µl of 4.75% PEG and mix thoroughly

b. ____ Centrifuge at 16,000 rpm for 30 minutes at room temperature

c. ____ Carefully remove the top 145 µl

- This should be done very carefully as it is easy to disturb the pellet it should take roughly 30 seconds to slowly pipette out the supernatant in one smooth draw. It helps to constantly be pipetting near the fluid-air boundary as to be as far away from the pellet as possible

d. ____ Add 115 µl of 3.5% PEG and mix thoroughly

e. ____ Centrifuge at 16,000 rpm for 30 minutes at room temperatur

f. ____ Carefully remove the top 115 µl

- This should be done very carefully as it is easy to disturb the pellet it should take roughly 30 seconds to slowly pipette out the supernatant in one smooth draw. It helps to constantly be pipetting near the fluid-air boundary as to be as far away from the pellet as possible

- ____ Add 115 µl of 3.5% PEG and mix thoroughly

- ____ Centrifuge at 16,000 rpm for 30 minutes at room temperature

- ____ Carefully remove the top 115 µl

- This should be done very carefully as it is easy to disturb the pellet it should take roughly 30 seconds to slowly pipette out the supernatant in one smooth draw. It helps to constantly be pipetting near the fluid-air boundary as to be as far away from the pellet as possible

- The remaining 10 µl should have the hybridized DNA scaffold free of any detectable amount of free floating oligonucleotides

This construct is now ready for use in on-rate experiments.

4. On-rate Experiments:

To avoid the formation of aggregates (streptavidin molecules linking multiple scaffolds) we work at low construct concentrations (i.e. the concentration of the construct should be lower than the effective concentration of the two biotins on the scaffold, which in the case of Vars 4 and 8, is ~30nM. The construct prepared in the above protocol (3.2) is at a concentration of ~16nM. To ensure that aggregation is not an issue we will dilute this 100 fold.

4.1 Dilute the construct 100 fold to achieve a concentration of 160 pM. (note if you used oligonucleotides at lower concentration your construct may already be less concentrated than 16nM if you used different volumes in creating your construct you must calculate the final construct concentration)

4.1.1 ____ In an Eppendorf protein LoBind tube(0030 108.094), mix 1µl of your construct with 99µl of the buffer in which you wish to do the experiment

One buffer condition that we recommend for biotin streptavidin experiments is 1x NEBuffer 2 supplemented with an additional 150mM NaCl (total 200mM NaCl)

4.1.2 To make 2 ml of this mix the following

a. ____ 200 µl of 10x NEBuffer 2

b. ____ 100 µl of 3M NaCl in nuclease-free water

c. ____ 1,700 µl of nuclease-free water

To avoid capping (i.e. the binding of two streptavidin molecules to one construct thus rendering that construct unloopable) the streptavidin concentration should also be well below the effective concentration of the ligands on the scaffold which for Vars 4 and 8 is ~30nM. To achieve this we will dilute the streptavidin to ~6nM so that when mixed in equal volumes with the scaffold the final concentration of streptavidin is one-tenth of the effective concentration of the two biotins on the loop.

1mg/ml streptavidin (Rockland catalog number: S000-01) has a concentration of ~15µM diluting this 2,500 fold will bring the streptavidin to a nominal concentration of 6nM. We measured the concentration of our streptavidin, and its activity (using a HABA assay) and found that our results closely match the data sheet provided by Rockland yielding a final streptavidin concentration of 6.88 nM which when mixed 1:1 with the construct yielded a streptavidin concentration of 3.44nM

4.2 Dilute the streptavidin 2,500 fold

4.2.1 ____ In an Eppendorf protein LoBind tube, mix 4µl of 1mg/ml streptavidin with 196µl of the same buffer used to dilute the construct. This yields a ~300nM stock of streptavidin

4.2.2 ____ In another Eppendorf protein LoBind tube, mix 4µl of the ~300nM streptavidin with 196µl of the same buffer used to dilute the construct. This yields a ~6nM stock of streptavidin (This low concentration solution should be made fresh before each experiment)

4.3 Preparation for on-rate experiments

To do the on-rate measurement equal volumes of 160pM construct and 6nM streptavidin will be combined. Loops will immediately start forming. To halt loop formation the construct can be quenched with free biotin to occupy all free sites on streptavidin thus preventing further loop closure events. If fractions of the construct are quenched with biotin at different times this yields an on-rate time series.

The rate of loop closure with 3 nM streptavidin and 80 pM scaffold saturates after roughly 2 minutes. A good series of time points to cover this range well is 5 seconds, 10 seconds, 15 seconds, 20 seconds, 30 seconds, 40 seconds, 60 seconds, 80 seconds, 120 seconds, 360 seconds.

As you will only have 5 seconds between the first couple of time points you will want to prepare all of your tubes and quencher ahead of time. Below we provide a very detailed approach to doing these experiments which we have found greatly facilitates performing on-rate measurements.

To prepare the biotin quencher you will want to make a saturated solution of biotin (Sigma-

Aldrich B4501-100MG) (0.22mg/ml ~1mM) in nuclease free water. To ensure the solution is saturated we recommend having excess powder in the tube. The tube can be vortexed then centrifuged before each use.

4.4 Performing an on-rate experiment with the above mentioned time series:

4.4.1 ____ 10 Eppendorf protein LoBind tubes should be labeled and arranged in an easily accessible manner in a tube rack.

4.4.2 ____ 2 µl of the saturated biotin solution should be pipetted into the very bottom of each tube

- Tube caps can be closed now, but during the on-rate experiments it will help save time to leave all your tubes open
- We recommend having an ample supply of tips 1-200µl LowBind tips and three pipettors at hand (1 that can pipette 60 µl and two that can pipette 10 µl)

4.4.3 ____ Add 60 µl of the 160 pM construct to a new protein LoBind tube

4.4.4 ____ Load tips onto all three pipettors and have them at close reach

4.4.5 ____ Set a timer, that counts up after the alarm rings, for 30 seconds

4.4.6 ____ Aspirate 60 µl of the ~6 nM streptavidin mixture into the pipette

4.4.7 ____ When the alarm sounds mix 60 µl of streptavidin with the 60 µl of DNA

- Do not handle the tube near the bottom as this will heat the sample to your body temperature yielding an artificially higher room-temperature on rate.

4.4.8 ____ Grab the first 10 µl pipettor and aspirate 10 µl of the mixture

4.4.9 ____ When the count-up timer hits 5 seconds pipette the mixture into the bottom of the 5 second tube esnsuring good mixing with the 2 µl of saturated biotin

4.4.10 ____ Grab the second pipette and repeat this procedure for the 10 second tube

4.4.11 ____ Now continue with the remaining time points changing tips between samples

Notes:

This procedure can take a couple of tries to nail the early time points. We recommend practicing with empty tubes to get the timing and positioning down. Additionally having more time between samples i.e. 10 seconds rather than 5 may help for the first couple of experiments.

We have also found that doing the experiment on parafilm can help with speed, but we tend to prefer using the low bind tubes

There should be roughly 20 µl of the mixture left after completion. This can be left unquenched, or can be quenched at a later time point to provide a true plateau value.

5. Pouring, running, and staining the gel:

We recommend running the loops on a 0.7% agarose gel in 0.5x TBE at 4V/cm (100V in a 25cm Owl gel box) for 100 minutes. It is important to use TBE instead of TAE, since the separation of looped from unlooped is significantly better in TBE under these conditions. Other running buffers have not been extensively tested. Other agarose percentages can be used, but we recommend staying between 0.6% and 1%. Adjusting times and voltages to suit your needs is possible, but we have not extensively tested this, so it is recommended to follow the protocol for a baseline before tweaking parameters.

5.1 Preparing and running the gel:

5.1.1 ____ Add 0.7 g of ultrapure agarose (Invitrogen catalog # 16500-500) to a 500 ml Erlenmeyer flask

5.1.2 ____ Make 1 L of 0.5x TBE by diluting 50 ml of 10x TBE (BioRad 161-0770EDU) with 950 ml of Reverse Osmosis, MilliQ, or double-distilled water

5.1.3 ____ Add 100 ml of 0.5x TBE and a magnetic stir bar to the Erlenmeyer flask

- It is important to use the same buffer for making the gel and for running buffer. Even slight mismatches in buffer can cause gel artifacts that make quantification difficult. Make sure you have enough 0.5x TBE to make the gel and to fill the gel box with running buffer.

5.1.4 ____ Cover the top of the flask with aluminum foil to prevent vapor from escaping

5.1.5 ____ Place the Erlenmeyer flask on a hot plate with stirring capability

5.1.6 ____ Bring to a rolling boil while stirring at ~400 rpm, and allow to boil for several seconds

5.1.7 ____ Cool the flask until it is cool enough that it can be held comfortably in a gloved

hand for 60 seconds

- If the gel cools too much it will not pour evenly. It is better to error on the side of too hot than too cold
- We find that cooling by running cool water over the flask for a minute or submerging in ice water for 20 seconds tends to provide quick and adequate cooling
- Ensure that you swirl the contents while doing this so that liquid doesn't gel at the walls of the flask

5.1.8 ____ Pour the gel into a molding tray with a gel comb containing at least 13 wells and allow to solidify

- We find that pouring the gel in the cold room (4°C) helps expedite the gelling process (10 minutes in the cold room should be ample time, at 25°C the gel should be allowed at least 45 minutes to solidify)

5.1.9 ____ To each of the 12 µl samples (2 µl biotin + 10 µl construct/streptavidin) add 2 µl of 6x-ficoll loading-dye (Promega catalog # G1881)

5.1.10 ____ We recommend running a ladder alongside the on rate samples to aid in verification of the looped and unlooped bands

5.1.11 ____ To prepare the ladder mix the following

i. ____ 0.5 µl of 1kb extension ladder (Invitrogen catalog # 10511-012)

ii. ____ 4 µl of 6x ficoll loading dye

iii. ____ 19.5 µl of 0.5x TBE

5.1.12 ____ Fill the gel box with the 0.5x TBE running buffer (to the fill line)

- It is important to use the same buffer for making the gel and for running buffer. Even slight mismatches in buffer can cause gel artifacts that make quantification difficult. Make sure you have enough 0.5x TBE to make the gel and to fill the gel box with running buffer.

5.1.13 ____ Load 4 µl of the ladder mix into the first lane

5.1.14 ____ Load the full 14 µl of each of the time points into the next 10 lanes

- Additionally 10 µl of the unquenched sample can be mixed with 2 µl of 6x ficoll loading dye and the 12 µl can be loaded

5.1.15 ____ In the final lane load 4 µl of the ladder mix

- Having a ladder on both sides helps if there is skew at the running or imaging stages

5.1.16 ____ Run the gel by applying 4V/cm (distance measured electrode to electrode) for 100 minutes

- Note that if the interaction of interest has a lifetime shorter than the gel run time, the loops will fall apart during the gel running process and no looped band will be seen
- To circumvent this we have shown separation of the looped and unlooped, for a Var 4 – Var 8 construct, in as little as 9 minutes at 300 V (Figure 2.4)
- Additionally for short lived interactions, crosslinkers, such as glutaraldehyde, could be used to stabilize the loops to prevent loop opening during the gel running process

5.2 Staining the gel:

We recommend using SYBR-gold (Life technologies catalog # S-11494) for maximal sensitivity

5.2.1 ____ In a container slightly larger than the gel dilute the SYBR-gold 1 in 10,000 in running buffer (i.e. 6 µl of stock SYBR-gold in 60 ml of 0.5x TBE)

5.2.2 ____ Allow the gel to sit in stain on a rocker for at least 30 minutes

- one hour usually leads to more even staining

5.3 Imaging the gel:

We have found similar results using several imagers (including a point and shoot camera) but for the highest sensitivity and repeatability we recommend using a laser scanning gel imager such as the Typhoon FLA 9000. Note that some gel imaging formats save with non-linear

intensity profiles. This will affect your analysis as intensity will no longer be linearly proportional to the amount of material. Either make sure that you save the images with a linear intensity profile or that you linearize the images with freely available tools in imageJ (see methods).

SYBR-gold can be excited at 488. On the Typhoon FLA 9000 we usually image using the standard SYBR-gold settings with a PMT value of 500 and a resolution of 100μm or 10μm if we want to resolve two bands that are very close to one another.

See methods and supplemental for details about image analysis, quantification, and kinetic modeling.

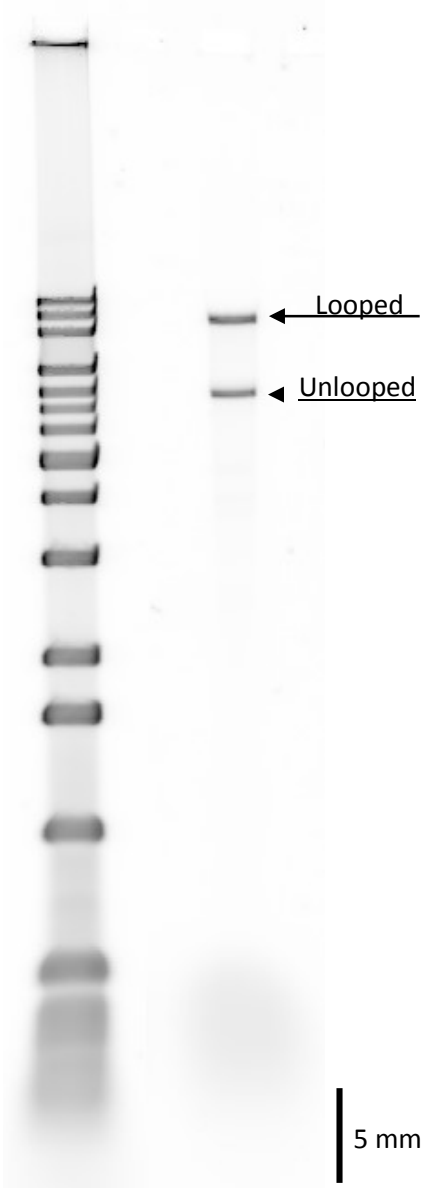

Figure 2.12| An image of a gel prepared, run, and stained under these conditions showing where the looped and unlooped bands appear relative to the 1kb extension ladder (Invitrogen catalog # 10511-012).

6. Performing Off-rate experiments:

To perform off-rate experiments you must first form loops and allow them to equilibrate. This can be done by following the steps in the on-rate experiment with the exception of the quenching steps (4.1-4.3, 4.4.3, and 4.4.6). Simply mix equal volumes of 160 pM construct and 6nM streptavidin, and allow this to form loops for 10 minutes.

To perform the off-rate experiments samples of loops will be allowed to sit in quenching conditions for different amounts of time with the idea being that if a loop opens it will do so irreversibly as the now available binding site will quickly be quenched by the large excess of free floating biotin in solution. To avoid having to run many gels it is easiest to do the longest time point first so that all the samples can be run on the same gel. For example, if you wanted your longest time point to be 72 hours you would mix 10 μl of loops with 2 μl of saturated biotin 72 hours before you planned on running the gel.

An example time series for the biotin streptavidin system would be to take time points over ~5 days at room temperature in the presence of 200 mM salt. Alternatively, for a quicker experiment time points can be taken over 3 hours at 50°C and 200 mM NaCl.

To form the loops follow the protocols above to generate linear DNA(1), hybridize on the functionalized and unfunctionalized oligonucleotides(3), dilute the construct (4.1), and dilute the streptavidin(4.2).

Once you have the required materials (See 1-4.3) You may proceed to do an off-rate experiment:

6.1 Forming loops

6.1.1 ____ Add 70 μl of the 160 pM construct to a new protein LoBind tube

6.1.2 ____ Add 70 μl of the 6nM streptavidin to the 40 μl of DNA

6.1.3 ____ Allow this to sit at 25° C for 10 minutes to allow loop formation to go to completion

The following protocol illustrates an off-rate with the following time points 0, 1 min, 5 min, 10 min, 15 min, 30 min, 45 min, 60 min, 90 min, 120 min, and 180 min.(These times do not need to be adhered to strictly, but this range of times is good to show a significant off rate).

6.2 Performing an off-rate experiment with the above mentioned time points:

6.2.1 ____ Select a date and time when you wish to run the gel

6.2.2 ____ 180 min before running the gel, mix 10 μl of the looped mixture with 2 μl of saturated biotin in an Eppendorf protein LoBind tube

6.2.3 ____ Allow this to sit at 50°C (in a thermocycler or water bath)

6.2.4 ____ 120 min before running the gel, mix 10 μl of the looped mixture with 2 μl of saturated biotin in another Eppendorf protein LoBind tube

6.2.5 ____ Allow this to sit at 50°C (in a thermocycler or water bath

6.2.6 ____ 90 min before running the gel, mix 10 μl of the looped mixture with 2 μl of saturated biotin in another Eppendorf protein LoBind tube

6.2.7 ____ Allow this to sit at 50°C (in a thermocycler or water bath)

6.2.8 ____ Cast a gel and get everything ready to run the gel (see section 5)

6.2.9 ____ 60 min before running the gel, mix 10 µl of the looped mixture with 2 µl of saturated biotin in another Eppendorf protein LoBind tube

6.2.10 ____ Allow this to sit at 50°C (in a thermocycler or water bath)

6.2.11 ____ 45 min before running the gel, mix 10 µl of the looped mixture with 2 µl of saturated biotin in another Eppendorf protein LoBind tube

6.2.12 ____ Allow this to sit at 50°C (in a thermocycler or water bath)

6.2.13 ____ 30 min before running the gel, mix 10 µl of the looped mixture with 2 µl of saturated biotin in another Eppendorf protein LoBind tube

6.2.14 ____ Allow this to sit at 50°C (in a thermocycler or water bath)

6.2.15 ____ 15 min before running the gel, mix 10 µl of the looped mixture with 2 µl of saturated biotin in another Eppendorf protein LoBind tube

6.2.16 ____ Allow this to sit at 50°C (in a thermocycler or water bath)

6.2.17 ____ 10 min before running the gel, mix 10 µl of the looped mixture with 2 µl of saturated biotin in another Eppendorf protein LoBind tube

6.2.18 ____ Allow this to sit at 50°C (in a thermocycler or water bath)

6.2.19 ____ 5 min before running the gel, mix 10 µl of the looped mixture with 2 µl of saturated biotin in another Eppendorf protein LoBind tube

6.2.20 ____ Allow this to sit at 50°C (in a thermocycler or water bath)

6.2.21 ____ 1 min before running the gel, mix 10 μl of the looped mixture with 2 μl of saturated biotin in another Eppendorf protein LoBind tube

6.2.22 ____ Allow this to sit at 50°C (in a thermocycler or water bath)

6.2.23 ____ 10 μl of an unquenched sample held at the same temperature can be used as your 0 point

6.2.24 ____ Add 2 μl of 6x ficoll loading dye to each of the samples right before loading and running the gel

- Some of the liquid may have condensed on the cap. Mild centrifugation can help ensure that all of your volumes are the same

6.2.25 ____ Load, run, stain, and image the gel as described in section 5

Note: if you wish to do the off-rate in different solution conditions, all you need to do is alter the buffer in which you dilute your streptavidin and your construct. If you wish to do the off rate at a different temperature you simply need to let the samples sit in a water bath or thermocycler set to the desired temperature rather than at room temperature.

See methods, Halvorsen et al. 2011 and Koussa et al. 2014 for information on how to implement the nanoswitch platform for non-biotin-streptavidin systems.

Chapter Three

Protocol for sortase-mediated construction of DNA-protein hybrids and functional nanostructures

Mounir A. Koussa[1], Marcos Sotomayor[2], Wesley P. Wong[3,4,5]*

[1]Program in Neuroscience, Department of Neurobiology, Harvard Medical School, Boston, MA

[2]Department of Chemistry and Biochemistry, The Ohio State University, Columbus, OH

[3]Program in Cellular and Molecular Medicine, Boston Children's Hospital, Boston, MA

[4]Department of Biological Chemistry and Molecular Pharmacology, Harvard Medical School, Boston, MA

[5]Wyss Institute for Biologically Inspired Engineering, Harvard University, Boston, MA

Methods. 2014 May 15; 67(2):134-41

Contributions: MS guided MAK through all molecular biology and protein expression, purification, and refolding. MAK designed and carried out the experiments and characterization for the sortase conjugation.

Abstract

Recent methods in DNA nanotechnology are enabling the creation of intricate nanostructures through the use of programmable, bottom-up self-assembly. However, structures consisting only of DNA are limited in their ability to act on other biomolecules. Proteins, on the other hand, perform a variety of functions on biological materials, but directed control of the self-assembly process remains a challenge. While DNA-protein hybrids have the potential to provide the best-of-both-worlds, they can be difficult to create as many of the conventional

techniques for linking proteins to DNA render proteins dysfunctional. We present here a sortase-based protocol for covalently coupling proteins to DNA with minimal disturbance to protein function. To accomplish this we have developed a two-step process. First, a small synthetic peptide is bioorthogonally and covalently coupled to a DNA oligo using click chemistry. Next, the DNA-peptide chimera is covalently linked to a protein of interest under protein-compatible conditions using the enzyme sortase. Our protocol allows for the simple coupling and purification of a functional DNA-protein hybrid. We use this technique to form oligos bearing cadherin-23 and protocadherin-15 protein fragments. Upon incorporation into a linear M13 scaffold, these protein-DNA hybrids serve as the gate to a binary nanoswitch. The outlined protocol is reliable and modular, facilitating the construction of libraries of oligos and proteins that can be combined to form functional DNA-protein nanostructures. These structures will enable a new class of functional nanostructures, which could be used for therapeutic and industrial processes.

Keywords: DNA-protein hybrids/chimeras; Molecular self-assembly; Sortase coupling; Bioconjugation; DNA origami; site-directed

1. *Introduction*

DNA is emerging as the platform of choice for the bottom-up self-assembly of intricate, biocompatible nanostructures. As techniques for the programmed patterning of these structures have advanced, it is now possible to create complex assemblies, ranging from two dimensional shapes to three-dimensional nano-robots [1, 2, 3]. Structures built using only DNA, although intricate, are limited in their ability to interact with biological substrates. Proteins, on the other

hand, are the molecular machines of biology, and have a wide range of functions including chemically modifying, binding to, and applying forces to other molecules. However, to build intricate machines using DNA-protein hybrids, which harness the advantages of both materials, one needs to attach the proteins in a targetable and biocompatible way [4,5].

One approach is to attach the proteins to the oligonucleotides (oligos) that bind to designated locations on the DNA origami scaffold. The challenge, however, is to attach these proteins to oligos while preserving protein function. Existing chemistries, such as disulfide and SMCC (sulfosuccinimidyl-4-(N-maleimidomethyl)cyclohexane-1-carboxylate) linkage [9], are sometimes effective, but they react with functional groups ubiquitous in biology. This reactivity hinders both the ability to link to a desired location on the protein, and to control the number of linkers bound to each molecule (stoichiometry), as one biomolecule may contain many reactive species. To overcome this issue, bioorthogonal techniques, such as copper-free click-chemistry, have been developed [6]. Although these techniques do in fact overcome the issues of regioselectivity and stoichiometry, they still suffer from the problem common to all of these techniques: reaction conditions are suboptimal for many proteins, be it due to long incubation periods at room temperature, extreme oxidizing/reducing conditions, or non-physiological pH. These methods also fail when working with non-thermostable proteins that have a tendency to aggregate and/or precipitate out of solution under the requisite conditions. Additionally, purification can be difficult due to the challenge of easily distinguishing products from reactants—as we will see, our technique solves this problem by directly marking successful reactions by the simultaneous removal of an affinity label. Finally, each protein has specific

considerations with regards to its reactivity and structural stability. Thus protocols optimized for one protein may not be suitable for another protein.

Here, we present a protocol for covalent coupling developed to meet the challenges outlined above. In order to preserve protein function, protein-DNA coupling is performed under physiological conditions. In this two-step process, a small synthetic peptide is first coupled to a DNA oligo. Next, utilizing the enzyme sortase [7, 8], the protein is coupled to the DNA-peptide chimera under physiological conditions. This strategy frontloads all of the protein-incompatible chemistry so that it is performed on an oligo and a synthetic peptide, which are far more tolerant of non-physiological conditions. The use of sortase also facilitates purification, as coupling of the oligo is accompanied by the removal of an affinity tag. Our protocol, detailed below, allows for the use of commercially available purification resins to yield the product of interest free of any side products and reactants. This technique can be used to generate libraries of oligo nucleotides and proteins such that any proteins in the library can be easily and reliably attached anywhere along the DNA origami scaffold.

To demonstrate the utility of this technique we build the simplest DNA-protein nanomachine, a binary DNA-nanoswitch [9, 18], gated by the interacting pair of cadherin-23 and protocadherin-15 protein fragments (CDH23 and PCDH15) [10, 11]. This self-assembled mechanical switch changes state to report the formation or rupture of biomolecular bonds: in this case, the switch is closed when CDH23 is bound to PCDH15 and open otherwise. The CDH23 fragment is covalently linked to an oligo that hybridizes one-third of the way in from one edge of the DNA scaffold (M13). In addition, the PCDH15 fragment is linked to an oligo that hybridizes one-third

of the way in from the other edge of the scaffold (Figure 3.1). The result is a nanoswitch with an end-to-end length of 3μm when the proteins are not interacting, and an end-to-end length of 2μm when the proteins are interacting. These two states are resolvable via gel electrophoresis as described in [9].*In vivo* some variants of Sortase, such as Sortase-A are used to anchor proteins to the cell surface by covalently linking proteins to the peptidoglycan on the cell walls of bacteria. In this in vitro system Sortase covalently links the N-terminus of one protein to a location near (within ~100 amino acids of) the C-terminus of another protein. Sortase recognizes an N-terminal GGG and a C-terminal LPX_1TGX_2, where X_1 can be any amino acid, and X_2 can be any string of amino acids of length 1-99. Sortase then facilitates the transposition of the glycine residues in the two proteins resulting in a covalent linkage between the two proteins and the release of GX_2 (Figure 3.2).

Maximillian Popp et al. in 2007 [8] first described using sortase to selectively attach fluorescent markers to a protein of interest. Chen et al. in 2011 [7] evolved a sortase variant with 140-fold increased activity, lowering coupling times from hours to minutes. Sortase has also been used to link peptide nucleic acids (PNA) to peptides [12], to label proteins N-terminally [13], C-terminally, and in loops [14]. Additionally sortase has been used in combination with click chemistry to make unnatural N-N- and C-C- linked protein chimeras [15].

Our goal was to use sortase technology to generate DNA-protein hybrids for self-assembled nanostructures. While synthetic PNA oligos offer the ability to append amino acids directly to a string of nucleic acids, they are less soluble than DNA oligos, and harder to synthesize. Thus, we wanted instead to develop a convenient way to couple proteins to DNA

oligos which are more readily-available. To do this we needed a means of attaching a peptide to an oligo. Click chemistry was chosen to allow for the process to be both bioorthogonal and efficient.

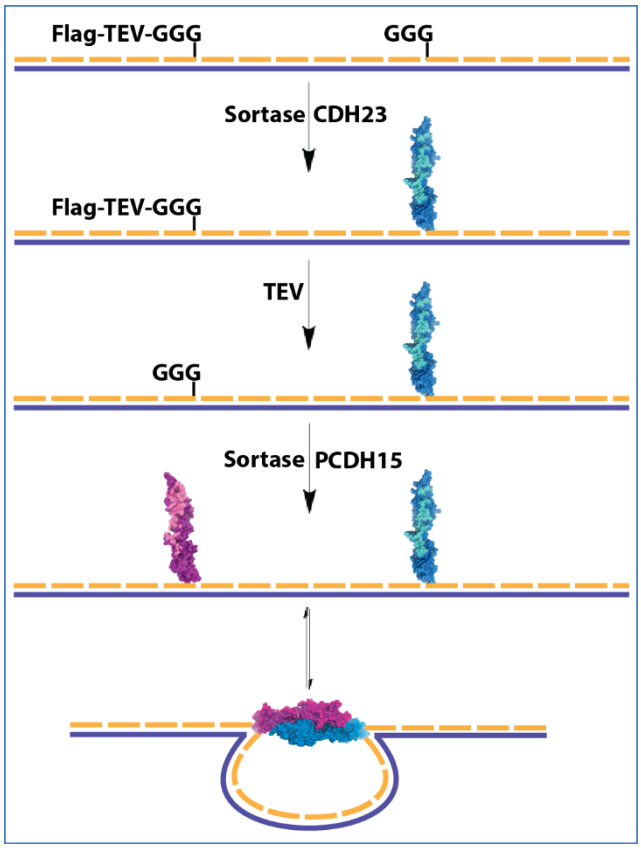

Figure 3.1| A method for the formation of the binary DNA-nanoswitch. Linearized M13 single-stranded DNA (dark blue), complimentary oligonucleotides (golden-rods), CDH23 EC1 + 2 (cyan), and PCDH15 EC1 + 2 (magenta). (A–>B) Annealing of functionalized and non-functionalized oligo nucleotides to the M13 ssDNA scaffold (see Figs. 3–6 for functionalization of oligos). (B–>C) Sortase is used to link an LPETG-containing CDH23 fragment (2.4.4) to the Gly–Gly–Gly-modified oligo (the other oligo is protected by having the N-terminus blocked by a Flag-TEV sequence) (2.1). (C–>D) After successful coupling, the TEV protease is used to

deprotect the second Gly–Gly–Gly-oligo, thereby priming it for sortase coupling (2.4.4 e). (D–>E) sortase is then used again to attach an LPETG-containing PCDH15 fragment (2.4.4 k). (E<–>F) Upon binding of CDH23 to PCDH15 the DNA-nanoswitch is closed. In the paper we also outline a method for attaching thermo-stable proteins to a DNA origami scaffold. For thermo-stable proteins, one can perform the sortasebased coupling reactions on the individual oligos separately prior to thermally annealing the oligos to the M13 scaffold, thus obviating the need for the protecting Flag-tag (2.3).

2. Methods

Here we present four protocols describing: *2.1)* the formation of a DNA-oligo bearing a sortase-compatible GGG-peptide, *2.2)* the sortase-catalyzed coupling of a protein to the DNA-peptide chimera, and *2.3/2.4)* the integration of DNA-protein hybrids into self-assembling nanostructures for thermostable/non-thermostable proteins. The oligos we were interested in functionalizing for our application were both 60bp oligos herein referred to as oligo 1 and oligo 2. We ordered oligo 1 with a 3'-azide and oligo 2 was ordered with a 5'-azide (IDT custom oligo). The following peptide was synthesized by NeoBioLab: (N->C) Flag-TEV-GGG-Pra (DYKDDDDK-ENLYFQ-GGG-Pra) where Pra is the unnatural amino acid propargylglycine. This can be incorporated into a synthetic peptide to provide an alkyne, the complimentary click reagent. Additionally, to facilitate purification, a Flag-tag was added to the N-terminus. As the Sortase requires the GGG to be on a free N-terminus a tobacco etch virus cleavage site (TEV) was inserted to allow for removal of the Flag-tag.

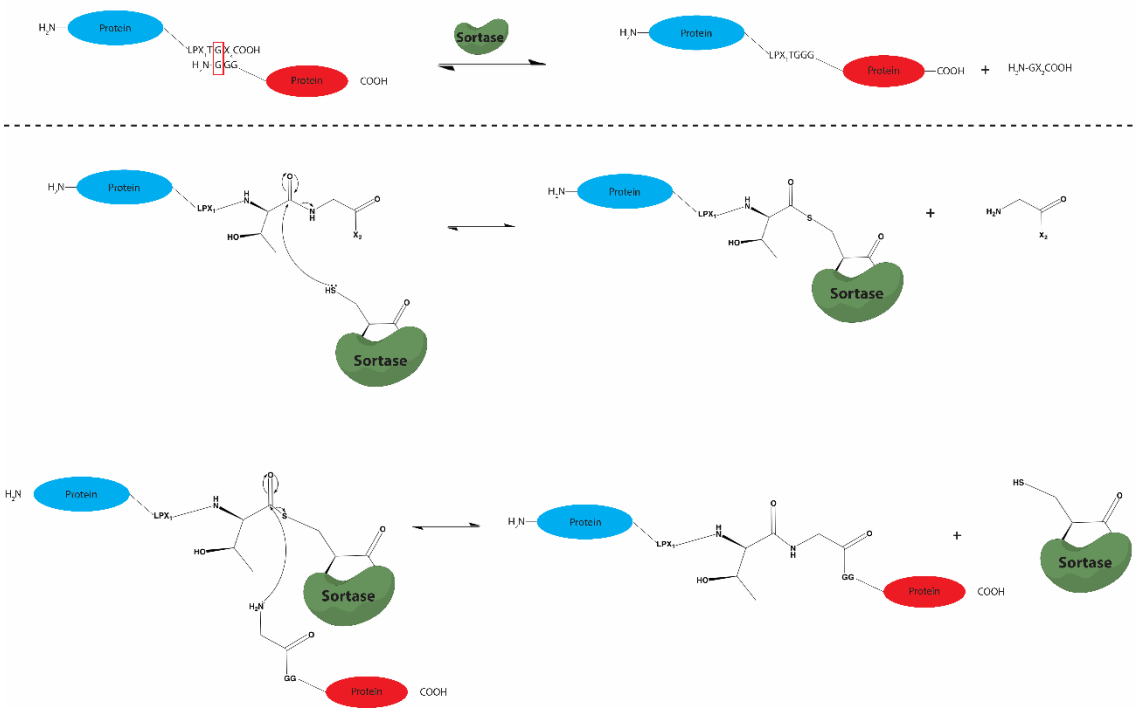

Figure 3.2| (Top). Sortase coupling schematic: The sortase enzyme catalyzes the formation of a covalent bond between two proteins by recognizing, and then coupling two specific peptide sequences. Note that the recognition sequences do not first align, but rather, sortase binds to the LPX1TGX2 sequence first, as described below. (Bottom). Reaction Diagram: Sortase first recognizes a C-terminal LPX1TGX2 sequence, in which X1 can be any one amino acid, and X2 can be any string of 1–99 amino acids. Sortase then transposes the Nterminal-most glycine from the Gly–Gly–Gly sequence with the glycine from the LPX1TGX2 sequence (red box), resulting in a peptide bond between the two proteins and the release of GX2. (G and T refer to the amino acids Glycine and Threonine respectively.)

2.1 Protocol for the formation of oligonucleotides with sortase-compatible GGG peptide

2.1.1 Preparation of reagents

a. Solubilize the peptide to 1mg/ml (0.5mM) in nuclease-free water
    i. Note: The propargylglycine reduces solubility of the peptide and a small amount of ammonium bicarbonate can be added to solubilize the peptide.
b. Solubilize the oligo at 100μM in nuclease-free water
c. Prepare a 94.2g/L (59mM) aqueous $CuSO_4$ stock
    i. Anhydrous $CuSO_4$ should be used
d. Prepare a 264.2g/L (0.21M) aqueous ascorbic acid stock
    i. The ascorbic acid serves to reduce the Cu(II) (blue) to the catalytically active Cu(I) (green)

2.1.2 Click-coupling of the peptide to the oligo (Figure 3.3)

a. Combine the following in a 250uL DNA-lowbind tube
    ii. 35μL of the azide-oligo
    iii. 30μL of the peptide
    iv. 12μL of the ascorbic acid
        1. CO_2(g) is produced from the ammonium bicarbonate
        2. Although the peptide is insoluble at neutral pH it is soluble under both the slightly basic ammonium bicarbonate conditions and the acidic ascorbic acid conditions
    v. 8.5μL of the $CuSO_4$
b. Allow the reaction to sit for 2 hours at room temperature to ensure completion
c. Note: some of the Cu will be reduced to Cu(0) metal, which will precipitate out.

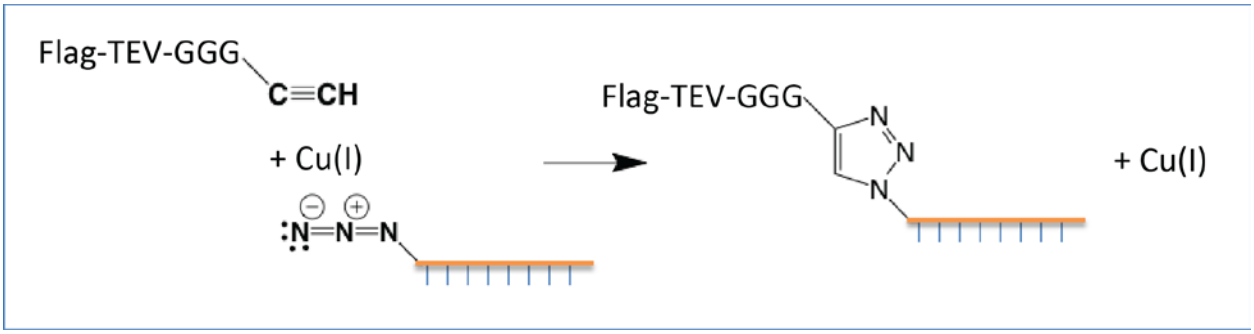

Figure 3.3| Click coupling of peptide to oligo. The Flag-TEV-GGG-Pra (DYKDDDDKENLYFQ-GGG-Pra) peptide is attached to an azide oligo (golden-rod) through copper(I)-catalyzed click chemistry.

2.1.3 Purification of the peptide-oligo chimera

a. Removal of uncoupled peptide (select either *Method 1* or *Method 2*) (Figure 3.4)

Method 1: Neutralization

1. Neutralizing the solution via the addition of 250µL of TBS (50mM TrisHCl, 300mM NaCl pH 7.6) will cause uncoupled peptide to precipitate.
2. The copper metal and precipitated peptide can be pelleted by centrifugation at 16,000 g for 5 min. The supernatant will contain coupled and uncoupled oligo and excess Cu(I) can be dialyzed out using a 6-8kDa membrane (Mini GeBAflex-tube, T070-6)

Method 2: QiaQuick Nucleotide Removal Kit (Qiagen) (The Qiagen kit works by precipitating out DNA, passing it over a membrane, and washing

away any soluble products such as unconjugated peptides, small molecules, soluble copper etc.)

1. Following the kit protocol will remove the copper metal, Cu(I), Cu(II), and the uncoupled peptide.
2. The protocol should be followed as instructed by the manufacturer, but the wash step should be repeated a second time.
3. Perform the elution with 200µL of TBS

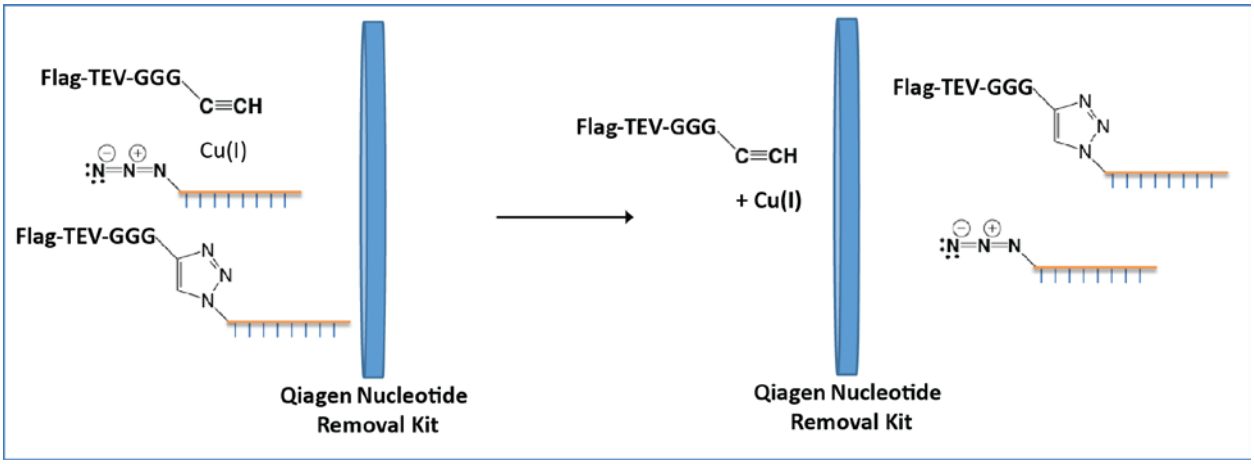

Figure 3.4| Removal of Cu and uncoupled peptide. Running the reaction product through a Qiagen nucleotide removal kit allows for the isolation of the coupled and uncoupled oligo. Excess peptide and copper will remain on the membrane and/or be removed in the wash steps.

2.1.4 Removal of uncoupled oligo (Figure 3.5)

a. Wash 1ml of Anti-Flag M2 magnetic beads (Sigma-Aldrich, M8823) three times with 1ml of TBS

b. Apply the product of the Qiagen purification column and allow to bind for 1-2hrs rotating at room temperature.

c. Wash the beads at least 4 times with 500µl of TBS being sure to agitate the beads to remove any uncoupled oligo

    i. Note: A wide boar pipette is recommended when agitating the beads

d. Elute with 1ml of 0.1mg/ml (Sigma) Flag peptide in eTBS (50mM TrisHCl, 150mM NaCl)

    i. Allow 1 hour rotating at room temperature for elution

e. A second elution can be performed, but >85% will be recovered in the first elution

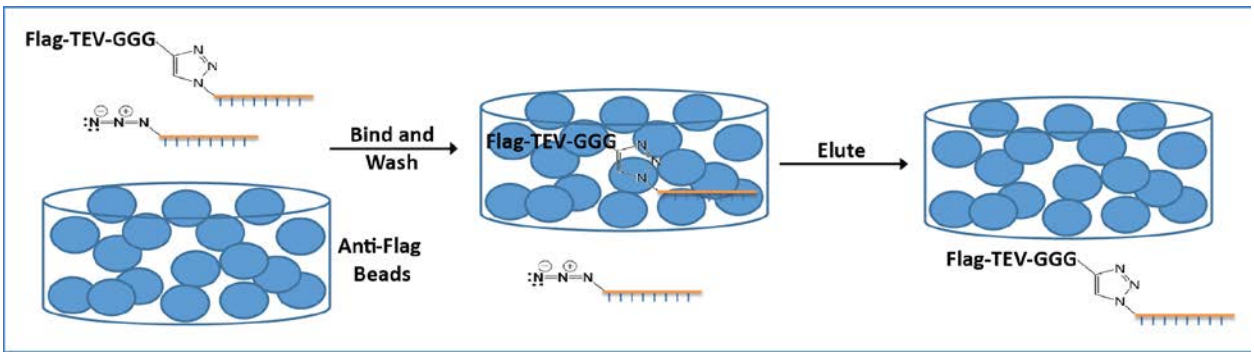

Figure 3.5| Removal of uncoupled oligo. Binding the product of the Qiagen nucleotide removal kit to Anti-Flag beads allows one to wash away uncoupled oligo. Elution with Flag-peptide releases the oligo from the affinity matrix.

2.1.5 TEV-cleavage of the Flag-tag (Figure 3.6)

a. Add 2µL of 2mg/ml TEV protease (Sigma-Aldrich, T4455) to each ml of eluted product

b. Incubate in a 30°C water bath over night

c. Running a 4-20% gradient poly-acrylamide gel with the binding, wash, and elution (cleaved and uncleaved) supernatants reveals that the product has been successfully purified of uncoupled oligo (The 60bp band is eliminated with successive washes) and cleaved (after cleavage the band shifts back near 60bp)

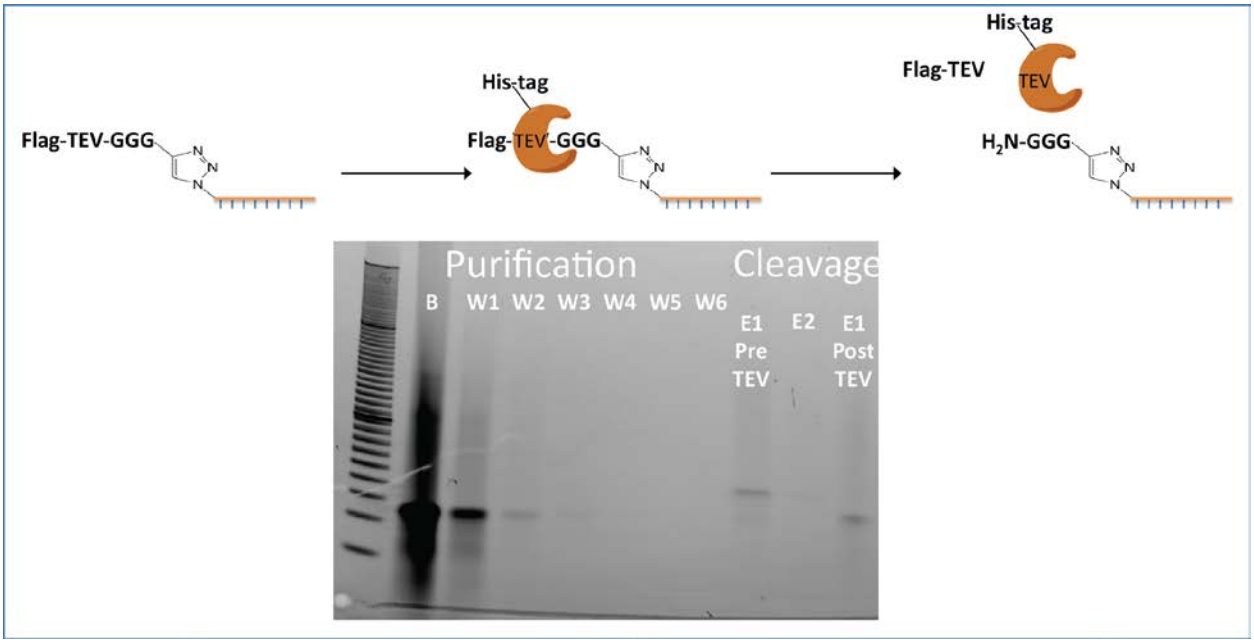

Figure 3.6| TEV cleavage of Flag-tag. The TEV protease (brown) can be applied to cleave the Flag-tag resulting in an oligo with a sortase-compatible GGG-peptide. The left-most lane is a Bio-Rad 20 bp Molecular Ruler.

2.1.6 The final product will herein be referred to as GGG-oligo

a. Additionally the TEV and cleaved peptide can be removed by repeating the Qiagen nucleotide removal kit as described above. This step has not proven to be necessary

2.2 Protocol for sortase coupling LPETG-tagged proteins to GGG-oligonucleotides

2.2.1 Preparation of reagents

a. The GGG-oligo should be at a concentration of ~2μM as judged by band intensity on the polyacrylamide gel.
    i. Gel was stained with SYBR-Gold (Invitrogen, S11494), imaged using a GE Typhoon FLA-9500, and analyzed using ImageJ (NIH, 1.46r)
b. Two proteins, protein1 and 2, are coupled to two different oligos, oligo1 and 2
    i. In this example protein 1 is a fragment of the CDH23 protein containing two (out of 27) extracellular repeats. Likewise, protein 2 is a PCDH15 fragment containing two (out of 11) extracellular repeats. Both proteins were modified by appending the LPETG amino-acid sequence between the protein fragment C-terminus and a His-tag. Protein fragments were produced as described in [11, 16].
c. Proteins should be used at a minimum concentration of 0.1mM.
    i. CDH23 and PCDH15 stocks were at 2.5 and 2.7 mg/ml respectively in TBS + 5mM $CaCl_2$ (~0.1mM)
        1. CDH23-LPETG and PCDH15-LPETG were fragments, each containing two extracellular domains used in a crystallographic study [11]. The proteins was were modified by appending LPETG between the His-tag and the C-terminus of the protein
        2.

d. Sortase stock was at 1.5mg/ml in TBS + 10%-glycerol

    i. An evolved variant of sortase-A from S. aureus [7] was expressed and purified from E. coli (plasmids and expression protocol provided by Brent Dorr in David Liu's lab [7])

e. Sortase Reaction buffer consisted of the following:

    i. 300mM TrisHCl pH7.5

    ii. 5mM $MgCl_2$

    iii. 5mM $CaCl_2$

    iv. 150mM NaCl

2.2.2 Sortase coupling of protein1 to oligo1 (Figure 3.7)

a. Mix the following in a 250µL mini GEBAflex-tube

    i. 140µL of 2µM GGG-oligo1

    ii. 40µL of 0.1mM protein1-LPETG-HHHHHH

        1. The protein is added in large excess to drive coupling to completion with respect to the oligo

    iii. 5µL of Sortase

    iv. 65µL of Sortase Rxn Buffer

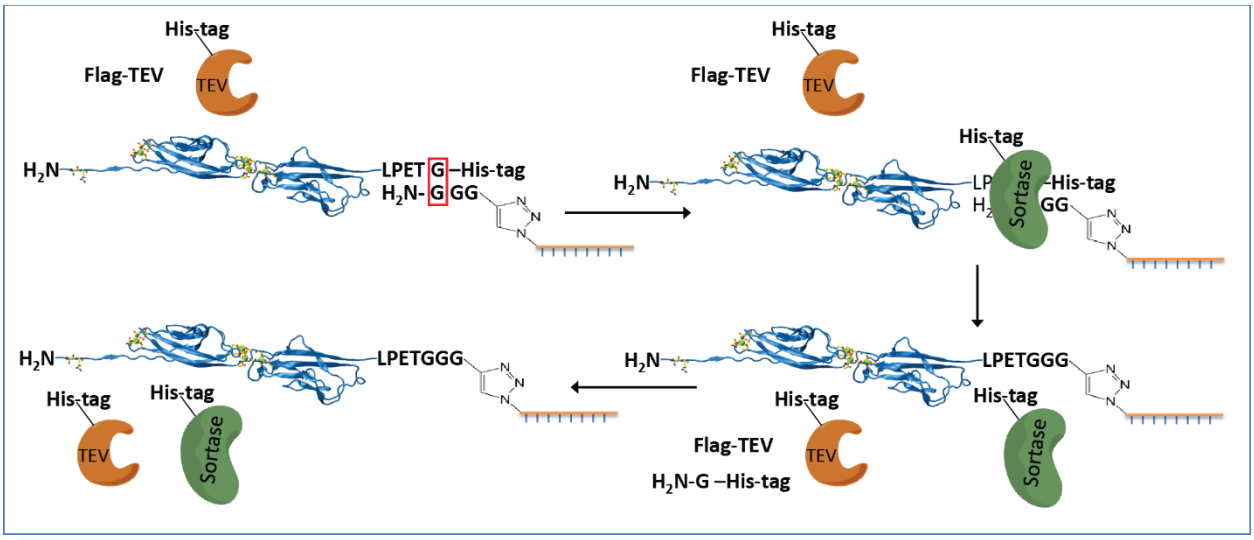

Figure 3.7| Sortase-catalyzed production of protein–DNA hybrids. An LPETG-containing protein, in this case CDH23 EC1 + 2, is coupled to the Gly–Gly–Gly-oligo via sortase. Sortase transposes the two glycine residues highlighted by the red box, resulting in the formation of a peptide bond between the protein and the Gly–Gly–Gly-oligo (we note that the recognition sequences do not first align, but rather, sortase binds to the LPX1TGX2 sequence first, as described in Figure 3.2b). In this case the sequence after the Cterminal-most glycine on the protein was a 6xHis-tag. Sortase cleaves and releases this affinity tag, replacing it with the Gly–Gly–Gly-oligo. The procedure is carried out in a dialysis membrane so the Flag-TEV and G-His-tag peptides are dialyzed out.

b. Place the GEBA Flex tube in 1L of Sortase RXN buffer and allow the reaction to go for 1hr at RT or 4-5 hours at 4°C
    i. The dialysis column will allow any Flag Peptide to dialyze out and will remove the sortase reaction byproduct, G-HHHHHH, which can compete with the Oligo

c. Figure 3.8 shows SDS-PAGE analysis indicating that the protein oligo chimera is only formed when all components are present

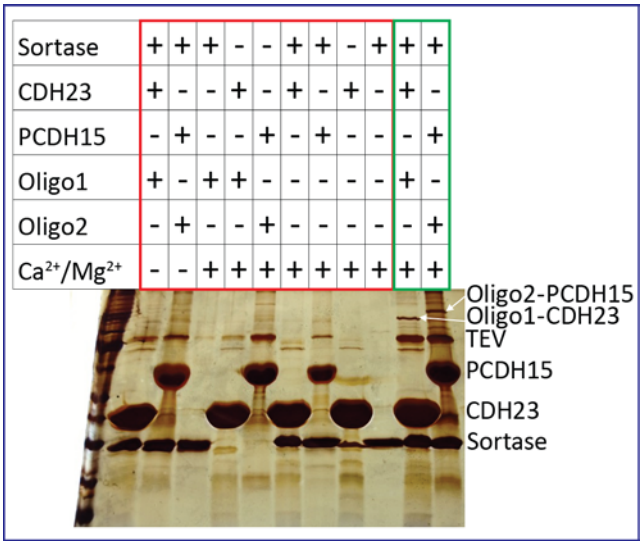

Figure 3.8| SDS–PAGE verification of protein–DNA coupling. Successful coupling requires an LPETG-containing protein, a GGG-oligo, the sortase enzyme, and divalent cations (primarily Ca2+). Only when all the requisite constituents are present (green box), do coupled products appear.

2.2.3 Purification of protein-oligo chimera (Figure 3.9)

a. The TEV, sortase, protein 1, and protein 2 all bear His tags. The sortase reaction, however, selectively cleaves the His tag off of the final product. Thus passing the product over anti-His magnetic beads will remove these reactants leaving the final product in the supernatant

i. Note: anti-His beads should be used rather than Ni-NTA. The Ni-NTA beads tend to bind the oligos quite strongly and very high salt is required to remove them

b. If your protein buffer contains Ca^{2+} wash 1ml of magnetic Anti-His beads (GenScript, L00275) 2 times with 1ml of TBS. If, however, your protein buffer does not contain Ca^{2+} PBS can be used for these washes and the washes in step c

    i. This is to remove any phosphate from the storage solution to prevent calcium-phosphate crystal formation. Omitting this step will result in large losses in later steps

c. Wash 3 more times with 1 ml of TBS + 5mM $CaCl_2$

d. Apply the product of the sortase reaction and allow 2 hours rotating at 4°C for binding

e. The supernatant contains the DNA-protein hybrid, free of any other proteins. In our molecular system we obtain a yield of ~65% with respect to the amount of starting oligo.

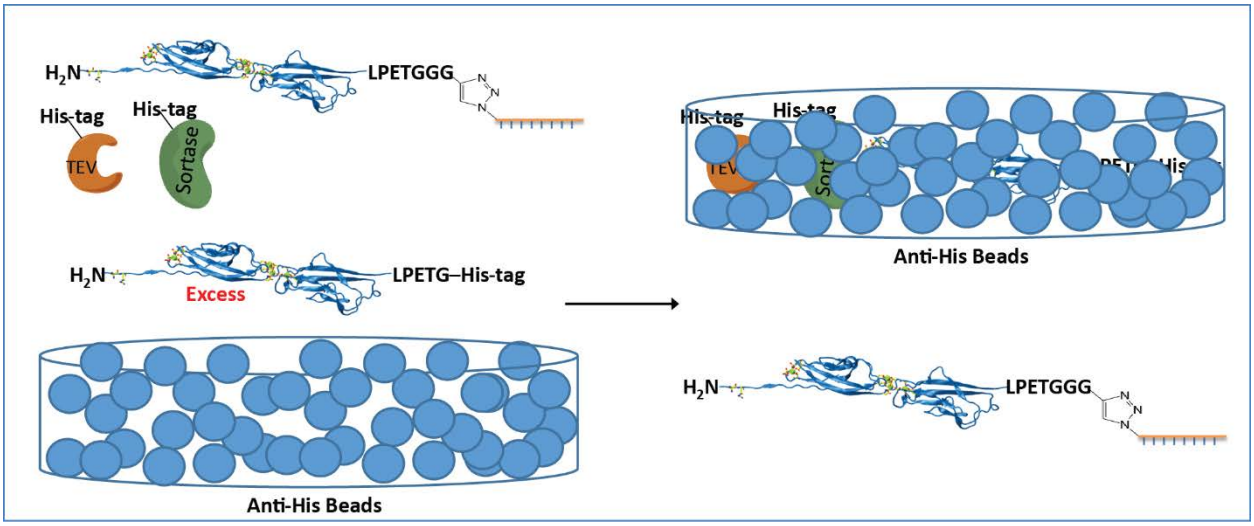

Figure 3.9| Removal of reactants and catalysts. Upon completion of coupling the product is amidst TEV, sortase, and excess protein. While all of these components initially bear a His-tag,

sortase cleaves the His-tag when coupling the protein and oligo. Thus, by running the sample over anti-His beads, everything but the product of interest will bind to the affinity matrix leaving the DNA–protein hybrid in the supernatant.

2.3 Protocol for hybridization of DNA-protein hybrid to scaffold (Thermostable Proteins)

If the protein used can withstand being heated to 40°C, the oligos can be hybridized to the scaffold, in this case linearized M13 [9], by adding the oligos in a one-to-one ratio to the scaffold, then ramping the temperature from 40°C to 20°C at half a degree per minute in a thermocycler [9].

2.3.1 One can anneal all unfunctionalized oligos from 95°C in 0.5 degree steps to 20°C. The functionalized oligos can be added during this run by pausing the thermocycler once it hits 40°C, adding the functionalized oligos, and

a. If the protein is not thermostable an alternate approach can be taken as described below in section 2.4.

2.4 Protocol for hybridization of DNA-protein hybrid to scaffold (Non-thermostable Proteins)

In this example the CDH23 and PCDH15 fragments are not very thermostable and hybridization through temperature annealing was not an option. For this system the GGG-oligos were hybridized onto the scaffold and the sortase coupling was done *in situ* directly on the scaffold. Performing the coupling on the oligos before hybridization allows one to easily control which protein is attached to which oligo. For this system selective coupling was

achieved using the Flag-tag as a protecting group. That is, Oligo 1 was processed fully, resulting in a GGG-oligo, while Oligo 2 did not undergo TEV cleavage of its Flag tag (Figure 3.1).

An additional concern is ensuring that each site on the scaffold receives its complimentary oligo. To accomplish this, the oligos are added at 50-fold excess. This, however, results in a large surplus of free floating oligos. This can be a problem if there is an excess of GGG-oligo floating around which will compete with the *in situ* reaction. To overcome this issue excess oligos had to be removed from the solution.

2.4.1 Preparation of reagents

a. The GGG- and Flag-TEV-GGG- oligos should be concentrated to ~10μM
    i. This can be achieved by using a speedvac (Thermo-Savant, SC210A) or a 3kDa spin column (Vivaspin 500, VS0191)
        1. If a speed vac is used the oligos should first be dialyzed into water to remove salts before concentration

2.4.2 Annealing oligos

a. Mix the following in a low-bind 250μL PCR tube
    ii. 5μL of 20nM origami scaffold (linear M13 in this case) [9]
    iii. 1.19μL of 100nM mixture (equal parts) of all unfunctionalized oligos
    iv. 0.5μL of 10nM GGG-Oligo 1
    v. 0.5μL of 10nM Flag-TEV-GGG-Oligo 2
b. Subject the mixture to a temperature ramp from 95°C to 20°C at 0.5 degree increments to anneal the oligos to the scaffold.

2.4.3 Removal of excess oligos by PEG-precipitation (modified from [17])

a. Dilute the product of the annealing in 115µL of 4%, by weight, 8K PEG (Amresco, 0159) in 30mM $MgCl_2$
b. Mix thoroughly
c. Centrifuge at 16,000 g for 30min at 25°C
d. Remove the top 112µL leaving the bottom 10µL which should contain the precipitated scaffold
e. Dilute the remaining 10µL with another 115µL of 4%, by weight, 8K PEG (Amresco, 0159) in 30mM $MgCl_2$
    vi. Be sure to mix thoroughly.
f. Centrifuge at 16,000 g for 30min at 25°C
g. Remove the top 115µL of supernatant
h. The remaining 10µL should have the scaffold free of any detectable amount of unhybridized oligo

2.4.4 *In situ* coupling of protein 1-LPETG-HHHHHH to the GGG-Oligo

a. Mix the following
    vii. 40µL 1M Tris HCl pH 7.5
    viii. 0.8µL 1M $CaCl_2$
    ix. 8µL 3M NaCl
    x. 10µL of PEG-precipitated scaffold
    xi. 50µL of 14mg/ml sortase
    xii. 15µL of 0.1M protein1-LPETG-HHHHHH

b. Place the mixture into a dialysis membrane (Spectra/Por MicroFloat-a-lyzer, F235053)

c. Place the Floatalyzer in 1 L of sortase reaction buffer

d. Allow this reaction to run for 0.5-1hr at RT before moving to 4°C for an additional 2 hours (upon transferring to 4°C it is best to transfer to a pre-chilled liter of sortase reaction buffer)

e. Add 4μL of 2mg/ml TEV and allow to sit at room temperature for 1hr

f. If your protein buffer contains Ca^{2+} wash 1ml of magnetic Anti-His beads (GenScript, L00275) 2 times with 1ml of TBS. If, however, your protein buffer does not contain Ca^{2+} PBS can be used for these washes and the washes in step g

    xiii. This is to remove any phosphate from the storage solution to prevent calcium-phosphate crystal formation. Omitting this step will result in large losses in later steps

g. Wash 3 more times with 1 ml of TBS + 5mM $CaCl_2$

h. Apply the product of the sortase reaction and allow 2 hours rotating at 4°C for binding

i. The supernatant contains the DNA-protein hybrid. Free of TEV and excess CDH23

j. Add the following to the supernatant and place in a new Floatalyzer

    xiv. 15μL of 0.1M protein 2-LPETG-HHHHHH

    xv. 50μL of 14mg/ml sortase

k. Repeat Steps b,c,d,f, g, and h

l. The supernatant contains the pure site-directedly bi-functionalized DNA-protein hybrid.

m. Functionality of the nanoswitch can be assayed by gel electrophoresis as previously described in [9]

3. Conclusions

We have presented detailed protocols for a reliable approach for linking proteins to DNA-oligos, while preserving protein function. Additionally we outline methods for the incorporation of these chimeras into self-assembling nanostructures. These techniques frontload all harsh chemistries to synthetic oligos and peptides, which are more amenable to these non-physiological conditions. The use of click chemistry ensures that linkages are bioorthogonal, site directed, and efficient. The use of an evolved sortase allows for protein coupling to occur under conditions favorable for protein stability. The protocols have been designed to be resilient to changes in the protein of interest. All materials are commercially avaliable, with the exception of the sortase (for which the plasmid is available from the Liu Lab [7]). The built in purification schemes allow for fast and efficient purification, allowing for the immediate use of the chimeric product. When combined with a library of sortase compatible oligos and peptides, this flexible and modular approach could enable the creation of a wide range of functional nanostructures on demand. Furthermore, our approach expands the range of functional DNA-protein chimeras that can be constructed, enabling the incorporation of previously inaccessible protein machinery to generate nanostructures with previously unobtainable functionalities.

References:

1. P.W.K. Rothemund

   Nature 440 (2006), 297-302

2. S.M. Douglas, I. Bachelet, G.M. Church

   Nature 335 (2012), 831-834

3. V. Linko and H. Dietz

   Cur. Op. in Biotech. 24 (2013), 555-561

4. C.M. Niemeyer

   Trends. in Biotech. 20 (2002), 395-401

5. C.M. Niemeyer and B. Saccà

   Chem. Soc. Rev. 40 (2011), 5910-5921

6. C.G. Gordon, J.L. Mackey, J.C. Jewett, E.M. Sletten, K.N. Houk, and C.R. Bertozzi

   Journal of the American Chamical Society 134 (2012), 9199-9208

7. I. Chen, B.M. Dorr, and D.R. Liu

   Proceedings of the National Academy of Sciences. 108 (2011), 11399-11404

8. M. Popp, J. Antos, G. Grotenbreg, E. Spooner, H. Ploegh

Nature chemical biology 3 (2007), 707-708

9. K. Halvorsen, D. Schaak, W. Wong

Nanotechnology 22 (2011), 494005-494012

10. P. Kazmierczak, H. Sakaguchi, J. Tokita, E. Wilson-Kubalek, R. Milligan, U. Müller, and B. Kachar

Nature 449 (2007), 87–91

11. M. Sotomayor, W. Weihofen, R. Gaudet, and D. Corey

Nature 492 (2012), 128–32

12. S. Pritz, Y. Wolf, O. Kraetke, J. Klose, M. Bienert, and M. BeyermannThe Journal of organic chemistry 72 (2007), 3909–3912

13. C. Theile, M. Witte, A. Blom, L. Kundrat, H. Ploegh, and C. Guimaraes

Nature protocols 8 (2013), 1800–1807

14. C. Guimaraes, M. Witte, C. Theile, G. Bozkurt, L. Kundrat, A. Blom, and H. Ploegh

Nature protocols 8 (2013), 1787–1799

15. M. Witte, C. Theile, T. Wu, C. Guimaraes, A. Blom, and H. Ploegh

Nature protocols 8 (2013), 1808–1819

16. M. Sotomayor, W. Weihofen, R. Gaudet, and D. Corey

Neuron 66 (2010), 85–100

17. J.L. Hartley, H. Bowen

Focus 66 (1996), 27-28

Acknowledgments:

The authors gratefully acknowledge the help of Brent Dorr, for providing the plasmid for the evolved sortase, Rachelle Gaudet, for allowing us to use her facilities for protein production and purification; David P. Corey, Gary Yellen, Rachel Wilson, Jeffery Holt, Ahmed Badran, Zhi-Yang Tsun, and members of the Wong and Corey Labs for critical discussions; The labs of Sun Hur and Timothy Springer, for assistance in protein production; Lynne Oland, for scientific training, discussions, and instruction on the proper use of hyphens. Funding for this project was provided by NIH R01 DC02281 to D.P.C and R.G.; NIH K99/R00 DC012534-01 to M.S. M.K. was supported by NSF GRFP 2012147612.

Chapter Four

Towards Force Spectroscopy of Single Tip-Link Bonds[1]

Mounir A. Koussa[1, a)], Marcos Sotomayor[2, a)], Wesley P. Wong[3-5], David P. Corey[6,7]

[1]*Program in Neuroscience, Department of Neurobiology, Harvard Medical School, Boston, MA, United States.*

[2] *Department of Chemistry and Biochemistry, The Ohio State University, Columbus, OH 43210.*

[3]*Program in Cellular and Molecular Medicine, Boston Children's Hospital, Boston, MA, United States*

[4] *Department of Biological Chemistry and Molecular Pharmacology, Harvard Medical School, Boston, MA, United States*

[5] *Wyss Institute for Biologically Inspired Engineering, Harvard University, Boston, MA, United States*

[6] *Howard Hughes Medical Institute, Boston, MA 02115, USA*

[7] *Department of Neurobiology, Harvard Medical School, Boston, MA 02115, USA*

Abstract. Inner-ear mechanotransduction relies on tip links, fine protein filaments made of cadherin-23 and protocadherin-15 that convey tension to mechanosensitive channels at the tips of hair-cell stereocilia. The tip-link cadherins are thought to form a heterotetrameric complex, with two cadherin-23 molecules forming the upper part of the filament and two protocadherin-15 molecules forming the lower end. The interaction between cadherin-23 and protocadherin-15 is mediated by their N-terminal tips. Missense mutations that modify the interaction interface impair binding and lead to deafness. Molecular dynamics

[1] This chapter is a condensed version of [8] and [10] and also lays out the critical concepts for performing force spectroscopy on tip-link proteins.

simulations predict that the tip-link bond is mechanically strong enough to withstand forces in hair cells, but its experimentally determined strength is unknown. We have developed molecular tools to facilitate single-molecule force spectroscopy on the tip link bond. Self-assembling DNA nanoswitches are functionalized with the interacting tips of cadherin-23 and protocadherin-15 using the enzyme sortase under conditions that preserve protein function. These tip link nanoswitches are designed to provide a signature force-extension profile. This molecular signature should allow us to identify single-molecule rupture events in pulling experiments.

Introduction

Hair cells are the mechanoreceptors of the inner ear that transform mechanical stimuli into electrical signals and that can be passed along to the brain by the eighth nerve [1]. Hair-cell mechanotransduction occurs within stereocilia, actin-filled, hair-like projections that bundle together and are deflected by mechanical stimulation. Positive deflection results in tension applied to tip links, fine protein filaments linking the tip of each stereocilium to the side of its tallest neighbor. The tip links, acting in series with an elastic 'gating spring,' pull open transduction channels to initiate sensory perception [2, 3, 4, 5].

The tip link is made of protocadherin-15 (Pcdh15) and cadherin-23 (Cdh23), two deafness-related atypical cadherins that feature exceptionally long extracellular domains containing 11 and 27 extracellular cadherin (EC) repeats, respectively [6, 7]. The crystallographic structure of the Pcdh15 and Cdh23 interacting N-termini revealed a unique cadherin binding mechanism in

which the two most amino-terminal cadherin repeats of each protein form an overlapped, antiparallel heterodimer (**Figure 4.1**). The interaction resembles an 'extended handshake' and involves repeats EC1 and EC2 from both proteins. Site directed mutagenesis, size-exclusion chromatography (SEC), and microcalorimetry (ITC) experiments validated the handshake interaction *in vitro* [8] and subsequent work validated it *in vivo* [9].

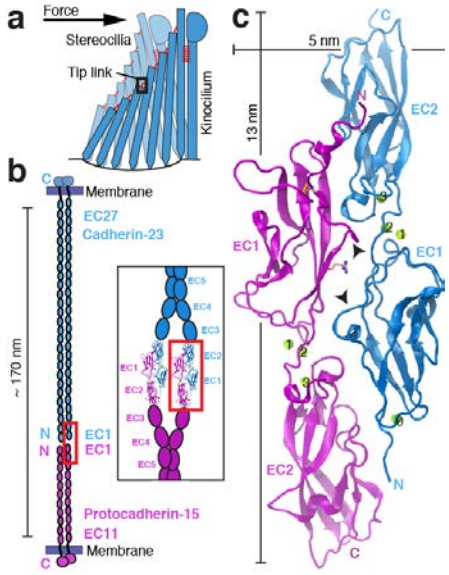

FIGURE 4.1| Structure of tip-link Pcdh15 bound to Cdh23. **a**, Hair-cell stereocilia bundle. A tip-link filament extends from the tip of each stereocilium to the side of its tallest neighbor. **b**, The tip link formed by a Pcdh15 parallel dimer interacting tip-to-tip with a Cdh23 parallel dimer. These proteins feature 11 and 27 EC repeats, respectively. Inset shows possible arrangement at the junction. **c**, Ribbon diagram of Pcdh15-EC1+2 (purple) bound to Cdh23-EC1+2 (blue) with calcium ions as green spheres. All panels adapted from [8]

Tip links are regularly subjected to (and must withstand) forces ranging from 10 to 100 pN, both in vivo and in electrophysiological experiments. Although SEC and ITC experiments provided a characterization of the bond in thermodynamic equilibrium, they did not probe its response to mechanical force. Here we discuss steered molecular dynamics simulations that predict the

strength of the tip link bond, as well as self-assembling DNA nanoswitches designed to probe the mechanical response of the tip link bond *in vitro*.

METHODS

Steered molecular dynamics simulations

Molecular dynamics simulations were performed using NAMD 2.7 [11], the CHARMM27 force field for proteins with CMAP correction [12] , and the TIP3P model for water. Simulation parameters were as in [8] . Each system was energy minimized, then equilibrated in the constant number, pressure and temperature (*NpT*) ensemble, and the resulting state used to perform subsequent SMD simulations. All simulations used T = 310 K. Coordinates of all atoms were saved for analysis every picosecond. Constant-velocity stretching simulations used the SMD method and NAMD Tcl Forces interface.

Cloning, expression, and purification of Cdh23 and Pcdh15 fragments

Clones of mouse Cdh23 repeats EC1 and EC1+2 were previously described in [13]. Numbering corresponds to mouse cadherin-23 (Cdh23) and protocadherin-15 (Pcdh15) without their signal sequences. Mouse Pcdh15 EC1+2 comprising residues Q1–D233 (Q27–D259 in mouse NCBI reference sequence NP_001136218.1) was subcloned into the NdeI and XhoI sites of the vector pET21a (C-terminal His-tag). The signal sequence was replaced by a methionine at position 0. All constructs were verified by DNA sequencing. Pcdh15-EC1+2 and Cdh23-EC1+2 were expressed independently in BL21CodonPlus(DE3)-RIPL (Stratagene) cultured in Luria-Bertani

medium and induced at OD600 ~0.6 with 100 μM IPTG at 20 ºC for ~16 h. Cells were lysed by sonication in denaturing buffer (20mM HEPES at pH7.5, 6M guanidine hydrochloride (GuHCl), 10mM $CaCl_2$, 20mM imidazole at pH7.0). The cleared lysates were loaded onto nickel sepharose (GE Healthcare) and eluted with denaturing buffer supplemented with 500mM imidazole. Wild-type Pcdh15-EC1+2 protein fragments were reduced by adding 1mM dithiothreitol and incubating at 37 ºC for ~30 min. Purified and denatured Pcdh15 samples were refolded in six steps at 4 ºC using membranes with a molecular weight cutoff of 2,000. Refolded protein used for DNA nanoswitch functionalization was further purified in size exclusion chromatography experiments on a Superdex75 column (GE Healthcare) in 20mM Tris HCl, pH8.0, 200mM KCl, with 1mM $CaCl_2$.

Sortase-mediated construction of DNA-protein hybrids

Linearized M13 single-stranded DNA was used as a scaffold upon which CDH23-EC1+2 and PCDH15-EC1+2 were localized for use in single molecule force spectroscopy. A C-terminal Leu-Pro-Glu-Thr-Gly sequence for sortase recognition was engineered into the C-terminal tail of Cdh23 and Pcdh15. A Gly-Gly-Gly sequence was incorporated to the oligonucleotides of interest. The latter was accomplished via the use of copper-catalyzed click chemistry. An azide functionalized synthetic oligonucleotide was coupled to an alkyne containing synthetic peptide (Pra-Gly-Gly-Gly-TEV-Flag, where Pra is a propargyl glycine which provides an alkyne functionality, Flag is a Flag tag for purification purposes, and the TEV is a TEV protease recognition site to allow the removal of the Flag tag to expose the N-terminal Gly-Gly-Gly).

Upon processing and purification with commercially available resins and kits, the final Gly-Gly-Gly-oligonucleotide can be obtained free of any side products [10].

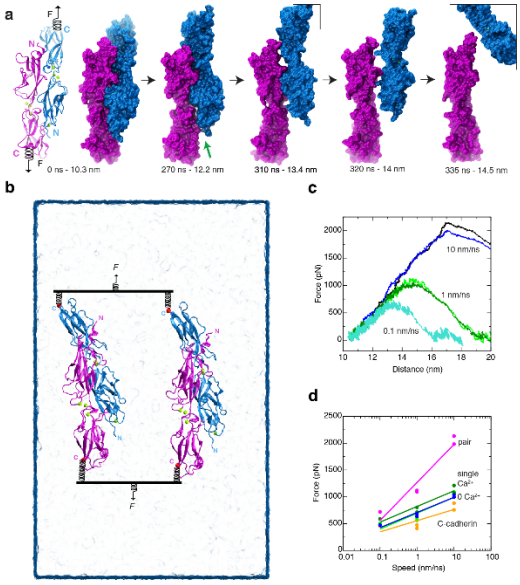

FIGURE 4.2| Mechanical strength of the Pcdh15-EC1+2–Cdh23-EC1+2 complex probed by SMD simulations. **a**, Snapshots of Pcdh15-EC1+2 (purple) and Cdh23-EC1+2 (blue) unbinding. The complex is shown in both cartoon and surface representations at the beginning, and in surface representation at indicated time points. Force (*F*) was applied to the C termini of both protomers. **b**, Mechanical strength of two Pcdh15-EC1+2–Cdh23-EC1+2 complexes connected in parallel by slabs. **c**, Force applied to one of the slabs versus distance between slabs. Different traces correspond to independent simulations performed at stretching speeds of 10 (blue and black), 1 (light and dark green), and 0.1 nm/ns (cyan). **d**, Maximum force-peak values vs. stretching speed for unbinding simulations of the pair of complexes shown in magenta. Unbinding force-peak values for simulations of single complexes with (green) and without Ca^{2+} (blue), as well as for C-cadherin (orange) are shown. All panels adapted from [8]

This sortase compatible oligonucleotide can be added to the sortase compatible protein for sortase catalyzed transpeptidation resulting in a peptide bond (Protein-Leu-Pro-Glu-Thr-Gly-Gly-Gly-Oligonucleotide + Gly-6xHis). The reaction was done with a large excess of protein to ensure that all the oligos were driven into the coupled state. During the transpeptidation, the sortase enzyme selectively cleaved the 6xHis tag off of the final product. All excess protein, the

TEV protease, and the sortase enzyme (all of which contain 6xHis tags), were removed by washing the product over anti-his beads. The final coupled oligonucleotides were hybridized onto the M13 scaffold in addition to digoxigenin and biotin containing oligos to facilitate single molecule force spectroscopy measurements using anti-digoxigenin beads and streptavidin beads in an optical tweezer system to measure the rupture force of the Cdh23 Pcdh15 interaction.

RESULTS

Simulated unbinding of the tip link bond

Steered molecular dynamics simulations [14], in which forces are applied to the carboxy terminus of each protomer to induce complex dissociation, showed unbinding without unfolding of repeats. Simulations performed using different stretching speeds, initial conditions, and thermodynamic ensembles revealed a similar scenario, with at least one force peak of ~400 pN associated with complex unbinding (**Figure 4.2**; [8]).

Unbinding forces followed the well-known dependence on stretching speeds, with less force required when the stretch was slower. The slowest speed used in our simulations matched the measured velocity of the basilar membrane induced by loud sound [15] as well as speed of mechanical stimulators used in *ex vivo* electrophysiological experiments [16]. In all the simulations the Pcdh15-EC1+2-Cdh23-EC1+2 interface was stronger than that of the classical C-cadherin interface pulled under identical conditions. Furthermore, the force required to unbind parallel complexes was almost double that required to unbind a single Pcdh15-EC1+2-Cdh23-

EC1+2 complex, which may correspond to the actual force that heterotetrameric tip links can withstand *in vivo* before rupture due to severe mechanical stimuli, such as loud sound.

A DNA nanoswitch for force spectroscopy of tip link bonds

To test the predictions from simulations and determine the strength of the Pcdh15-EC1+2-Cdh23-EC1+2 bond we developed a nanoswitch for single molecule measurements. We use the recently developed modular single molecule platform inspired by DNA origami [17]. This platform uses a single stranded DNA scaffold onto which a series of 121 complementary oligonucleotides bind to their sequence-specified locations. This allows for easy customization of the construct as individual oligonucleotides can be functionalized; the desired construct will self-assemble upon mixing with the scaffold. In this case we wanted to design a system in which the construct has strong handle for bead attachment at each end (digoxigenin at one end and biotin at the other end). Additionally the construct needed to have Cdh23EC1+2 and Pcdh15EC1+2 at different locations along the scaffold. Traditional protein coupling techniques are often incompatible with the proteins of interest, due either to a lack of site specificity and/or coupling conditions do not that maintain protein stability and function.

To solve this problem, we developed a technique which combines an evolved version of the enzyme sortase [18] with copper-catalyzed click chemistry to frontload all harsh coupling conditions to a short synthetic peptide and a synthetic oligonucleotide. This technique results in the protein of interest only being subjected to ~30 minutes of conjugation time under physiological buffer and salt conditions at room temperature [10]. Alternatively, the coupling can be done directly onto the scaffold as illustrated in **Figure 4.3**.

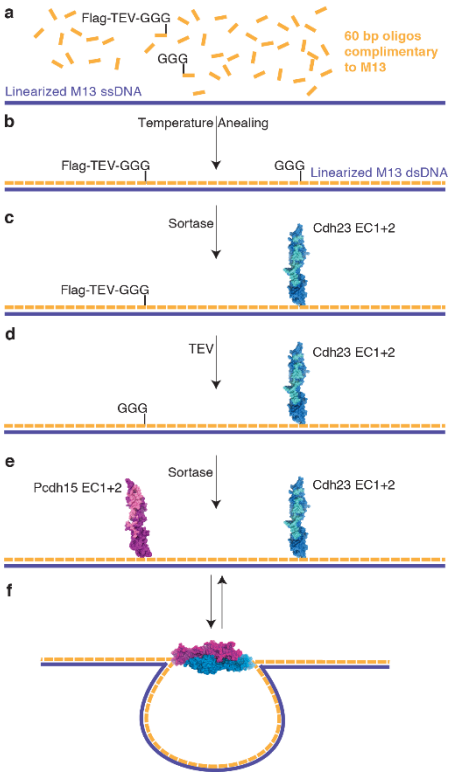

FIGURE 4.3| A method for the formation of the binary DNA-nanoswitch. Linearized M13 single-stranded DNA (dark blue), complimentary oligonucleotides (golden-rods), Cdh23-EC1+2 (cyan), and Pcdh15-EC1+2 (magenta). Adapted from [10].

CONCLUSIONS

The use of the DNA-nanoswitch platform will allow for high throughput read out of single-molecule force-spectroscopy measurements. The well-defined lengths of DNA-nanoswitch in the bound and unbound states provide a unique molecular signature that greatly facilitates the identification of rupture events of the protein pair of interest (**Figure 4.4**). The DNA-nanoswitches also provide a means of verifying that rupture force measurements were made on a single interacting pair, by utilizing the well characterized force extension properties of double stranded DNA (**Figure 4.4**). Upon pulling on the Cdh23-Pcdh15 interaction we can measure the

rupture force at the wide range of loading rates and solution conditions comparable to those experienced by tip links in the inner ear. We expect that the rupture forces measured at these lower loading rates will be significantly lower than the rupture forces measured at loading rates used in the molecular dynamics simulations that were comparable to the upper end of the physiological range.

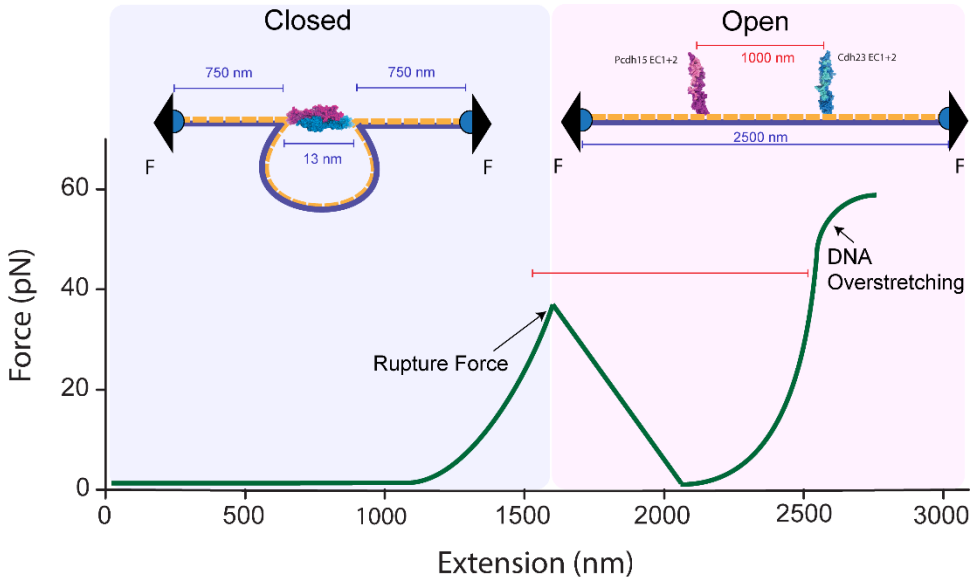

FIGURE 4.4| A predicted force-extension trace resulting from pulling on a nanoswitch functionalized with Cdh23-EC1+2 and Pcdh15-EC1+2 roughly one third of the way in from each end.

Acknowledgments

The authors gratefully acknowledge the help of Brent Dorr for providing the plasmid for the evolved sortase; Rachelle Gaudet for use of her facilities for protein production and purification; Gary Yellen, Rachel Wilson, Jeffrey Holt, Hidde Ploegh, Ahmed Badran, Zhi-Yang Tsun, and members of the Wong and Corey Labs for critical discussions; and the labs of Sun Hur and Timothy Springer for assistance in protein production. Funding for this project was provided by

NIH R01 DC02281 to D.P.C and R.G. and NIH K99/R00 DC012534-01 to M.S. M.K. was supported by NSF GRFP 2012147612; W.W. was supported by BCH startup funds.

References

1. Gillespie PG and Muller U (2009) Mechanotransduction by hair cells: models, molecules, and mechanisms. *Cell*

2. Corey DP and Hudspeth AJ (1983) Kinetics of the receptor current in bullfrog saccular hair cells. *Journal of Neuroscience*

3. Pickles JO, Comis SD, and Osborne MP (1984) Cross-links between stereocilia in the guinea pig organ of Corti, and their possible relation to sensory transduction. *Hearing Research*

4. Howard J, Hudspeth AJ (1988) Compliance of the hair bundle associated with gating of mechanoelectrical transduction channels in the bullfrog's saccular hair cell. *Neuron*

5. Assad JA, Shepherd GM, and Corey DP (1991) Tip-link integrity and mechanical transduction in vertebrate hair cells. *Neuron*

6. Kazmierczak P, Sakaguchi H, Tokita J, Wilson-Kubalek EM, Milligan RA, Müller U, and Kachar B (2007) Cadherin 23 and protocadherin 15 interact to form tip-link filaments in sensory hair cells. *Nature*

7. Ahmed ZM, Goodyear R, Riazuddin S, Lagziel A, Legan PK, Behra M, Burgess SM, Lilley KS, Wilcox ER, Riazuddin S, Griffith AJ, Frolenkov GI, Belyantseva IA, Richardson GP, and Friedman TB (2006)The tip-link antigen, a protein associated with the transduction complex of sensory hair cells, is protocadherin-15. *Journal of Neuroscience.*

8. Sotomayor M, Weihofen WA, Gaudet R, Corey DP (2012) Structure of a force-conveying cadherin bond essential for inner-ear mechanotransduction. *Nature*

9. Geng R, Sotomayor M, Kinder KJ, Gopal SR, Gerka-Stuyt J, Chen DH, Hardisty-Hughes RE, Ball G, Parker A, Gaudet R, Furness D, Brown SD, Corey DP, Alagramam KN (2013) Noddy, a mouse harboring a missense mutation in protocadherin-15, reveals the impact of disrupting a critical interaction site between tip-link cadherins in inner ear hair cells. *Journal of Neuroscience*

10. Koussa MA, Sotomayor M, and Wong WP (2014) Protocol for sortase-mediated construction of DNA-protein hybrids and functional nanostructures. *Methods*

11. Phillips JC, Braun R, Wang W, Gumbart J, Tajkhorshid E, Villa E, Chipot C, Skeel RD, Kalé L, Schulten K (2005) Scalable molecular dynamics with NAMD. *Journal of Computational Chemistry*

12. Mackerell AD Jr, Feig M, Brooks CL 3rd (2004) Extending the treatment of backbone energetics in protein force fields: limitations of gas-phase quantum mechanics in reproducing protein conformational distributions in molecular dynamics simulations. *Journal of Computational Chemistry*

13. Sotomayor M, Weihofen WA, Gaudet R, and Corey DP (2010) Structural determinants of cadherin-23 function in hearing and deafness. *Neuron*

14. Sotomayor M and Schulten K (2007) Single-molecule experiments in vitro and in silico

15. Robles L and Ruggero. MA (2001) Mechanics of the mammalian cochlea. *Physiology Review*

16. Stauffer EA, Holt JR (2007) Sensory transduction and adaptation in inner and outer hair cells of the mouse auditory system. *Journal of Neurophysiology*

17. Halvorsen K, Schaak D, Wong WP (2011) Nanoengineering a single-molecule mechanical switch using DNA self-assembly. *Nanotechnology*

18. Chen I, Dorr BM, Liu DR (2011) A general strategy for the evolution of bond-forming enzymes using yeast display. *PNAS*

Chapter Five

Force Spectroscopy of Single Tip-Link Bonds

Abstract

Inner-ear mechanotransduction relies on tip links, fine protein filaments made of cadherin-23 and protocadherin-15 that convey tension to mechanosensitive channels at the tips of hair-cell stereocilia. The tip-link cadherins are thought to form a heterotetrameric complex, with two cadherin-23 molecules forming the upper part of the filament and two protocadherin-15 molecules forming the lower end. The interaction between cadherin-23 and protocadherin-15 is mediated by their N-terminal tips. Missense mutations that modify the interaction interface impair binding and lead to deafness. We have developed molecular tools to perform single-molecule force spectroscopy on the tip-link bond. Self-assembling DNA nanoswitches are functionalized with the interacting tips of cadherin-23 and protocadherin-15 using the enzyme sortase under conditions that preserve protein function. These tip-link-functionalized nanoswitches are designed to provide a signature force-extension profile, which allows us to identify single-molecule rupture events that result from applying force. Using this system, we have been able to measure the cadherin-23-protocadherin-15 single-molecule force-dependent off rate, as well as the concentration-dependent on rate for a single pair of these proteins. The rates suggest that a single bond is inadequate to withstand physiological forces for physiological times, but we construct a new model for tip-link dynamics which greatly alters our understanding of tip-link function and explains the necessity for a two-filament tip link.

Introduction

Hearing in humans is unique among the senses in that it allows simultaneous detection of stimuli from any direction. Beyond providing us additional senses, mechanotransduction complements our other senses. We are primarily visual creatures but our vision is limited to having high acuity only at the fovea. This is not very noticeable in daily life as a result of compensatory mechanisms, some of which rely on mechanotransduction in the inner ear. For instance, the vestibular-ocular reflex (VOR) allows one to remain foveated on a target while the head moves. In order to do this the semi-circular canals in the inner ear must sense angular accelerations of the head which are converted to electrical signals. In the brainstem these signals are integrated and relayed to the ocular muscles to counter roll the eyes, resulting in the eye remaining still while the head rotates. Similarly, although we usually use vision to track a target, it is often an auditory signal which first alerts us to the presence of something that requires our visual attention.

In addition to complementing vision, the inner ear provides us with our sense of balance, a sense of linear acceleration, of head position, and of up and down. The auditory part of the inner ear, the cochlea, is central to our means of communicating with one another; it affords us the ability to listen to and appreciate music and the ability to detect threats from visually occluded regions of our environment. Our hearing works over a large dynamic range. This results in the ability to hear the sound of a pin drop in a quiet room, while also allowing us to hold and maintain a conversation with an individual in a noisy environment. Although much of this ability comes from higher order rejection of sound, the sensory epithelium of the cochlea

is sensitive to motions of atomic dimensions and has built-in mechanisms for adapting to constant stimuli.

All these senses rely on mechano-electrical transduction carried out by cells in the ear known as hair cells, so named for the bundle of "hairs" or modified microvilli at their apical surface. These specialized microvilli, referred to as stereocilia, are arranged in a staircase formation from shortest to tallest. Mechanical stimuli from sound or head movements ultimately result in deflection of the bundle and shearing between the tips of individual stereocilia. This applies tension to a set of fine filaments called tip links that connect the tip of each stereocilium to the side of its tallest neighbor (**Figure 5.1a**).

The tip link conveys this tension to mechanosensitive ion channels at the tips of stereocilia, inducing stimulus-locked changes in the hair cell's membrane potential (Corey &Hudspeth 1979, Hudspeth 1982, Castellano-Muñoz et al., 2012). These tip links are composed of two different proteins which interact in a non-covalent fashion. The upper end of the tip link is composed of cadherin-23 (CDH23) while the lower end is composed of protocadherin-15 (PCDH15) (Kazmierczak et al., 2007). Crystal structures reveal that these proteins interact in an anti-parallel fashion through an interaction interface which spans extracellular domains one and two (EC1 and EC2), such that ECs 1 and 2 of CDH23 interact with ECs 2 and 1 of PCDH15 respectively (Sotomayor et al., 2012). This two component nature of the tip link means that the tip link has the potential to break. The integrity of the tip link has been shown to be dependent on Ca2+, as chelation of Ca2+ severs tip links (Assad et al., 1991). Furthermore, tip links have been shown to be ruptured by exposure to loud sounds (Husbands et al., 1999). Once tip links

are ruptured, no force will be conveyed to the mechanosensitive ion channels when stereocilia shear, meaning that the mechanical signal is never transduced. Thus investigation of the mechanical properties of tip links is crucial for our understanding of both noise-induced, and in some cases hereditary, hearing loss. Sotomayor et al. in 2012 performed steered molecular dynamics simulations to apply forces in silico to the crystal structure of the complex. This work has set up a framework for designing single molecule experiments to probe the mechanical nature of the interaction, described here.

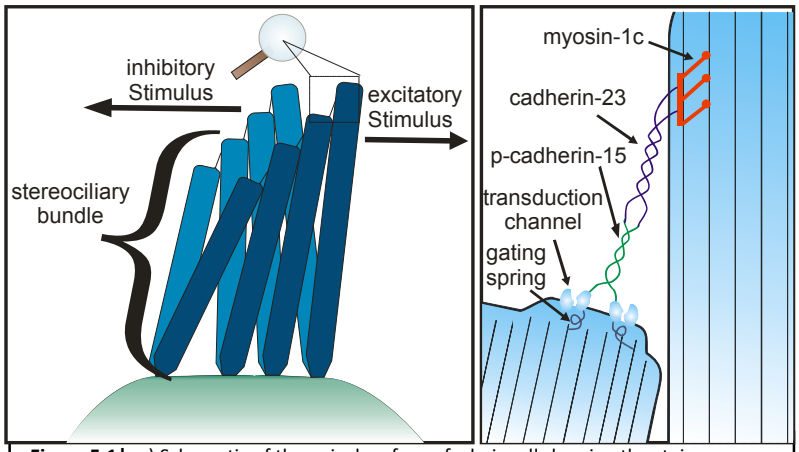

Figure 5.1|. a) Schematic of the apical surface of a hair cell showing the staircase arrangement of stereocilia at rest (light blue) and experiencing an excitatory stimulus (dark blue). b) Magnification of the region indicated in a. Highlighting the putative organization of components of the mechanotransduction apparatus.**b.**

Materials and Methods:

Looped Linkers:

Scaffold preparation: DNA scaffolds for single molecule studies were made using methods described in Halvorsen et al., 2011. In short, circular single-stranded M13mp18 DNA was linearized by hybridizing an oligonucleotide complementary to a region containing a BtsCI

restriction site, and incubating with BtsCI at 50°C for 1 hour. The enzyme was then heat-deactivated by raising the temperature to 95°C. The scaffold was then tiled with 121 oligonucleotides (118 oligonucleotides of 60nt, one of which has a 5′ dual biotin and one has a 3′ digoxigenin; 1 of 30nt; 1 of 49nt; and one of 58nt). The 58-nt oligo has the last 28nt complementary to Var6(30-58) on M13mp18 and the first 30nt of this oligonucleotide is herein referred to as VarA. This covers the entirety of the M13mp18 scaffold leaving one 29nt, single-stranded region, Var4.08(14-42) herein referred to as VarD, on the M13mp18 and adding another through the oligonucleotide that is only complementary to 28nt on the M13mp18. These two single stranded regions lack secondary structure at room temperature allowing for room-temperature hybridization of protein-functionalized oligonucleotides (see Koussa et al., 2015 for Var nomenclature and sequence map).

Sortase coupling: A method for using the enzyme sortase to couple CDH23 and PCDH15 is detailed in Koussa et al., 2014). In short, a synthetic peptide with (N-to-C) a Flag tag, a tobacco-etch-virus (TEV) protease cleavage site, the sequence Gly-Gly-Gly, and a propargylglycine, (Flag-TEV-GGG-Pra) was coupled via copper-catalyzed click chemistry to an oligonucleotide by attaching the propargylglycine's alkyne to an Azide on the 3′ end of VarD or to an oligonucleotide complementary to VarA (VarA Comp). The coupled product was purified via gel extraction, and the Flag tag was cleaved by treatment with TEV protease leaving a sortase-compatible N-terminal Gly-Gly-Gly peptide sequence on the 3′ end of the oligonucleotides. The oligonucleotides were then concentrated to ~10μM. CDH23-LPETG(H_6) and PCDH15-LPETG(H_6) stocks are used at ~0.1 mM concentrations, and the sortase stock is at ~1 mM. VarD-GGG (5 μl) was combined with 0.5 μl of the CDH23-LPETG(H_6) stock and 0.5 μl of the sortase

stock. The final buffer contains 150mM Tris buffer pH 7.4, 300mM KCl, 5mM $CaCl_2$ and 5mM $MgCl_2$. Similarly, VarA Comp-GGG (5 μl) was combined with 0.5 μl of the PCDH15-LPETG(H_6) stock and 0.5 μl of the sortase stock. The final buffer contains 150mM Tris buffer pH 7.4, 300 mM KCl, 5 mM $CaCl_2$ and 5 mM $MgCl_2$. These were allowed to sit at 22 C for 2 hours in the dark before combining with 5 μl of the tiled M13mp18 scaffold (~16nM). This was then allowed to hybridize for 2 hours at 22 C. The sample was either used immediately, or aliquoted, flash frozen, and thawed right before use in optical trap experiments.

Optical Trap experiments:

Sample Prep: 5μm carboxylic-acid-functionalized silica beads were conjugated to either digoxigenin antibodies (Roche) or streptavidin molecules (Rockland) using EDC-NHS chemistry (Ward et al., 2015). Post conjugation, 2 μl of streptavidin beads was washed 3 times in 20 μl of 150 mM Tris buffer pH 7.4, 300 mM KCl, 5 mM $CaCl_2$. After the final centrifugation step, 20 μl of supernatant was removed, and the beads were resuspended in 5 μl of 15x dilute protein containing DNA scaffold. This was left to rotate for 30min at 22 C. Meanwhile, 2 μl of anti-digoxigenin beads was washed 3 times in 20 μl of 150 mM Tris buffer pH 7.4, 300 mM KCl, 5 mM $CaCl_2$, then resuspended in 20 μl of wash buffer. Anti-digoxigenin beads (10 μl) were added to 200 μl of the same buffer and mixed thoroughly before adding 3.5 μl of the streptavidin-DNA bead mixture. This was then quickly added to a 10 μl channel made with double-sided Captain tape on a polyacrylamide-passivated slide.

Trapping: Beads were manipulated using a dual-beam 1064-nm optical trap system similar to that described in Halvorsen et al. 2011. One beam is equipped with coarse steering via a

Newport piezo mirror mount. The second beam is afforded finer control via a Mad City piezo mirror mount. Both steering mirrors are placed in the back focal plane of the objective such that rotation of the mirrors results in pure beam translation in the chamber. The trap stiffnesses were calibrated by measuring thermal fluctuations at ~50 mW laser power (split roughly evenly between the two traps). Typically the trap stiffness is around 0.1 pN/nm when using ~900 mW of laser power. Beads were brought in close proximity to one another for 0-2 seconds by steering with the Mad City mirror to form single molecule tethers. Bead positions were determined in real time at 1500-3000 frames per second with sub-pixel fitting of a 3rd order polynomial to the dark edges of the beads. Loading rates were controlled by controlling the speed of beam motion rather than using force-based feedback this results in a ~10% spread in loading rates across conditions. Tethers were usually pulled out until the anchor ruptured. In some experiments, however, once a tether was formed and a rupture of the CDH23-PCDH15 interaction was observed, the force would be lowered for 1-5 seconds to enable rebinding of the complex. Rebinding was assessed by pulling on the tether again to see if the bond had reformed.

Results:

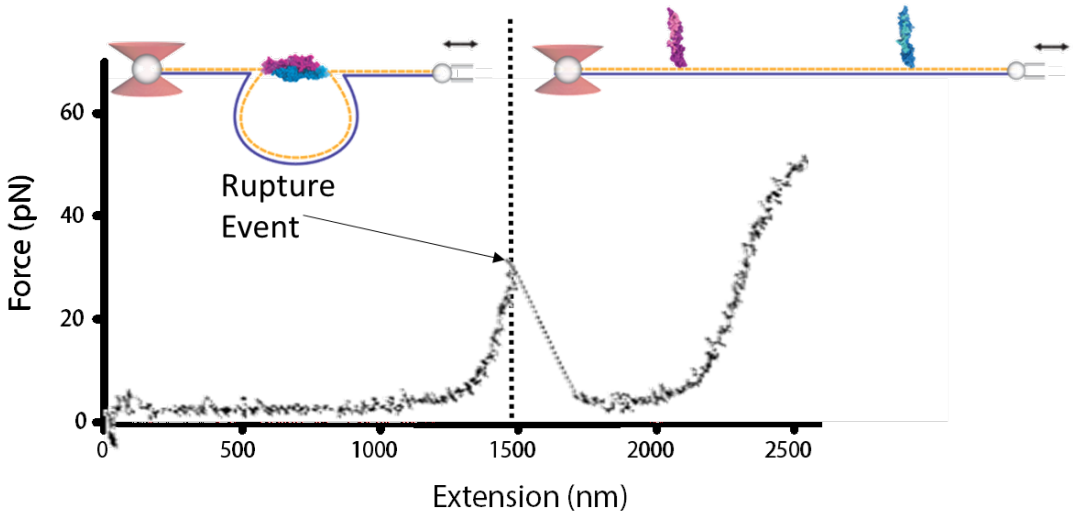

Figure 5.2| Force extension plot of a CDH23-PCDH15 rupture event.

Dynamic force spectroscopy (DFS): DFS was used to measure the force dependence of the CDH23-PCDH15 off-rate. Rupture forces were measured, as shown in **Figure 5.2**, at three different loading rates (15, 150, and 1500 pN/s). The simplest way to describe a system that can exist in one of two states is to use the first order kinetic equation. $\frac{dP}{dt} = -k_{\text{off}} \cdot P + k_{\text{on}} \cdot (1 - P)$ in which P is the probability of being in one state, and 1-P is then probability of being in the other state. If we assume the system is far from equilibrium and can only transition out of P, then we can write $\frac{dP}{dt} = -k_{off} \cdot P$. This would apply for example for a bound complex which would be unlikely to rebind after rupture of the interaction. By taking the derivative of this function and setting it equal to zero, we can find the most likely rupture time. $\frac{d^2P}{dt^2} = -\frac{dk_{\text{off}}}{dt} \cdot$

$P - k_{\text{off}} \cdot \frac{dP}{dt} = 0$. We can simplify this to $\frac{dk_{\text{off}}}{dt}(t^*) = k_{\text{off}}^2(t^*)$. From the Arrhenius equation, we know that $k_{\text{off}}^0 = A_0 e^{\frac{-E_a}{k_B T}}$ in which k_{off}^0 is the zero-force off rate, A_0 is an attempt frequency, E_a is the activation energy, k_B is Boltzmann's constant, and T is the temperature in Kelvin. When force is applied to a system along the reaction coordinate, that reduces the energy barrier by the amount of work done on the particle of $f \cdot x_{\text{ts}}$ where f is the force, and $x_{\text{ts}}$is the distance to the transition state. Thus the force dependent off-rate can be written as $k_{\text{off}}(f) = A_0 e^{\frac{-(E_a - f \cdot x_{\text{ts}})}{k_B T}}$ or $k_{\text{off}}(f) = k_{\text{off}}^0 e^{\frac{f \cdot x_{\text{ts}}}{k_B T}}$. If we define a force scale $f_\beta = \frac{k_B T}{x_{\text{ts}}}$ then we can write $k_{\text{off}}(f) = k_{\text{off}}^0 e^{\frac{f}{f_\beta}}$. If we alter that force linearly with time at some loading rate, r_l, then we can write that $\frac{dk_{\text{off}}}{dt} = \frac{dk_{\text{off}}}{df}\frac{df}{dt}$ or $\frac{dk_{\text{off}}}{dt} = \frac{dk_{\text{off}}}{df} r_f$. Differentiating k_{off} with respect to force, yields $\frac{dk_{\text{off}}}{dt} = \frac{r_l}{f_\beta} k_{\text{off}}$. By substituting in our expression for the most likely rupture time, $\frac{dk_{\text{off}}}{dt}(t^*) = k_{\text{off}}^2(t^*)$, we find $k_{\text{off}} = \frac{r_l}{f_\beta} = k_{\text{off}}^0 e^{\frac{f^*}{f_\beta}}$ where f^* is the most likely rupture force. This can be rearranged to yield $f^* = f_\beta \ln\left(\frac{r_l}{f_\beta \cdot k_{\text{off}}^0}\right)$. This can then be fit to the peak of the rupture force histograms as a function of loading rate (**Figure 5.3**). The curve fitting yielded an f_β of 3.43 pN, and a k_{off}^0 of 2.1x10^{-3} s^{-1}.

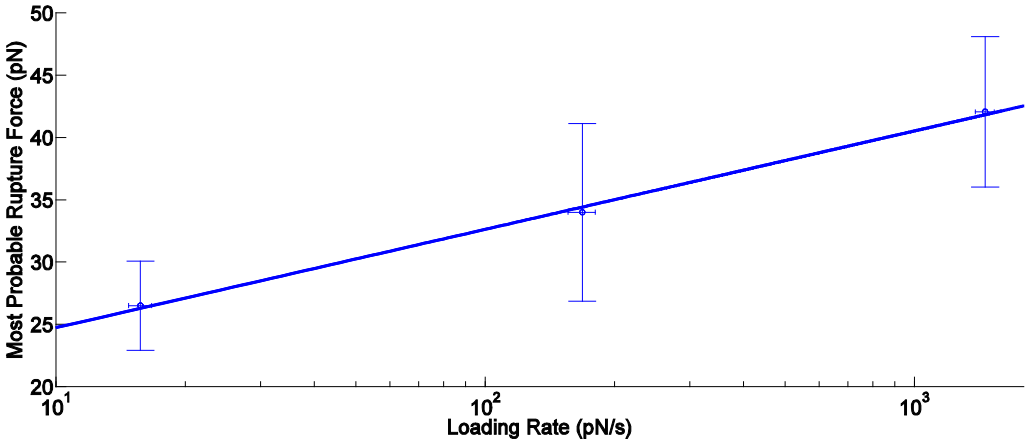

Figure 5.3| Dynamic Force Spectroscopy fit to the most likely rupture forces measured at various loading rates. Error bars represent standard deviations.

On-rate measurements: After a CDH23-PCDH15 rupture we brought the beads into close proximity to lower the force and allow the bond to reform. By pulling on the construct again we were able to assess bond formation (**Figure 5.4**). We found that 43% of one-second-long trials resulted in bond formation. The effective concentration of ligands on a loop of this size has been theoretically calculated by using a worm-like-chain treatment of the polymer, and experimentally verified to be ~500nM. It is important to note however, that this assumes a free polymer in solution, and does not account for the fact that the ends are fixed to beads held a distance apart thus the following concentration-dependent on rate is an under estimate. Using the single-molecule rebinding probability at a given waiting time, and the effective concentration, we were able to determine a concentration-dependent on-rate of 1.1×10^{6} M^{-1} s^{-1} (N =7).

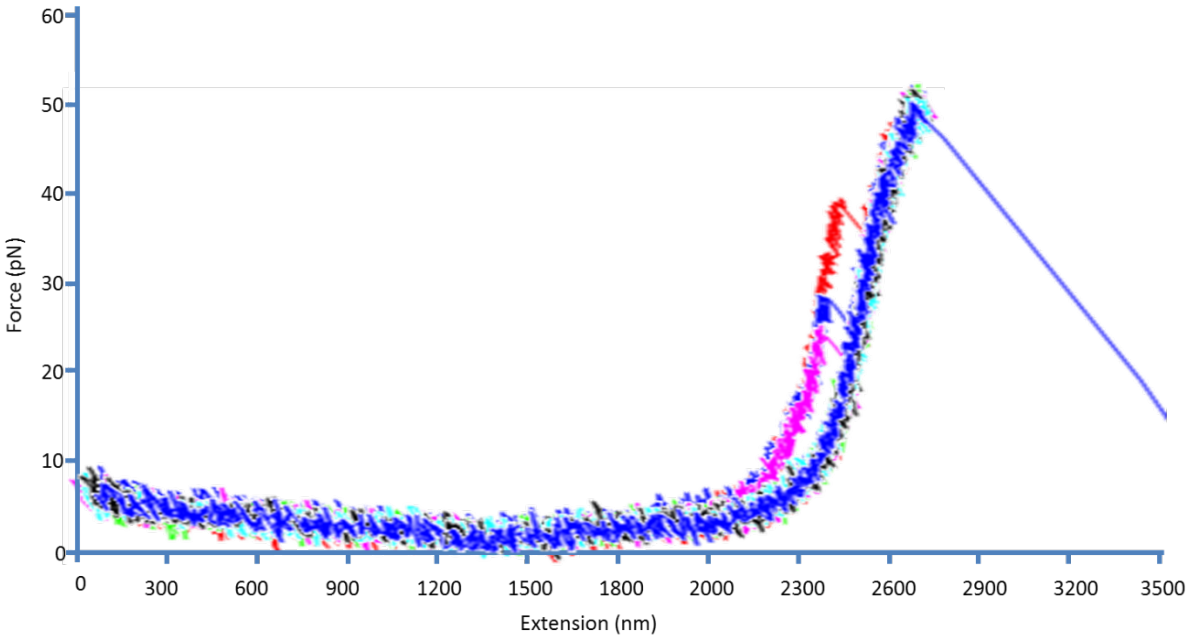

Figure 5.4| Force extension plot showing 3 repeated CDH23-PCDH15 rupture and rebinding

Discussion:

These data provide insights into the dynamics of tip links under physiological forces. First, we can use the force dependence, f_β, to understand how far the cadherins slip under the influence of force, x_{ts}, in moving between the resting bound state and the transition state for unbinding. Taking $k_b T = 4.1\ pN \cdot nm$ we calculate an x_{ts} of 1.19 nm. This indicates that the CDH23-PCDH15 interaction can slip by ~25% the length of an extracellular domain without a catastrophic rupture. Forces that induce slipping greater than 1.19 nm, however, surmount the energy of the transition state and cause a complete rupture of the interaction.

The force-dependent off rate is given by $k_{off}(f) = k_{off}^0 \cdot e^{\left(\frac{f}{f_\beta}\right)}$. Taking the lifetime as $\frac{1}{k_{off}(f)}$ yields a zero-force lifetime of 7.96 minutes, and a lifetime of only 26 seconds under the 10

pN of resting tension thought to be applied by the myosin motor. These lifetimes do not seem conducive to a functioning auditory system, in that we expect the lifetime of a tip link to be much longer than eight minutes.

It is important, however, to consider that the tip link is thought to exist as a dimer of dimers, constituting two sets of parallel strands interacting with one another in an antiparallel fashion. Thus if one CDH23/PCDH15 dimer ruptures, the tip link can hold together so long as the ruptured strand can rebind before the other strand ruptures.

The average lifetime of the divalent system can be expressed as follows: $\frac{c \cdot k_{on} + 3k_{off}(f)}{2(k_{off}(f))^2}$ (Yang D. et al. unpublished) where c is the effective concentration of the tethered binding partners, k_{on} is the concentration-dependent on rate, derived from the single-molecule rebinding experiments to be 1.11×10^6 $M^{-1}s^{-1}$, and $k_{off}(f)$ is the force-dependent, single-molecule off rate given by $k_{off}(f) = k_{off}^0 \cdot e^{\left(\frac{f}{f_\beta}\right)}$. Combining these two expressions enables calculation of the average lifetime as a function of force, if the tip link exists as a dimer of dimers. With this, we find that the zero-force lifetime becomes 9.33 months rather than 7.96 minutes. The lifetime under the 10 pN of resting tension is nearly one day rather than under one second.

By fitting optical coherence tomography measurements of hair-bundle motions resulting from stimuli at varying stimuli (Lee et al., 2014) to an exponential assuming a maximum operating range of 2 μm we can develop a function to determine bundle deflection as a function of sound pressure level. With this fit, assuming a gamma factor (the geometric factor relating bundle displacement to displacement at the tip link) of 0.1 (Hudspeth, 1983), and a gating-

spring stiffness of 0.38pN/nM (Benser et al., 1993), we can express the force experienced by a tip link as a function of sound pressure level. Using this, we can generate the expected lifetime of divalent tip-links under different sound pressure levels associated with daily activities (**Figure 5.5**).

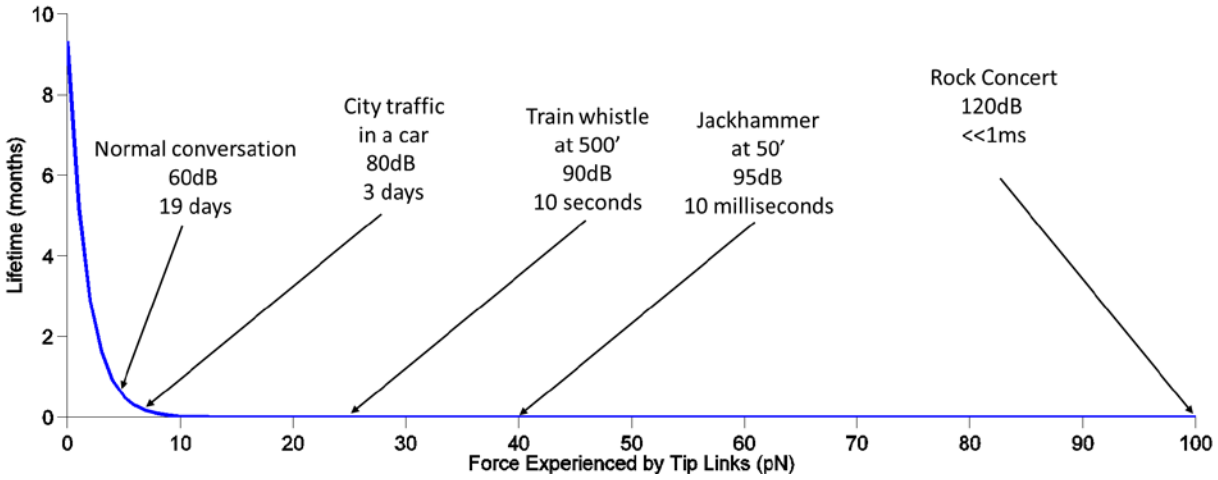

Figure 5.5| Tip link lifetime as a function of force. Predicted lifetimes at for specific auditory stimuli are highlighted.

One must also account for adaptation. The adaptation motor will try to maintain tip-link tension at ~10pN. To survive, a tip link's lifetime during a given sound stimulus simply needs to exceed the time-course of adaptation, which occurs in tens of milliseconds. From **Figure 5.5** we see that the 95dB jackhammer at 50 feet seems to be the threshold for rupturing tip links faster than the time course of adaptation.

It is interesting to speculate about the utility of having a two-strand tip link. There are no vesicles in stereocilia, thus all membrane proteins need to be inserted at the apical surface of the cell body, and transported up the stereocilia. As it would be difficult to coordinate the transport of a molecule that spans two cellular compartments isolated by up to 800 nm, it may have been simpler to evolve a two component system such in which individual components

could be transported to the tips of stereocilia, then combined to form a tip link. At the same time, this lack of a covalent bond, introduces a weak link in the chain.

It is also interesting to speculate further that the tip link may have evolved to be just strong enough. Acting like a circuit breaker, cadherin unbunding may be a more desirable failure mode than ripping the entire mechanotransduction apparatus out of the membrane.

These single-molecule measurements not only reveal the underlying mechanical properties of tip-link proteins, but also fundamentally alter the way we think about tip-link dynamics, the evolution of tip links, and the molecular implications of prolonged exposure to loud sounds.

References:

1. Corey, D. & Hudspeth, A. (1979), 'Ionic basis of the receptor potential in a vertebrate hair cell.', *Nature* **281**(5733), 675--677Hudspeth 1982,
2. Castellano-Muñoz M, Peng AW, Salles FT, Ricci AJ (2012), 'Swept field laser confocal microscopy for enhanced spatial and temporal resolution in live-cell imaging'
3. Sotomayor, M.; Weihofen, W.; Gaudet, R. & Corey, D. (2012) Structure of a force-conveying cadherin bond essential for inner-ear mechanotransduction.' Nature
4. Assad, J.; Shepherd, G. & Corey, D. (1991), 'Tip-link integrity and mechanical transduction in vertebrate hair cells.', *Neuron* **7**(6), 985--994.
5. Husbands, J.; Steinberg, S.; Kurian, R. & Saunders, J. (1999), 'Tip-link integrity on chick tall hair cell stereocilia following intense sound exposure.', *Hearing research* **135**(1-2), 135--145.
6. Halvorsen, K.; Schaak, D. & Wong, W. (2011), 'Nanoengineering a single-molecule mechanical switch using DNA self-assembly.', *Nanotechnology* **22**(49), 494005--.
7. Koussa, M.A.; Halvorsen, K; Ward, A.; Wong, W.P. (2015) 'DNA nanoswitches: a quantitative platform for gel-based biomolecular interaction analysis.', *Nature Methods* **12, 123-126.**
8. Koussa, M.A.; Sotomayor, M.; Wong, W.P. (2014) 'Protocol for sortase-mediated construction of DNA-protein hybrids and functional nanostructures', *Methods* **67(2), 134-141.**
9. Ward, A.; Hilitski, F; Schwenger, W.; Welch, D.; Lau, A.W.; Vitelli, V.; Mahadevan, L.; Dogic, Z. (2015), 'Solid friction between soft filaments.' *Nature Materials* **(epub)**

10. Yang, D.; Wong, W.P.; Prentiss, M. 'Kinetic Modeling of Reaction Dwell Time of Polyvalent Biological and Chemical System' **(unpublished)**
11. Wong, W.P. and Halvorsen, K. (2006) 'Theeffectofintegrationtime on fluctuation measurements: calibrating an optical trap in the presence of motion blur' *Opt. Express* **14**, **12517–31**
12. Lee, H.Y.; Raphael P.D.; Ellerbee, A.K.; Applegate, B.E.; and Oghalai J.S. (2014). 'Swept source optical coherence tomography for in vivo imaging and vibrometry in the apex of the mouse cochlea' Mechanics of Hearing 2014 Proceedings **(in press)**
13. Benser, M.; Issa, N. & Hudspeth, A. (1993), 'Hair-bundle stiffness dominates the elastic reactance to otolithic-membrane shear.', *Hearing research* **68**(2), 243--252.

Chapter Six: Closing Remarks

In closing, it may be worthwhile to articulate some of the insight gained in the course of this work into the design of experiments and the scientific method, and to suggest future experiments that could carry our understanding further.

The study of the underpinnings of inner-ear mechanotransduction has enriched the lives of thousands of scientists over the last 150 years. The study of mechanotransduction, and especially that in the inner ear, exemplifies the utility of biophysical approaches to neuroscience and to biology as a whole. The intricate molecular architecture of the mechanotransduction apparatus has certainly been my inspiration and motivation during the course of my doctoral work. The system is innately mechanical, exquisitely sensitive, and simply awe-inspiring.

In an effort to develop tools to study the mechanotransduction apparatus with single molecule precision, we have developed tools with far wider, and more general utility. The gel-based DNA-nanoswitch platform, brought high-precision molecular-interaction analysis within the reach of thousands of scientists by providing a low-cost and easy-to-use system that works with a common biology technique, gel electrophoresis. Additionally, the platform affords researchers the ability to study complex multi-state systems. We also developed a generally useful technique for the production of DNA-protein chimera's without disrupting protein structure or function.

In studying the rupture force of tip links, we were initially perplexed at the extremely low rupture forces and the very short interaction lifetimes. The clear and well-defined experiments and clear results leave very little possibility of artifact. This forced us to look back to the physiology for understanding. It was only by combining this highly focused and

extremely precise experimental approach with the more holistic understanding of the physiology that we were able to make sense of the data. To go beyond a qualitative justification, and move to a more analytical statement, mathematical modeling was crucial.

This is a theme that has proved very successful in neuroscience. General phenomena are discovered; specialized tools are developed to study them; and mathematical modeling is used to interpret the data, explain the phenomenon, and lay the groundwork for further study. Andrew Huxley and Alan Hodgkin built high-speed amplifiers to more precisely study the electrical phenomena generating the action potential in the squid giant axon. They then built beautiful mathematical models to interpret the data, laying the framework for further electrophysiological study of ion channels and cellular currents.

Pickles et al. first described the tip links in 1984; Assad et al. showed, in 1991, that the tip links can be cleaved by chelating calcium, and that this abolishes mechanotransduction; Ahmed et al. showed, in 2006, that protocadherin-15 (PCDH15) is involved in the tip link; and Kazmierczak et al. showed, in 2007, that the tip link is composed of cadherin-23 (CDH23) and PCDH15; and in 2012 Sotomayor et al. developed techniques to produce and crystalize a complex of extracellular domains 1 and 2 of CDH23 and PCDH15. Sotomayor et al. then used conventional and steered molecular dynamics simulations to study the properties of this interaction. I have been very fortunate to be able to build on all of this work, taking the simulations of this protein-protein interaction, developing tools to experimentally study the way single pairs of these proteins react to the types of forces they would experience nature, and

developing mathematical models to interpret the data and hopefully pave the road for further study.

The data presented in this thesis build upon a lot of previous understanding, ultimately changing our view of tip-link dynamics and their force-dependent lifetimes. This new understanding, however, sets up several new questions. For example, it would be very interesting to study how these force-dependent properties change with differing calcium concentrations. From the simulations that Marcos Sotomayor has performed (Sotomayor et al. 2010; 2012) I would predict that low calcium would increase the zero-force off rate more than it would affect the force-dependent off rate. I say this because the removal of Ca^{2+} seems to act by increasing flexure in the protein rather than by compromising the interaction interface. I would also predict that the increased flexure resulting from lower calcium would alter the on rate, because the effective volume explored by the ruptured pair of molecules increases with increased flexure and their effective concentration is thus lowered. Additionally, it would be very interesting to look at mutations such as the R113G mutant in PCDH15, which results in deafness, but does not affect vestibular function especially to see how this mutation alters the energy landscape of this interaction, and to elucidate the mechanism by which mechanotransduction is conserved in the vestibular system.

Beyond the tip link, this work sets up an experimental platform for further study of the mechanotransduction complex. The mechanotransduction channel is directly gated by force and thus converts motions of the bundle into changes in channel open probability. Opening affects the membrane potential, ultimately resulting in the release of neurotransmitter. Although the

identity of the mechanotransduction channel is not yet known, much has been done to characterize it functionally (Sukharev & Corey 2004). Unfortunately, the majority of this characterization has relied not on direct stimulation of the channel but on stimulation of the entire hair bundle. Although deflections of the entire bundle mimic the physiological stimulus, one must decouple bundle mechanics from the measurement if the goal is to understand the biophysical properties of the channel itself. To achieve this, I propose using a unique approach of applying force directly to a single channel while monitoring the cell's electrical activity. One could do this by utilizing the tip link itself as a molecular handle to apply force to the channel. A hair cell's tip links are each a tetramer of cadherin-23 and protocadherin-15 (Kazmierczak et al., 2007). These two strands are joined together in an overlapping grasp stabilized by calcium (Sotomayor et al., 2012). Removal of calcium from the external solution severs this connection (Assad et al., 1991) (**Figure 6.1**). PCDH15—thought to bind the transduction channel directly—has been shown to remain at the tip of the stereocilium even after the tip link has been severed with EGTA or BAPTA (Indzhykulian et al., 2011) and is thus likely to remain associated with a transduction channel. CDH23 is likely to be pulled away by the myosin-1C motor (**Figure 6.1**) that mediates adaptation.

This situation creates a unique opportunity: By grabbing the free end of a PCDH15 molecule, a single channel can be stimulated and its ionic current recorded (**Figure 6.1b&c**). To grab the PCDH15, one can use N-terminal fragments of its normal binding partner, CDH23; or an antibody to PCDH15; or—if the PCDH15 is affinity tagged—the receptor for that tag. Each could be bound through a DNA linker to a bead that can be manipulated with an optical trap (**Figure 6.1**). Once functionalized, the bead can be initially positioned and experimentally

maneuvered via a 1064-nm continuous wave laser used in an optical trap configuration. The trap can simultaneously apply a calibrated force and measure the bead movement associated with the conformational change of channel opening. Beam deflections can be controlled via electro-optic deflectors to allow subnanometer and submillisecond adjustments of beam position (Valentine et al., 2008).

By correlating single-channel currents with the conformational changes measured by bead movement, one can learn how force alters the open probability of a single channel and the extent of the conformational change associated with the mechanical gating of the channel. Additionally, these experiments will shed light on the open time of the channel. The current estimate of the single channel open time is 3-5 ms (Crawford et al., 1991), but this is too long for a channel whose response latency is on the order of tens of microseconds (Corey and Hudspeth, 1979). These manipulations will also settle a longstanding question of whether there is an adaptation process intrinsic to single channels or whether all adaptation is a consequence of movement of myosin motors.

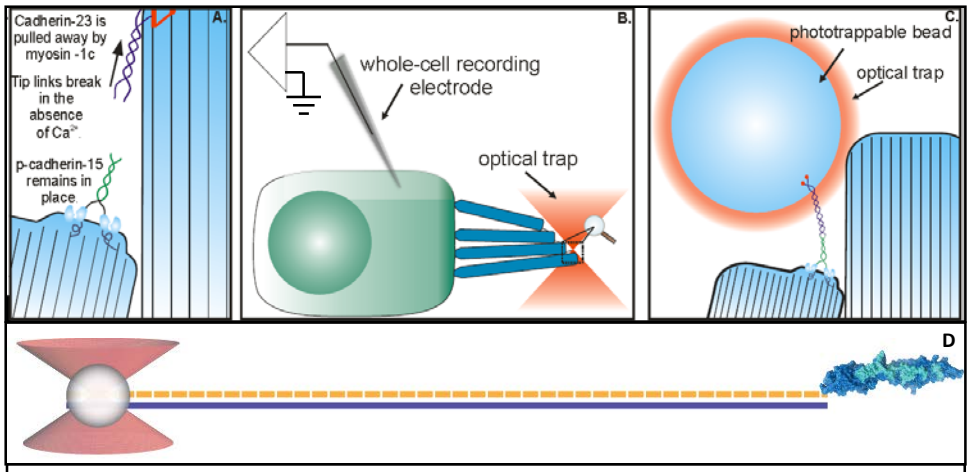

Figure 6.1| Stimulation and recording from a single transduction apparatus. D) shows an expansion of the probe that will be used. The last complimentary oligo will be functionalized with CDH23 fragments instead of a bead.

Although technically challenging, all the individual components of this experiment—attaching CDH23 to a flexible linker on a photo-trappable bead, binding exogenous CDH23 to endogenous PCDH15 (Lelli et al. 2010), using an optical trap in the vicinity of hair cells (Cheung & Corey 2006), and recording a single channel in a whole-cell configuration (Crawford et al. 1991)—are worked out.

These experiments may answer very fundamental questions concerning the mechanism of force transduction into an electrical signal, which will shed light on auditory transduction as well as on the general field of force-gated channels. Once precise measurements are made for channels in intact hair cells, it would be interesting to study the structural correlates of gating and ion permeability, and the means by which force is mechanically linked to the channel. These measurements may do for the field of force-gated channels what single-channel recordings did for the study of voltage-gated channels.

References:

1. Pickles, J.; Comis, S. & Osborne, M. (1984), 'Cross-links between stereocilia in the guinea pig organ of Corti, and their possible relation to sensory transduction.', *Hearing research* **15**(2), 103--112.

2. Assad, J.; Shepherd, G. & Corey, D. (1991), 'Tip-link integrity and mechanical transduction in vertebrate hair cells.', *Neuron* **7**(6), 985--994.

3. Ahmed, Z.M.; Goodyear, R.; Riazuddin, S.; Lagziel, A.; Legan, P.K.; Behra, M.; Burgess S.M.; Lilley, K.S.; Wilcox, E.R.; Riazuddin, S.; Griffith, A.J.; Frolenkov, G.I.; Belyantseva, I.A.; Richardson, G.P.; and Friedman, T.B. (2006). 'The tip-link antigen, a protein associated with the transduction complex of sensory hair cells, is protocadherin-15.' *Journal of Neuroscience.* **26(26) 7022-34**

4. Sotomayor, M.; Weihofen, W.; Gaudet, R. & Corey, D. (2010), 'Structural determinants of cadherin-23 function in hearing and deafness.', *Neuron* **66**(1), 85--100.

5. Sotomayor, M.; Weihofen, W.; Gaudet, R. & Corey, D. (2012) Structure of a force-conveying cadherin bond essential for inner-ear mechanotransduction.' Nature

6. Sukharev, S. & Corey, D. (2004), 'Mechanosensitive channels: multiplicity of families and gating paradigms.', *Science's STKE : signal transduction knowledge environment* **2004**(219)

7. Indzhykulian, A.A.; Stepanyan, R. ; Nelina, A.; Spinelli, K.J. ; Ahmed, Z.M.; Belyantseva, I.A.; Friedman, T.B.; Barr-Gillespie, P.G.; and Frolenkov, G.I. (2011), 'Molecular remodeling of tip links underlies mechanosensory regeneration in auditory hair cells.' *PLoS Biol.* **11(6), e1001583**

8. Crawford, A.; Evans, M. & Fettiplace, R. (1991), 'The actions of calcium on the mechano-electrical transducer current of turtle hair cells.', *The Journal of physiology* **434**, 369-398.

9. Cheung, E. & Corey, D. (2006), 'Ca2+ changes the force sensitivity of the hair-cell transduction channel.' *Biophysical journal* **90**(1), 124--139.

10. Valentine, M.T.; Guydosh, N.R.; Gutiérrez-Medina, B.; Fehr, A.N.; Andreasson, J.O.; Block, S.M; (2008), 'Precision steering of an optical trap by electro-optic deflection.' *Optics Letters* **33: 599-601**